University of Wroclaw

Faculty of Physics & Astronomy

Institute of Theoretical Physics

Modeling nuclear effects in NuWro Monte Carlo neutrino event generator

PhD thesis

Author:
Tomasz Golan

Supervisor:
Prof. Jan T. Sobczyk

Co-supervisor:
dr Krzysztof M. Graczyk

April 10, 2014

Modelowanie efektów jądrowych w generatorze Monte Carlo oddziaływań neutrin NuWro

Rozprawa doktorska

Autor:
Tomasz Golan

Promotor:
Prof. Jan T. Sobczyk

Kopromotor:
dr Krzysztof M. Graczyk

Streszczenie

Neutrina są neutralnymi cząstkami o znikomej masie, które niezwykle słabo oddziałują z materią. Ich detekcja jest możliwa, lecz wyjątkowo trudna - obserwuje się cząstki, które powstały w wyniku oddziaływań neutrin. Każdy pomiar bezpośrednio zależy od modeli teoretycznych użytych w analizie danych. Pomostem między teorią a pomiarem są generatory Monte Carlo. Umożliwiają one interpretację tego co się widzi w detektorze. W niniejszej rozprawie doktorskiej przedstawiony zostanie generator oddziaływań neutrin NuWro, rozwijany przez grupę fizyków z Uniwersytetu Wrocławskiego.

Pierwsza część doktoratu poświęcona jest opisowi modeli fizycznych zaimplementowanych w generatorze. Przedstawione zostaną oddziaływania neutrin na swobodnym nukleonie: rozpraszanie elastyczne, produkcja pojedynczego pionu przez wzbudzenie rezonansu $\Delta(1232)$ i oddziaływania głęboko nieelastyczne oraz koherentne rozpraszanie na jądrze, prowadzące do produkcji pionów. Szerzej omówione zostaną oddziaływania przez prądy wymiany mezonów. Zachodzą one na co najmniej dwóch nukleonach i nie to-

warzyszy im produkcja nowych cząstek. Z doświadczalnego punktu widzenia niezwykle trudno jest rozróżnić takie zdarzenia od elastycznych. Ostanie pomiary wskazują na to, że dla neutrin o energiach rzędu 1 GeV oddziaływania przez prądy wymiany mezonów mogą mieć istotny wkład do całkowitego przekroju czynnego.

W przypadku rozpraszania na jądrze dla wszystkich typów oddziaływań (oprócz koherentnego) cząstki wyprodukowane w pierwotnym wierzchołku propagowane są przez jądro. Jest to tzw. oddziaływanie stanów końcowych, które w NuWro realizuje się w ramach modelu kaskady wewnątrzjądrowej. Jest to semi-kwantowy opis propagacji cząstek, w którym zakłada się, że są one klasyczne i między zderzeniami poruszają się po liniach prostych. Prawdopodobieństwo oddziaływania wyznacza się na podstawie odpowiednich przekrojów czynnych. W NuWro rozważa się kaskadę pionów oraz nukleonów. W rozprawie przedstawiony zostanie szczegółowo model Oseta dla niskoenergetycznych pionów. Zaprezentowany będzie również fenomenologiczny model dla nukleonów oraz rozszerzenie modelu Oseta dla wyższych energii.

Prawdopodobieństwo oddziaływań stanów końcowych jest bezpośrednio związane z czasem kształtowania. Efekt ten przewidziany został przez Landaua i Pomeranchuka dla elektronów, które ulegają wielokrotnemu rozpraszaniu. Na bazie formuły Landaua-Pomeranchuka powstało wiele parametryzacji czasu kształtowania dla oddziaływań neutrin. Okazuje się jednak, że większość z nich działa tylko w określonym zakresie energii, który zależy od danych użytych do dopasowania. W rozprawie zaproponowane zostanie uniwersalne podejście, w którym dla każdej z dynamik używany jest inny model.

W drugiej części doktoratu dyskutowane będą wyniki otrzymane przy pomocy generatora NuWro. Zostaną zaprezentowane liczne porównania z danymi doświadczalnymi oraz przewidywaniami innych generatorów. Ostatni rozdział poświęcony będzie analizie danych eksperymentu MiniBooNE wykonanej przy użyciu generatora NuWro. Jest to pierwsza analiza tych danych, w której dyskutuje się wpływ oddziaływań przez prądy wymiany mezonów na oszacowanie parametrów czynników postaci.

Moja przygoda z fizyką neutrin zaczęła się w 2006 roku, gdy prof. Jan Sobczyk zaproponował mi udział w studenckim projekcie neutrinowym. Od tamtego czasu pozostawałem pod jego opieką naukową. Przez 8 lat wspólnej pracy był on zawsze gotowy, aby wyjaśniać mi zawiłości fizyki cząstek elementarnych. Prof. Jan Sobczyk był promotorem wymagającym, lecz cierpliwym. Motywował do samodzielnej pracy, lecz służył radą, gdy była ona niezbędna. Zawsze zachęcał mnie do starannego i krytycznego podejścia do pracy naukowej. Umożliwił mi uczestnictwo w międzynarodowych konferencjach i szkołach oraz udział w eksperymentach T2K i ICARUS. Za to wszystko chciałbym mu serdecznie podziękować.

Chciałbym również podziękować dr. Cezaremu Juszczakowi za wsparcie od strony programistycznej. Za wiele cennych rad i uwag dziękuję dr. Krzysztofowi Graczykowi.

Wszystkim wymienionym oraz dr. Jakubowi Żmudzie dziękuję za wieloletnią współpracę w miłej atmosferze, interesujące seminaria i ciekawe dyskusje (nie tylko o fizyce).

Abstract

The main goal of the PhD thesis is the investigation of nuclear effects and the implementation of them into a neutrino Monte Carlo event generator NuWro. A description of physical models used in the generator is presented. Model of final state interactions is described in a more detailed way, as it was an essential part of the PhD thesis. Many quantum effects related to a propagation of particles through a nucleus, like Fermi motion, Pauli blocking, or formation zone, are taken into account. NuWro predictions are compared to experimental data and other generators results. Finally, a full analysis of the data for neutral current elastic neutrino scattering off CH_2 measured by the MiniBooNE experiment made using NuWro generator is presented. An influence of two-body current contribution on the results is investigated.

List of publications

Theoretical papers

1. Tomasz Golan et al. “Extraction of Axial Mass and Strangeness Values from the MiniBooNE Neutral Current Elastic Cross Section Measurement”. Phys.Rev. C88 (2013), p. 024612

2. Tomasz Golan, Cezary Juszczak, and Jan T. Sobczyk. “Final State Interactions Effects in Neutrino-Nucleus Interactions”. Phys.Rev. C86 (2012), p. 015505

Proceedings

1. Tomasz Golan. “A comparison of Monte Carlo generators” . arXiv: 1402.1608 [hep-ph] (2014)

2. T. Golan, J.T. Sobczyk, and J. Zmuda. “NuWro: the Wroclaw Monte Carlo Generator of Neutrino Interactions”. Nucl.Phys.Proc.Suppl. 229-232 (2012), p. 499

3. Tomasz Golan, Cezary Juszczak, and Jan T. Sobczyk. “Final state interactions model in NuWro Monte Carlo event generator”. AIP Conf.Proc. 1405 (2011), pp. 219–222

4. M. Ziembicki et al. “The SMRD subdetector at the T2K near detector station”. Acta Phys.Polon. B41 (2010), pp. 1579–1584

5. Maddalena Antonello et al. “Study of Pion Production in nu(mu) CC Interactions on O-16 Using Different MC Generators”. Acta Phys.Polon. B40 (2009), pp. 2519–2535

Experimental papers

1. K. Abe et al. “Measurement of the intrinsic electron neutrino component in the T2K neutrino beam with the ND280 detector” . arXiv: 1403.2552 [hep-ex] (2014)

2. K. Abe et al. “Measurement of the neutrino-oxygen neutral-current interaction cross section by observing nuclear de-excitation γ-rays” . arXiv: 1403.3140 [hep-ex] (2014)

3. K. Abe et al. “Recent Results from the T2K Experiment”. Nucl.Phys.Proc.Suppl. 246-247 (2014), pp. 23–28

4. K. Abe et al. “Precise Measurement of the Neutrino Mixing Parameter theta23 from Muon Neutrino Disappearance in an Off-axis Beam” . arXiv: 1403.1532 [hep-ex] (2014)

5. K. Abe et al. “Observation of Electron Neutrino Appearance in a Muon Neutrino Beam” . arXiv: 1311.4750 [hep-ex] (2013)

6. K. Abe et al. “Measurement of Neutrino Oscillation Parameters from Muon Neutrino Disappearance with an Off-axis Beam”. Phys.Rev.Lett. 111 (2013), p. 211803

7. K. Abe et al. “Evidence of Electron Neutrino Appearance in a Muon Neutrino Beam”. Phys.Rev. D88 (2013), p. 032002

8. K. Abe et al. “Measurement of the Inclusive NuMu Charged Current Cross Section on Carbon in the Near Detector of the T2K Experiment”. Phys.Rev. D87 (2013), p. 092003

9. K. Abe et al. “The T2K Neutrino Flux Prediction”. Phys.Rev. D87 (2013), p. 012001

10. K. Abe et al. “First Muon-Neutrino Disappearance Study with an Off-Axis Beam”. Phys.Rev. D85 (2012), p. 031103

11. K. Abe et al. “Measurements of the T2K neutrino beam properties using the INGRID on-axis near detector”. Nucl.Instrum.Meth. A694 (2012), pp. 211–223

12. K. Abe et al. “Indication of Electron Neutrino Appearance from an Accelerator-produced Off-axis Muon Neutrino Beam”. Phys.Rev.Lett. 107 (2011), p. 041801

13. K. Abe et al. “The T2K Experiment”. Nucl.Instrum.Meth. A659 (2011), pp. 106–135

14. C. Rubbia et al. “Underground operation of the ICARUS T600 LAr-TPC: first results”. JINST. 6 (2011), P07011

Contents

List of Figures

List of Tables

List of abbreviations

CC Charged current

CEX Charge exchange

CL Coherence length

COH Coherent pion production

CMS Center-of-mass system

CVC Conserved vector vurrent

DIS Deep inelastic scattering

EL Elastic

FF Form factor

FG Fermi gas

FM Fermi motion

FSI Final state interactions

FT Formation time

FZ Formation zone

IA Impulse Approximation

INC Intranuclear cascade

LDA Local density approximation

LFG Local Fermi gas

LRC Long-range correlations

MB MiniBooNE

MC Monte Carlo

MEC Meson Exchange Currents

MF Mean field

NC Neutral current

NN Nucleon-nucleon

NRB Non-resonant background

np-nh n particles - n holes

PB Pauli blocking

PCAC Partially conserved axial current

PV Primary vertex

QEL Quasi-elastic

RES Resonance pion production

RPA Random phase approximation

SciB SciBooNE

SF Spectral function

SM Standard Model

SPP Single pion production

SRC Short-range correlations

TE Transverse Enhancement

Chapter 1

Introduction

Neutrino is perhaps the most fascinating elementary particle. Its unique and still not entirely understood properties make its research a challenge from both theoretical and experimental points of view. The studying of neutrino is interesting itself, but it may also be a key to understand the Universe. Neutrino interacts extremely weakly with other particles. Thus, it can travel a large distance without any interactions providing an undisturbed information about its source. The first step to extract this information is to understand neutrino.

Neutrino interactions are described within the electroweak theory of the Standard Model (SM). In the SM forces are expressed in terms of local gauge symmetries. In the case of the electroweak sector the symmetry group is $U(1) \times SU(2)$. As a consequence there are four gauge bosons, which mediate weak and electromagnetic interactions. The $W^{\pm}$ and Z^0 are the charged and neutral bosons of the weak force. Processes mediated by the $W^{\pm}$ bosons (called charged current) involve an exchange of electric charge, so particles change their identities through the emission or absorption of the $W^{\pm}$. Processes mediated by the Z^0 (called neutral current) maintain particles identities.

There are three families of particles within the SM. Each one is composed of a pair of quarks and a pair of leptons (a charged one and a neutrino). Charged current interactions change the identity of a quark or a lepton within a single family. However, there is a mechanism which allows the transition between families. It is based on the fact that weak (or flavor) states are not the same as mass states, but they are mixtures of them.

In the early formulation of the SM a neutrino was assumed to be a massless particle, so the mass mixing was expected only in the quark sector. Because of the mass mixing each quark mass state is in fact the superposition of three quark weak states. Thus, the gauge boson acting on one of these states allows the passage from one family to another.

If a neutrino had mass, the mass mixing would be also possible in the lepton sector. If so, a neutrino produced in a specific flavor could be later registered in another one. This phenomenon, called neutrino oscillations, was predicted by Bruno Pontecorvo.

There is no fundamental principle that requires a neutrino to be massless. In the SM picture particles gain mass through an interaction with the Higgs boson, which leads to a change of their handedness. Experiments have shown that observed neutrinos are always left-handed. Thus, in the early SM there are no right-handed neutrinos, so there is no mechanism for acquiring mass by neutrinos. However, there are possible extensions of the SM which allow to introduce massive neutrinos.

The straightforward extension is to simply add a right-handed neutrino into the SM and introduce a Dirac mass term as for other particles. However, this new field would not couple to any of the SM gauge bosons. Thus, it is called sterile neutrino. Another possibility is the assumption that a neutrino does satisfy the Majorana equation. This approach does not require any new fields. It violates the lepton number conservation instead and it would mean that neutrinos are their own antiparticles. It is also possible to include both Dirac and Majorana mass terms. It leads to so called see-saw mechanism, which may be an explanation for the smallness of neutrino masses.

The strength of the mass mixing in the lepton sector is defined by PMNS (Pontecorvo-Maki-Nakagawa-Sakata) matrix[1]. For Dirac neutrinos PMNS is expressed by three mixing angles (θ_{12}, θ_{23}, θ_{13}) and the CP phase factor (δ). CP is the combination of charge conjugation (C) and parity (P) symmetries. It is known from kaons decays studies, that CP is violated in the quark sector. A non-zero value of δ would indicate also the violation in the lepton sector.

The probability for neutrino oscillations depends on the mass mixing parameters as well as the actual neutrino masses, or more precisely on the differences of their squares ($\Delta m^2_{21} \equiv m^2_2 - m^2_1$, $\Delta m^2_{32} \equiv m^2_3 - m^2_2$, $\Delta m^2_{31} = \Delta m^2_{32} + \Delta m^2_{21}$). Together there are six free parameters within the oscillation model, which cannot be calculated and must be determined from the experiment.

The first indication for neutrino oscillations was observed in the late 1960s by the Homestake experiment. The neutrino flux produced in the Sun through nuclear fusion (called solar neutrinos) was measured to be 2-3 times smaller than predicted by the Standard Solar Model. The discrepancy was called the solar neutrino problem. Today it can be well explained by the oscillation phenomenon. Although the MSW (Mikheyev-Smirnov-Wolfenstein) effect must be taken into account in order to fully explain the measured rate. The MSW effect describes how the presence of electrons in matter affects

[1]If PMNS was an identity matrix, there would be no mass mixing and no neutrino oscillations.

the oscillations. Is is important at very large electron densities, like the core of the Sun, where solar neutrinos are produced.

The first model-independent experimental evidence of neutrino oscillations was announced in 1998 by the Super-Kamiokande collaboration. A large zenith angle asymmetry of atmospheric neutrinos events was observed. These neutrinos are produced in collisions of comic rays with the atmosphere. Thus, the distance traveled by them (so the probability for the oscillations) until they reach the detector depends on the zenith angle. At 90% confidence level the data was consistent with two-flavor oscillations model with $\sin^2(2\theta_{23}) \equiv \sin^2(2\theta_{atm}) > 0.82$ and $5 \cdot 10^{-4} < |\Delta m^2_{32}| \equiv \Delta m^2_{atm} < 6 \cdot 10^{-3}$ eV^2.

Many other experiments have been arranged in order to measure the oscillations parameters. The combined analysis of global data for solar neutrinos and the KamLAND results led to "solar" parameters values $\sin^2(2\theta_{12}) \equiv \sin^2(2\theta_{sol}) = 0.87 \pm 0.03$ and $\Delta m^2_{21} \equiv \Delta m^2_{sol} = 7.59 \cdot 10^{-5}$ eV^2. The sign of Δm^2_{32} is still unknown. However, the MINOS collaboration provided the high precision measurement of its absolute value, which was established to be $|\Delta m^2_{32}| = 2.43 \pm 0.13 \cdot 10^{-3}$ eV^2. The result was confirmed by the T2K collaboration about one month ago. From the muon neutrino disappearance studies the values of $|\Delta m^2_{32}| = 2.51 \pm 0.10 \cdot 10^{-3}$ eV^2 and $\sin^2(2\theta_{23}) = 0.514^{+0.055}_{-0.056}$ were obtained. About a year ago the T2K collaboration gave also for the first time an indication of non-zero value of the θ_{13} angle. From the electron neutrino appearance studies they obtained the value of $\sin^2(2\theta_{13}) = 0.140^{+0.038}_{-0.032}$. Shortly after, Daya Bay, RENO and Double Chooz experiments confirmed the results. The last of them provided the most precise measurement of $\sin^2(2\theta_{13}) = 0.092 \pm 0.017$.

T2K is one of several accelerator experiments focused on a studying of the oscillations phenomenon. Muon neutrinos produced at J-PARC (Japan Proton Accelerator Research Complex) travel 295 km to the Super-K water Cherenkov detector. It is positioned at 2.5 degree angle to the center of the neutrino beam. The off-axis part of the beam ensures a narrower spectrum of neutrino energies. There is an additional detector within the beam path, called ND280. It measures the number of muon neutrinos in the beam before any oscillations occur, allowing to minimize the systematic error coming from flux uncertainty (from 21-26% to 3-5%).

The reconstruction of events rests on the analysis of the final state particles. For typical neutrino energies in the T2K flux interactions are dominated by charged current quasi-elastic (CCQE) processes. However, there is about 15% contribution coming from single pion production. If a pion is absorbed by nuclear matter through final state interactions (FSI), these events will be indistinguishable from CCQE ones[2]. The systematic

[2]Experimentally, CCQE is defined as events with charged lepton and no meson in the final state.

error coming from FSI is estimated to be 3-8%.

Two-body current (or $np-nh$) interactions are another significant background for CCQE. They occur on at least two nucleons and no particles are created in the process, so there is a lepton and n nucleons in the final state. For neutrino energy around 1 GeV there is about 10% contribution to the CCQE cross section from these events. So far, the two-body current contribution has not been taken into account in any analysis. The interest in $np-nh$ processes in neutrino physics began after recent measurements of axial mass (the phenomenological parameter controls the CCQE cross section). They suggest significantly larger value than older experiments, which were performed on deuteron target or with the high energy neutrino beam - in both cases the two-body current contribution is negligible.

Monte Carlo (MC) method is the only possibility to analyze experimental data. There are several MC neutrino event generators and they are all based on similar assumptions. The primary neutrino interaction (primary vertex, PV) and FSI are considered separately. There are several dynamics distinguished in the case of PV, for both charged and neutral current channels. Each one is described individually within one of available theoretical models. Note, that neutrino cross sections are known with the precision of about 20-30% and generators can not do better. In the case of T2K the systematic error coming from neutrino interactions models was estimated to be 7-8%. Intranuclear cascade (INC) is the natural approach for the FSI in the MC picture. The knowledge of hadron-nucleon in medium cross sections is necessary.

During my Ph.D. I have been developing NuWro - Monte Carlo neutrino event generator, created by a group of physicist from the Wrocław University. My work was concentrated on the FSI model described within the INC picture[3]. I implemented many new models and quantum effects. Each update was tested by comparing NuWro predictions with experimental data and other generators results. I have been also studying the impact of the two-body current contribution on the estimation on the form factors parameters.

The general scheme of the cascade (based on the old Metropolis model) has already been done, when I started my work on NuWro. I implemented the Oset model for low-energy pions. It is a theoretical model, based on the pion-nucleon optical potential. The quasi-elastic scattering (including charge exchange processes) and absorption are considered. For high-energy pions I proposed a phenomenological model, where quasi-elastic and charge exchange scattering, absorption and pion production processes are

[3]Only propagation of nucleons and pion is considered.

distinguished. The angular distributions are based on SAID model. I also upgraded the nucleon cascade. High-energy extension to Metropolis model has been introduced. An effective approach to the impact of nuclear potential on nucleons energy has been implemented.

The probability of re-interactions is controlled by formation time effect. I implemented several parameterizations of the formation time and confronted them with experimental data. It turns out that typically each parameter works only in a certain energy range, which depends on experimental data uses for the fit. I proposed a universal approach, where various models of formation time are used for specific dynamics.

In 2009 the MiniBooNE collaboration published the data for the neutral current elastic neutrino-CH_2 cross section. Such measurement is difficult mainly due to a lack of charged lepton in the final state. The result are presented as the sum of reconstructed kinetic energy of all nucleons in the final state for events without any charged lepton or pion. The reconstructed energy is related to the true one with response matrices, which define the energy smearing out in the detector and the efficiency. In the MiniBooNE analysis five signals are considered: elastic scattering on hydrogen; elastic scattering on proton from carbon unaffected by final state interactions; elastic scattering on proton from carbon affected by final state interactions; elastic scattering on neutron and an irreducible background (pion production and its absorption by nuclear matter). The two-body current contribution is not taken into account. The measured value of axial mass (1.39 ± 0.11 GeV) is significantly larger then older estimations (~ 1 GeV).

I redone the analysis of MiniBooNE data using NuWro. I investigated the impact of two-body current contribution on the axial mass estimation and proposed the unfolding procedure for these processes. The Transverse Enhancement model for neutral current channel I implemented in NuWro was used in the analysis. The final results indicate that the inclusion of $np-nh$ interactions into the analysis lead to the axial mass value consistent with older measurements.

As I mentioned before, there are several MC neutrino event generators based on similar basis. However, their predictions still can differ significantly on the level of both primary vertex and final state interactions. The systematics errors coming from PV and FSI are of order 7-8% and 3-8%, respectively. There is an obvious need to improve the generators. It requires both theoretical and computer work. The main focus should be on pion production models and the two-body current contribution. Experimentally, it is hard to distinguished between $np-nh$ processes and single pion production with pion absorbed by nuclear matter. They are both significant background for CCQE reactions.

Good theoretical models as well as accurate experimental methods are necessary to understand neutrino interactions.

Chapter 2

NuWro

In this chapter NuWro Monte Carlo neutrino event generator is presented. Basic information about the generator is introduced in Sec. 2.1. In Sec. 2.2 there are details about the implementation of primary vertex (PV), including descriptions of all basic dynamics. Sec. 2.3 is devoted to nucleus models used in NuWro. Final state interactions model is presented in Sec. 2.4.

2.1 Generalities

NuWro [22] is a Monte Carlo (MC) neutrino event generator with a basic scheme similar to other generators, like NEUT [23], GENIE [24] or NUANCE [25]. It has been developed for over 9 years at the Wroclaw University by the group of theorists under the direction of Jan Sobczyk, who was encouraged by Danuta Kiełczewska[1]. The general structure of the code is prepared and maintained by Cezary Juszczak, who is an author of many parts of the generator. The basic model of pion production processes was implemented by Jarosław Nowak[2] during work on his PhD thesis. I was responsible for the improvement of the existing model of final state interactions (FSI). Many others, including Krzysztof Graczyk and Jakub Żmuda, have also contributed to the development of NuWro.

All basic dynamics for neutrino scattering processes are included in NuWro, for both neutral (NC) and charged (CC) currents:

- elastic scattering (EL) for NC, or quasi-elastic (QEL) for CC (see Subsec. 2.2.2);

[1]Professor of Physics at Warsaw University.
[2]Currently lecturer at Lancaster University.

- pion production through $\Delta(1232)$ resonance excitation with a non-resonant background (RES) (see Subsec. 2.2.3);
- more inelastic scattering, usually (in the MC community) called deep inelastic scattering (DIS) (see Subsec. 2.2.4);
- two-body current interaction, also called n particles - n holes ($np - nh$) (see Subsec. 2.2.5);
- coherent pion production (COH) (see Subsec. 2.2.6).

In the first three cases interactions occur on a single nucleon from a nucleus in the Impulse Approximation (IA) regime (see Subsec. 2.2.1). Two-body current scattering goes beyond IA and neutrino interacts with at least two nucleons. Coherent pion production occurs on a whole nucleus. For all dynamics, but the coherent, the primary vertex is followed by final state interactions based on the intra-nuclear cascade model (see Sec. 2.4).

In the case of scattering off free nucleon NuWro simulates reactions for neutrino energies from threshold to TeV. However, for neutrino-nucleus processes there is a limit coming from IA (discussed in Subsec. 2.2.1).

A beam can be set manually or can be loaded from a ROOT [26] format file. It is possible to use mixed beams with different kinds of neutrino flavors.

The generator provides a multiplicity of choices for a description of a target nucleus, including Fermi gas (FG) and spectral function (SF). Nuclear density distributions are tabulated for many nuclei. The tables are based on Ref. [27]. More information about the nucleus models can be found in Sec. 2.3. NuWro also contains various parameterizations of nuclear form factors (FF) and has a detector geometry module. Many quantum effects, like Pauli blocking (PB) or formation zone (FZ), are included. All together NuWro is a complete tool to use in neutrino experiments.

In the past few years NuWro has become appreciated by experimental physicists. Not being an official generator of any collaboration, it has more opportunity to quick updates. Many theoretical models appear in NuWro long before they are implemented in other MCs. Therefore, NuWro is very often used to crosscheck new models introduced to generators.

T2K collaboration [28] has used NuWro predictions to estimate systematic errors. NuWro was the only generator at that time with successfully implemented spectral function. Various distributions for QEL neutrino-oxygen scattering, obtained with FG and SF, was used to check the uncertainty coming from theoretical nucleus models.

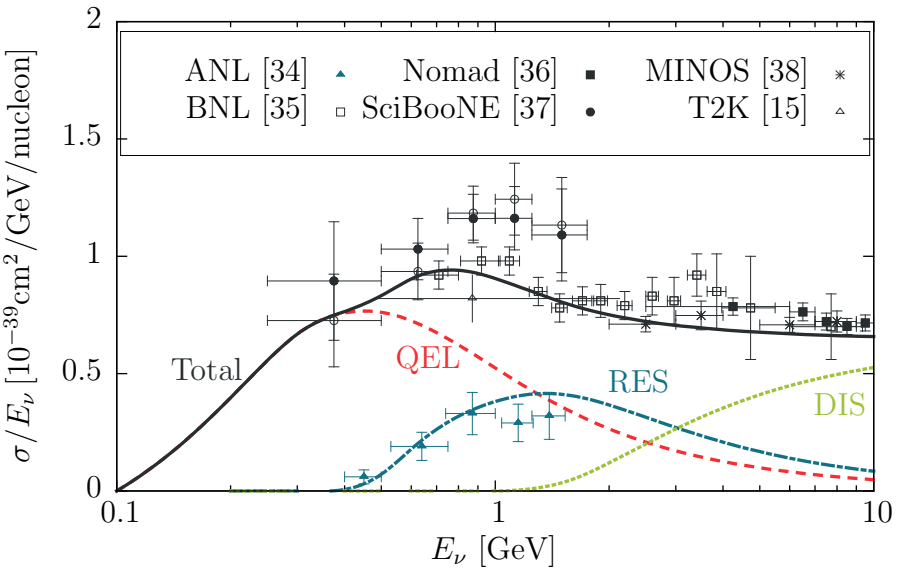

Figure 2.1: The NuWro cross sections predictions on an isoscalar target, compared to the ANL 12-feet, BNL 7-feet, NOMAD, SciBooNE (opened - NEUT based analysis, closed circles - NUANCE based analysis), MINOS and T2K data.

Recently, MINERvA collaboration published the measurement of the flux-averaged differential cross section $\mathrm{d}\sigma/\mathrm{d}Q^2$ (Refs [29, 30]). Data was compared to NuWro calculations to investigate the effect of using SF instead of FG model, as well as the impact of the two-body current contribution.

As an input, NuWro uses a text file (*params.txt*), where one can set a beam, target specifications and many other parameters, like axial mass or the form factor parameterization. For detailed description of *params.txt* file see Appx. A.

The results of a simulation are saved in a ROOT format file, which contains a complete tree with all information about the events. The output contains also a text file with total cross sections for each dynamics, normalized to cm^2/nucleon.

The NuWro code is written in C++ language. It is freely available from the repository [31]. The basic information necessary to install, run and analyze the output can be found in [22, 32, 33].

2.2 Primary vertex

Primary vertex describes an initial neutrino-nucleon (-nucleus) interaction. For all channels (but the coherent) the particles created in PV are propagated through nucleus (see Sec. 2.4). The NuWro predictions for QEL, RES (with non-resonant background), DIS and total cross section together with ANL, BNL, NOMAD, SciBooNE, MINOS and

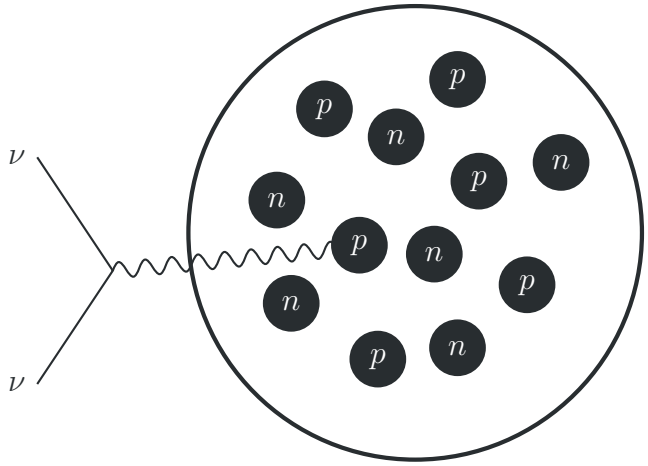

Figure 2.2: Impulse Approximation: interaction occurs on one nucleon; remaining are merely spectators.

T2K are presented in Fig. 2.1.

In this section all dynamics for primary vertex are described. First subsection is devoted to Impulse Approximation. (Quasi-)elastic scattering (Subsec. 2.2.2), resonance pion production (Subsec. 2.2.3) and deep inelastic scattering (Subsec. 2.2.4) are done under IA assumption. In the case of two-body current (Subsec. 2.2.5) the interaction occurs on at least two correlated nucleons. Coherent pion production (Subsec. 2.2.6) describes scattering on whole nucleus.

2.2.1 Impulse Approximation

The description of lepton-nucleus scattering processes depends on the momentum transfered to the nucleon system $\vec{q}$. For low $|\vec{q}|$ the impact area ($\sim \frac{1}{|\vec{q}|}$) usually includes many nucleons and the interaction leads to nuclear excitations. If $|\vec{q}|$ is high one can adopt a picture in which the lepton scattering occurs on a single nucleon (Impulse Approximation, see Fig. 2.2). It has been shown (Ref. [39]), that IA is reliable for the momentum transfer larger than $350 - 400$ MeV/c.

In IA squares of transition matrices for the lepton-nucleon scattering are summed up and interference terms are neglected. In terms of cross section it means that:

$$\sigma^A = \sum_{i=1}^{Z} \sigma_p(p_{F,i}^{(p)}) + \sum_{i=1}^{A-Z} \sigma_n(p_{F,i}^{(n)}) \tag{2.1}$$

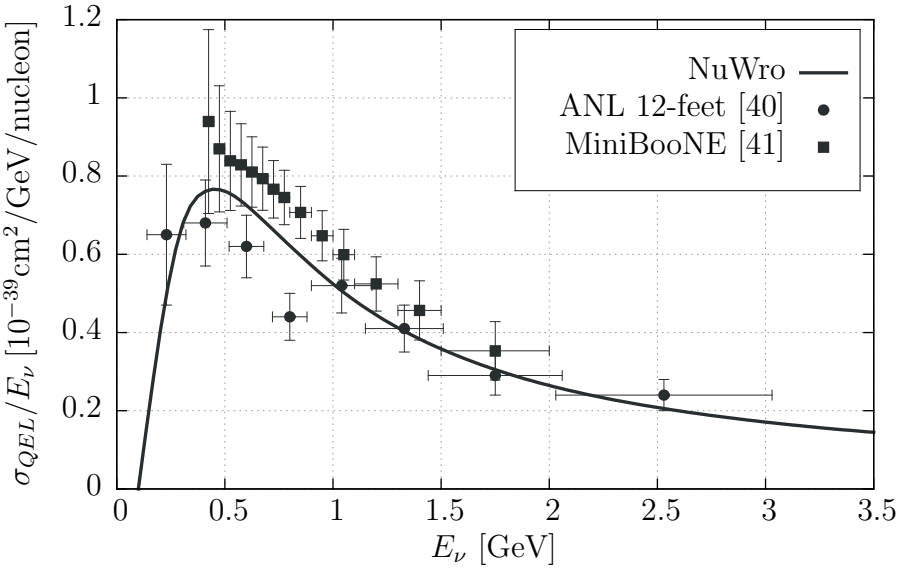

Figure 2.3: The NuWro prediction for the quasi-elastic scattering cross section (LFG, $M_A = 1.03$ GeV), compared to the ANL and MiniBooNE data.

2.2.2 (Quasi-)elastic scattering

For electron/muon scattering, the quasi-elastic term means that the elastic interaction occurs on a bound nucleon inside nucleus. In the case of neutrino the terminology is different. Elastic scattering is the process without charge exchange (neutral current):

$$\nu(\overline{\nu}) + p \;\rightarrow\; \nu(\overline{\nu}) + p \tag{2.2}$$

$$\nu(\overline{\nu}) + n \;\rightarrow\; \nu(\overline{\nu}) + n \tag{2.3}$$

while quasi-elastic scattering is an interaction with charged lepton in the final state (charged current):

$$\nu + n \;\rightarrow\; l^- + p \tag{2.4}$$

$$\overline{\nu} + p \;\rightarrow\; l^+ + n \tag{2.5}$$

In NuWro for (Q)EL cross sections the Llewellyn-Smith formula[3] (Ref. [42]) is used:

[3]The same model is used in most of MC generators.

$$\frac{\mathrm{d}\sigma^{\nu/\overline{\nu}}}{\mathrm{d}|q^2|} = \frac{M^2 G^2 \left(f^{CC/NC}\right)^2}{8\pi E_\nu^2} \left[A(q^2) \mp B(q^2)\left(\frac{s-u}{M^2}\right) + C(q^2)\left(\frac{s-u}{M^2}\right)^2\right] \tag{2.6}$$

where $M = (M_p + M_n)/2$ is average mass of nucleons, G - Fermi constant, $f^{CC} = \cos\theta_C$ (θ_C - Cabibbo angle), $f^{NC} = 1$, $q^2 = -Q^2$ is the square of four-momentum transfer, s and u are Mandelstam variables:

$$s = (k+p)^2 = (k'+p')^2 \tag{2.7}$$
$$u = (k-p')^2 = (k'-p)^2 \tag{2.8}$$

where $k(k')$ and $p(p')$ are four-momenta of incoming (outgoing) lepton and nucleon, respectively. A, B, C functions are expressed by nucleon form factors:

$$\begin{aligned} A &= \frac{1}{4}\left(\frac{m^2}{M^2} - z\right)\left[(4-z)\left(G_A\right)^2 - (4+z)\left(F_1^V\right)^2 - y\left(F_2^V\right)^2\left(1+\frac{1}{4}z\right)\right. \\ &- \left. 4F_1^V F_2^V z - \frac{m^2}{M^2}\left(\left(F_1^V + F_2^V\right)^2 + \left(G_A + 2F_P\right)^2 + (z-4)\left(F_P\right)^2\right)\right] \end{aligned} \tag{2.9}$$
$$B = -zG_A\left(F_1^V + F_2^V\right) \tag{2.10}$$
$$C = \frac{1}{4}\left[\left(G_A\right)^2 + \left(F_1^V\right)^2 - z\left(\frac{F_2^V}{2}\right)^2\right] \tag{2.11}$$

where $z \equiv \frac{q^2}{M^2}$, m is a mass of a charged lepton or a neutrino for CC or NC scattering, respectively. Note, that the vector ($F_{1,2}^V$) and axial (G_A) form factors are different for CC and NC interactions[4]. The vector FFs are related to electromagnetic ones due to CVC:

$$\left(F_{1,2}^V\right)^{CC} = F_{1,2}^p - F_{1,2}^n \tag{2.12}$$
$$\left(F_{1,2}^V\right)^{NC,p/n} = \pm\frac{1}{2}\left[F_{1,2}^p - F_{1,2}^n\right] - 2\sin^2\theta_W F_{1,2}^{p/n} - \frac{1}{2}F_{1,2}^s \tag{2.13}$$

where θ_W is the Weinberg angle. Proton and neutron electromagnetic form factors are normalized as following: $F_1^p(0) = 1$, $F_1^n(0) = 0$, $F_2^p(0) = \mu_p - 1$, $F_2^n(0) = \mu_n$ (μ_p

[4]All form factors are functions of Q^2. The argument is skipped to simplify the notation.

and μ_n are the magnetic moments of proton and neutron in the units of the nuclear magneton $\mu_n = e/2M_p$). They are expressed by:

$$F_1^{V,p/n} = \left(1 - \frac{1}{4}y\right)^{-1} \left[G_E^{p/n} - \frac{1}{4}yG_M^{p/n}\right] \tag{2.14}$$

$$F_2^{V,p/n} = \left(1 - \frac{1}{4}y\right)^{-1} \left[G_M^{p/n} - G_E^{p/n}\right] \tag{2.15}$$

where electric (G_E) and magnetic (G_M) form factors are extracted form the electron scattering data (for review see Ref. [43]). There are several parameterizations of electromagnetic FFs in NuWro - see App. A for details (parameter *qel_vector_ff_set*).

For the axial form factors and the vector strange form factor the dipole form is assumed:

$$G_A^{CC} = g_A \left(1 + Q^2/M_A^2\right)^{-2} \tag{2.16}$$

$$G_A^{NC,p/n} = \frac{1}{2}\left(1 + Q^2/M_A^2\right)^{-2} (\pm g_A - g_A^s) \tag{2.17}$$

$$F_{1,2}^s = F_{1,2}^s(0) \left(1 + Q^2/4M^2\right)^{-1} \left(1 + Q^2/M_V^2\right)^{-2} \tag{2.18}$$

where $g_A = 1.2670 \pm 0.0035$ is determined from nucleon β decay (Ref. [44]). M_A is the axial mass and g_A^s is the contribution of quark-antiquark pairs to the spin of the nucleon. Both parameters are discussed in details in Ch. 4. $F_1^s(0) = -\frac{1}{6}\langle r_s^2\rangle = 0.53 \pm 0.70$ and $F_2^s(0) = \mu_s = -0.40 \pm 0.72$ are established for vector mass $M_V = 0.84$ GeV (see Ref. [45]) with $\langle r_s^2\rangle$ interpreted as the mean square strangeness radius and μ_s - the strange magnetic moment of the nucleon. Alternative (but similar) values for vector strange form factors at $Q^2 = 0$ can be found in Ref. [46]. The pseudoscalar axial form factor can be expressed (according to PCAC) by the axial form factor:

$$F_P = \frac{4M^2}{m_\pi^2 + Q^2} G_A^{CC} \tag{2.19}$$

The NuWro prediction for QEL scattering on an isoscalar target together with ANL and MiniBooNE data is presented in Fig. 2.3.

2.2.3 Resonance pion production

The RES channel in NuWro is defined in terms of invariant mass W, which is given by the following formula:

$$W^2 = \left(\sum_i p_i\right)^2 \tag{2.20}$$

where p_i are four-momenta of all final state particles, but the lepton. All pion production processes with W from $W_{th} = M + m_\pi$ (the sum of pion and nucleon masses) to the res_dis_cut parameter value from *params.txt* (1.6 GeV by defualt, see App. A) are classified as RES events. Thus, RES contains resonance pion production, non-resonant background and also two pion production processes with $W < 1.6$ GeV (see 2.2.4.1).

For the neutrino energy of the order of few GeV inelastic interactions are dominated by single pion production (SPP) processes with the largest contribution coming from $\Delta(1232)$ resonance excitation:

$$\begin{aligned}
\nu + p &\rightarrow l^- + \left(\Delta^{++} \rightarrow p + \pi^+\right) && (2.21)\\
\nu + n &\rightarrow l^- + \left(\Delta^{+} \rightarrow p + \pi^0 \text{ or } n + \pi^+\right) && (2.22)\\
\overline{\nu} + p &\rightarrow l^+ + \left(\Delta^{0} \rightarrow p + \pi^- \text{ or } n + \pi^0\right) && (2.23)\\
\overline{\nu} + n &\rightarrow l^+ + \left(\Delta^{-} \rightarrow n + \pi^-\right) && (2.24)\\
\nu(\overline{\nu}) + p &\rightarrow \nu(\overline{\nu}) + \left(\Delta^{+} \rightarrow p + \pi^0 \text{ or } n + \pi^+\right) && (2.25)\\
\nu(\overline{\nu}) + n &\rightarrow \nu(\overline{\nu}) + \left(\Delta^{0} \rightarrow p + \pi^- \text{ or } n + \pi^0\right) && (2.26)
\end{aligned}$$

For each channel relative amplitudes can be calculated from Clebsh-Gordan coefficients (Ref. [47]). In NuWro the Adler-Rarita-Schwinger formalism (see Refs. [48] and [49]) is used to calculate the cross section:

$$\begin{aligned}
\frac{\mathrm{d}\sigma}{\mathrm{d}W\mathrm{d}Q^2} = G^2\cos^2\theta_C \frac{W g(W)}{\pi^2 M E_\nu^2}\Bigg[-(Q^2+m^2)W_1 + \frac{W_2}{M^2}\left(2\,(pq)\,(pk')\,\frac{M^2}{2}\left(Q^2+m^2\right)\right)\\
-\frac{W_3}{M^2}\left(Q^2\,(kp) - \frac{1}{2}\left(Q^2+m^2\right)(pq)\right) + \frac{W_4}{M^2}\frac{m^2}{2}\left(Q^2+m^2\right) - 2\frac{W_5}{M^2}m^2\,(kp)\Bigg] \qquad (2.27)
\end{aligned}$$

where $Q^2 = -q^2$, p, k, k' are four-momenta of initial nucleon, incoming and outgoing lepton and

$$g(W) = \frac{\Gamma_\Delta/2}{\left(W - M_\Delta\right)^2 + \Gamma_\Delta^2/4} \tag{2.28}$$

is the Breit-Wigner formula introducing the Δ width (Γ_Δ). W_i functions are expressed by the structure functions for Δ resonance (V_i): $W_i = V_i/2MM_\Delta$. The structure

functions depend on vector and axial form factors $C_i^{V,A}$:

$$V_1 = \frac{\left(C_3^V\right)^2}{M^2}\frac{2}{M_\Delta^2}\left[\alpha^2\beta + M_\Delta^2\left((qp)^2 + Q^2M^2 + Q^2MM_\Delta\right)\right] + 2\frac{\left(C_4^V\right)^2}{M^4}\alpha^2\beta_- \quad (2.29)$$
$$+ \frac{C_4^VC_3^V}{M^3}\frac{2}{M_\Delta}\alpha\left[\alpha\left(\beta_- - MM_\Delta\right) + M_\Delta^2 qp\right] + 2\left[\frac{\left(C_4^A\right)^2}{M^4}\alpha^2 + \left(C_5^A\right)^2 + 2\frac{C_4^AC_5^A}{M^2}\alpha\right]\beta_+$$

$$V_2 = \left(C_3^V\right)^2\frac{2}{M_\Delta^2}Q^2\left(\beta + M_\Delta^2\right) + \frac{2\left(C_4^A\right)^2}{M^2}Q^2\beta_+ + \frac{2C_3^VC_4^V}{MM_\Delta}Q^2\left(\beta_- - MM_\Delta + M_\Delta^2\right)$$
$$+ 2\left[\left(C_5^A\right)^2\frac{M^2}{M_\Delta^2} + \frac{\left(C_4^A\right)^2}{M^2}Q^2\right]\left(\beta + M_\Delta^2\right) \quad (2.30)$$

$$V_3 = \frac{4}{M_\Delta}\left(-\frac{C_3^VC_4^V}{M}\alpha - C_3^VC_5^AM\right)\left(2M_\Delta^2 + 2MM_\Delta - \alpha\right) + 4\alpha\left(\frac{C_4^VC_4^A}{M^2}\alpha - C_4^VC_5^A\right) \quad (2.31)$$

$$V_4 = \frac{2}{M_\Delta^2}\left(C_3^V\right)^2\left[(qp+\alpha)\beta - M_\Delta^2\left(M^2 + MM_\Delta\right)\right] + 2\left(C_4^V\right)^2(qp+\alpha)\beta_- \quad (2.32)$$
$$+ 2\frac{C_3^VC_4^V}{MM_\Delta}\left[(qp+\alpha)\left(\beta_- - MM_\Delta\right) + qpM_\Delta^2\right] + 2\left[\left(C_5^A\right)^2\frac{M^2}{M_\Delta^2} + \frac{\left(C_4^A\right)^2}{M^2}(qp+\alpha)\right.$$
$$\left. + \frac{\left(C_6^A\right)^2}{M^2M_\Delta^2}\left(\alpha^2 + Q^2M_\Delta^2\right) + 2C_4^AC_5^A - 2\frac{C_4^AC_6^A}{M^2}qp - 2\frac{C_5^AC_6^A}{M_\Delta^2}\left(M_\Delta^2 - \alpha\right)\right]\beta_+$$

$$V_5 = 2\frac{\left(C_3^V\right)^2}{M_\Delta^2}qp\left(\beta + M_\Delta^2\right) + 2\frac{\left(C_4^V\right)^2}{M^2}qp\beta_+ + 2\frac{C_3^VC_4^V}{MM_\Delta}qp\left(\beta_- - MM_\Delta + M_\Delta^2\right)$$
$$+ 2\left[\frac{\left(C_4^A\right)^2}{M^2}qp + \left(C_5^A\right)^2\frac{M^2}{M_\Delta^2} + C_4^AC_5^A - \frac{C_4^AC_6^A}{M^2}Q^2 + \frac{C_5^AC_6^A}{M_\Delta^2}\right]\beta_+ \quad (2.33)$$

where $\alpha \equiv qp - Q^2$, $\beta \equiv qp + M^2$, $\beta_- \equiv \beta - MM_\Delta$, $\beta_+ \equiv \beta + MM_\Delta$. There are several parameterizations of form factors ($C_i^{V,A}$) implemented in NuWro (for details see App. A, parameter *delta_FF_set*). As the default the ones from Ref. [50] are used.

NuWro's approach to the resonance pion production is different from other MC generators (e.g. NEUT, GENIE), which use Rein-Sehgal model (Ref. [51]).

2.2.4 Deep inelastic scattering

In this thesis all processes more inelastic than the ones defined in RES (with $W > 1.6$ GeV) are called deep inelastic scattering. For high energy neutrinos DIS:

$$\nu\left(\overline{\nu}\right) + N \rightarrow l^{-}\left(l^{+}\right) + X \tag{2.34}$$

$$\nu\left(\overline{\nu}\right) + N \rightarrow \nu\left(\overline{\nu}\right) + X \tag{2.35}$$

becomes a dominant process. In NuWro DIS processes are considered within the quark-parton model (Ref. [52]), so the neutrino-nucleon interactions are described by the scattering on quarks and gluons. This approach is based on quark-hadron duality (Ref. [53]) - the observation, that for high-energies resonances are averaged by the structure functions. The formalism used in NuWro is based on Ref. [54] with the cross section given by:

$$\begin{aligned}\frac{\mathrm{d}^2\sigma^{\nu/\overline{\nu}}}{\mathrm{d}x\mathrm{d}y} &= \frac{G^2 M E_\nu}{\pi\left(1+Q^2/M_{W,Z}^2\right)^2}\left[y\left(xy+\frac{m^2}{2E_\nu M}\right)F_1\right. \\ &+ \left.\left(1-y-\frac{Mxy}{2E_\nu}-\frac{m^2}{4E_\nu^2}-\frac{m^2}{2ME_\nu x}\right)F_2 \pm \left(xy\left(1-\frac{y}{2}\right)-y\frac{m^2}{4ME_\nu}\right)F_3\right]\end{aligned} \tag{2.36}$$

where $x = Q^2/2M\nu$, $y = \nu/E_\nu$, ν is the energy transfer and F_i are structure functions expressed by the parton distribution functions (PDF) q_j:

$$F_1\left(x,Q^2\right) = \sum_j\left[q_j\left(x,Q^2\right)+\bar{q}_j\left(x,Q^2\right)\right] \tag{2.37}$$

$$F_2\left(x,Q^2\right) = 2xF_1\left(x,Q^2\right) \tag{2.38}$$

$$F_3\left(x,Q^2\right) = 2x\sum_j\left[q_j\left(x,Q^2\right)-\bar{q}_j\left(x,Q^2\right)\right] \tag{2.39}$$

PDF's are taken from Ref. [55] with the modification from Ref. [56]. The final state hadrons are obtain using PYTHIA6 hadronization routine (Ref. [57]).

2.2.4.1 Non-resonant background

Experimental data indicate, that there is a contribution to the Δ resonance region coming from other resonances or non-resonant processes, usually called non-resonant background (NRB). According to quark-hadron duality NRB can be described in terms of parton distribution functions.

In NuWro NRB is modeled as a contribution to one-pion channels from DIS formalism. The smooth transition from Δ to DIS is made for the invariant mass range $W = (W_{min}, W_{max}) = (1.3, 1.6)$ GeV:

$$\frac{\mathrm{d}\sigma^{SPP}}{\mathrm{d}W} = \frac{\mathrm{d}\sigma^{\Delta}}{\mathrm{d}W}\left(1 - \alpha(W)\right) + \frac{\mathrm{d}\sigma^{DIS}}{\mathrm{d}W} F^{SPP}(W)\alpha(W) \tag{2.40}$$

where

$$\begin{aligned} \alpha(W) &= \Theta\left(W_{min} - W\right)\frac{W - W_{th}}{W_{min} - W_{th}}\alpha_0 \\ &+ \Theta\left(W_{max} - W\right)\Theta\left(W - W_{min}\right)\frac{W - W_{min} + \alpha_0\left(W_{max} - W\right)}{W_{max} - W_{min}} \\ &+ \Theta\left(W - W_{max}\right) \end{aligned} \tag{2.41}$$

The threshold for single pion production $W_{th} = M + m_\pi$. The NRB contribution is different for each SPP channel (Ref. [58]), so α_0 is fitted independently for each pion production process. The one-pion function:

$$F^{SPP}(W) = \frac{\mathrm{d}\sigma^{DIS-SPP}/\mathrm{d}W}{\mathrm{d}\sigma^{DIS}/\mathrm{d}W} \tag{2.42}$$

gives the probability for single pion in the final state in DIS formalism and it is calculated for each one-pion channel separately.

2.2.5 Two-body current contribution

It is well known from the electron scattering data that two-body current interactions give a significant contribution to the cross section between QEL and Δ peaks (so called "dip region"). The recent MiniBooNE measurement of the CC QEL double differential cross section (Ref. [41]) suggests, that $np - nh$ may be also important in neutrino-nucleus scattering interactions (see e.g. Refs. [59–61]). From theoretical point of view, two-body currents ensure the gauge invariance of the theory (Ref. [62]).

In $np-nh$ processes n nucleons are emitted from the primary vertex. Because of final

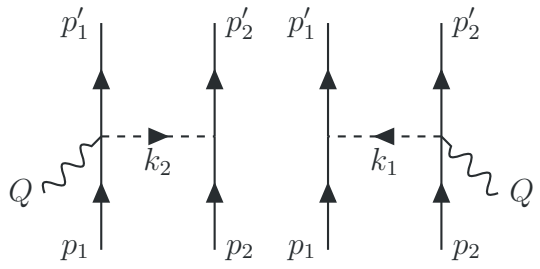

(a) Contact terms.

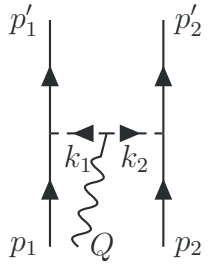

(b) The pion - in - flight term.

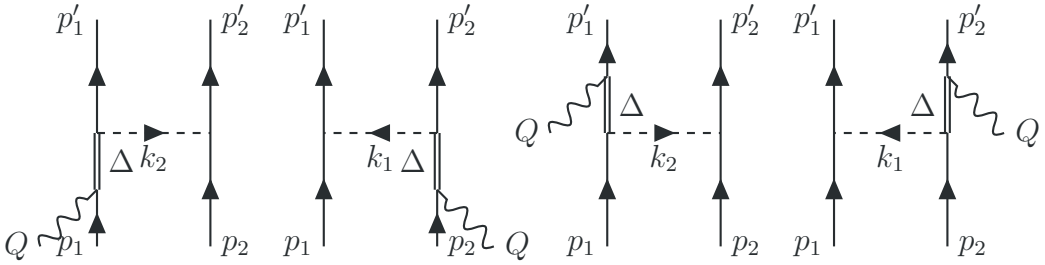

(c) Δ pole and Δ pole crossed terms.

Figure 2.4: Feynman diagrams for the two body current contribution.

state interactions it is difficult to distinguish between QEL, pion production (with π absorbed by the nuclear matter) and $np-nh$ events in the detector. A good theoretical model of $np-nh$ contribution within Monte Carlo generators is necessary to find the evidence of two-body current events in experimental data.

Some of Feynman diagrams for the $2p-2h$ interactions are presented in Fig. 2.4. Some authors refer to contact terms (Fig. 2.4a) and the so called pion-in-flight term (Fig. 2.4b) as Meson Exchange Currents (MEC) contributions, while another include also Δ-terms (Fig. 2.4c) into MEC. To avoid confusion in this thesis MEC term is no longer used.

There are four models of $np-nh$ available in NuWro:

- Nieves model (Ref. [63]) with the extension to higher energies (Ref. [64]) (only for CC);
- Marteau-like model (Ref. [65]) (only for CC);
- MEChM-like model (as above with new elementary response functions from Ref. [66]) (only for CC);
- Transverse Enhancement (TE) model (Ref. [60]) (for both NC and CC).

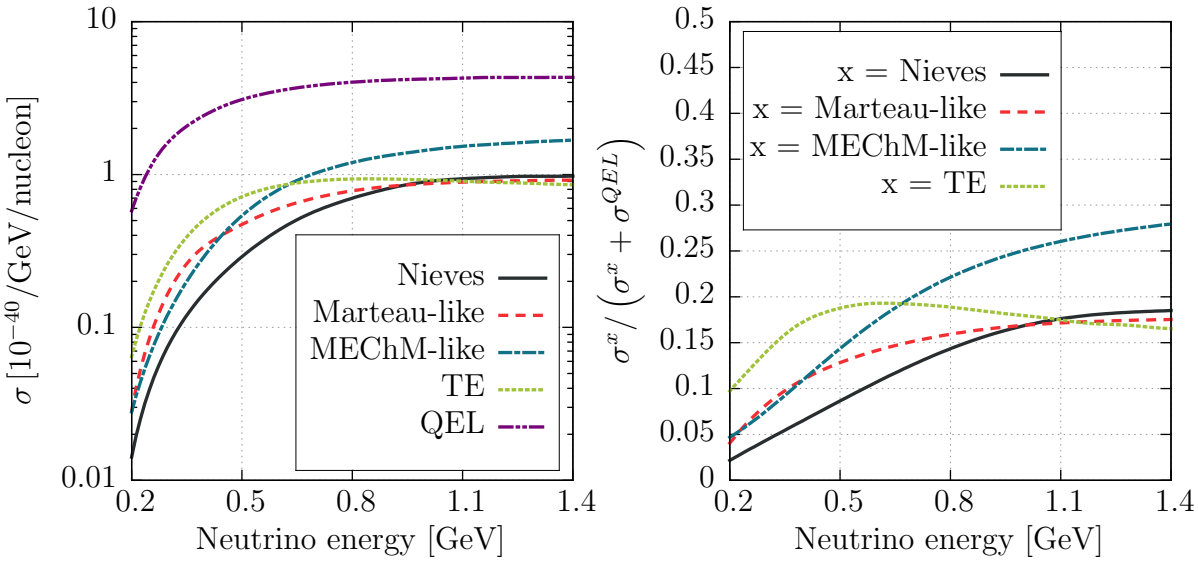

(a) The total cross section.

(b) The ratio of σ_{np-nh} to $\sigma_{np-nh} + \sigma_{QEL}$ cross sections.

Figure 2.5: The cross section for QEL (LFG, $M_A = 1.03$ GeV) neutrino-carbon scattering and the $np - nh$ contribution.

Nieves, as well as the original Marteau and MEChM models are microscopic calculations within the local Fermi gas picture. The Marteau model takes into account only Δ-terms (Fig. 2.4c) and so called nucleon correlations terms, while the Nieves model counts all diagrams presented in Fig. 2.4, nucleons correlations and so called pion pole terms. The virtual meson exchanged between the nucleons is just pion for Marteau, while Nieves considers also the ρ meson exchange contribution. Both models use Oset's parameterization for Δ self-energy (Ref. [67]). The medium polarization and collective effects are considered in the random phase approximation (RPA) picture in both models. Nieves model is relativistic, while the original Marteau model is not, but it has a relativistic correction (Ref. [61]). MEChM model is an upgraded version of the Marteau model done by Martini, Ericson, Chanfray and Marteau.

There are some simplifications in Marteau-like and MEChM-like respect to the original ones. The correlation part is not taken into account. The relativistic kinematics of nucleons is used. The constant value of Fermi momentum is kept and the local density effects are included in the approximate way.

Transverse Enhancement model is an effective approach to the two-body current interactions. It is based on the analysis of the electron-carbon scattering data. The $np-nh$ contribution to the (Q)EL cross section is introduced by the following modification

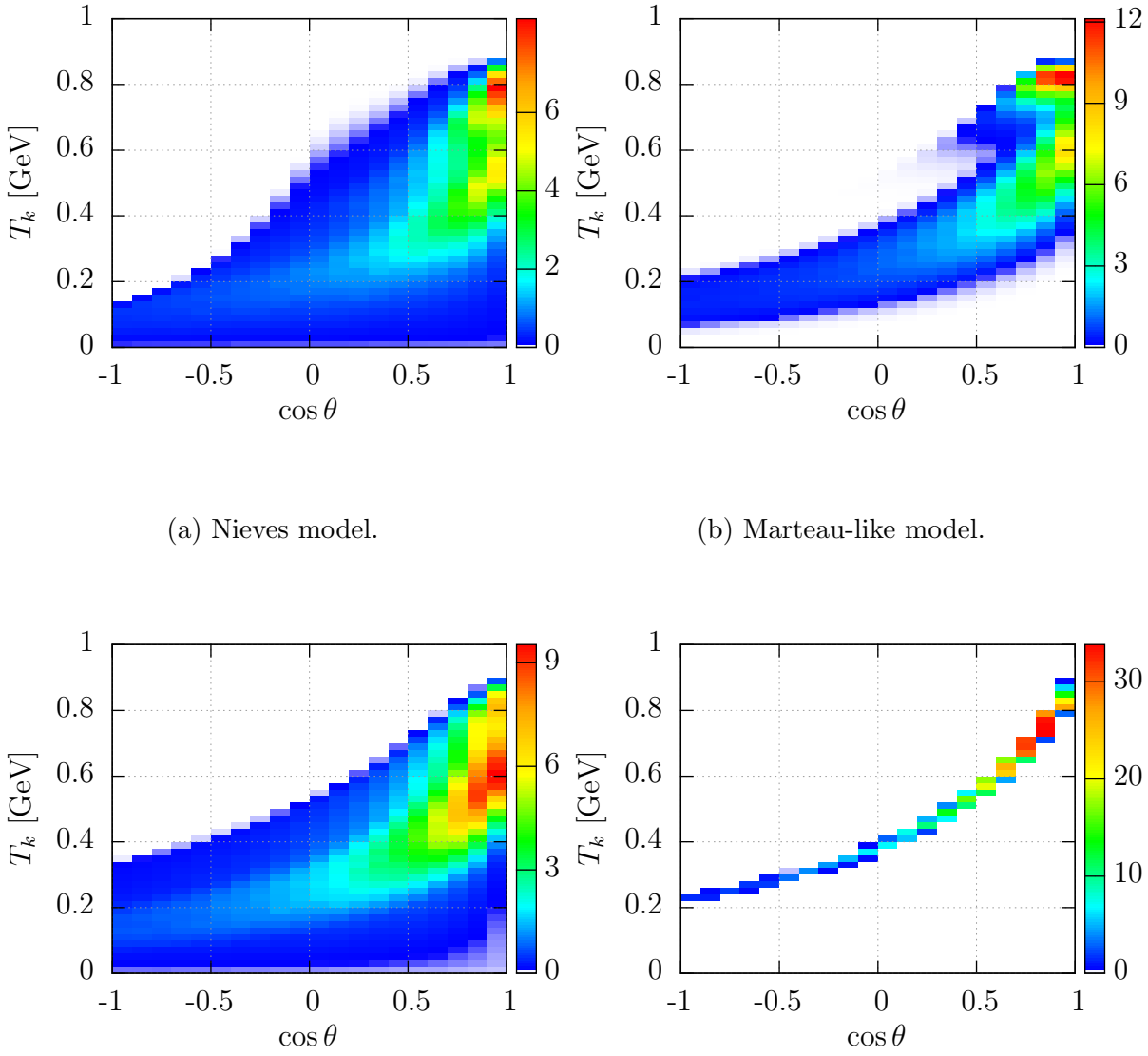

(a) Nieves model.

(b) Marteau-like model.

(c) MEChM-like model.

(d) TE model.

Figure 2.6: Lepton kinematics for the $np-nh$ contribution in the case of 1 GeV neutrino scattering off carbon.

of the vector magnetic form factors:

$$G_M^{p/n} \to \tilde{G}_M^{p/n} = \sqrt{1 + AQ^2 \exp -\frac{Q^2}{B}} G_M^{p/n} \tag{2.43}$$

where $A = 6$ GeV^{-2}, $B = 0.34$ GeV^2 and the axial mass value for TE model is fixed to be $M_A^{np-nh} = 1014$ MeV, as assumed in Ref. [60]. To obtain $np - nh$ cross section

one needs to subtract the (Q)EL contribution:

$$\left(\frac{\mathrm{d}\sigma^{\nu/\overline{\nu}}}{\mathrm{d}Q^2}\right)^{np-nh}_{CC} \equiv \frac{\mathrm{d}\sigma^{QEL}}{\mathrm{d}Q^2}(\tilde{G}_M^{p/n}) - \frac{\mathrm{d}\sigma^{QEL}}{\mathrm{d}Q^2}(G_M^{p/n}) \tag{2.44}$$

$$\begin{aligned}\left(\frac{\mathrm{d}\sigma^{\nu/\overline{\nu}}}{\mathrm{d}Q^2}\right)^{np-nh}_{NC} &\equiv \frac{1}{2}\left[\left(\frac{\mathrm{d}\sigma^{EL}}{\mathrm{d}Q^2}(\tilde{G}_M^{p}) - \frac{\mathrm{d}\sigma^{EL}}{\mathrm{d}Q^2}(G_M^{p})\right)\right. \\ &+ \left.\left(\frac{\mathrm{d}\sigma^{EL}}{\mathrm{d}Q^2}(\tilde{G}_M^{n}) - \frac{\mathrm{d}\sigma^{EL}}{\mathrm{d}Q^2}(G_M^{n})\right)\right]\end{aligned} \tag{2.45}$$

The cross section calculation for all four models (as implemented in NuWro) for the charge current neutrino-carbon scattering are presented in Fig. 2.5a. MEChM model predicts the highest two-body current contribution (note the logarithmic scale). Other models agree with each other for the neutrino energy around 1 GeV, but there is a large discrepancy for lower energies. It can be easily seen on Fig. 2.5b, which presents the fraction of $2p-2h$ events in the QEL+$(2p-2h)$ sample. Note, that original Nieves model breaks down for neutrino energies $E_\nu > 1.5$ GeV. However, there is a correction involving a cut on three-momentum transfer (Ref. [64]), which extends the model up to 10 GeV.

In Fig. 2.6 there are predictions for lepton kinematics for each model. In the TE model the lepton kinematics is based on QEL one with the assumption, that a target nucleon is at rest. Other models have two maximums related to contact and Δ terms.

NuWro is the only MC generator with all four models for $np-nh$ contribution implemented in the code. NEUT uses the Nieves model with the extension to higher energies (Ref. [64]), GENIE uses Dytman model (Ref. [68]), while other generators do not have the two-body current contribution implemented yet.

2.2.5.1 Multi-nucleon ejection model

All models for the two-body current contribution provide only the inclusive double differential cross section for the final state lepton. Nucleon kinematics is obtained using multi-nucleon ejection model (Ref. [69]) by the following scheme:

- set randomly the four-momenta (p_1 and p_2) of the initial nucleons from the Fermi sphere with a radius determined by the local nuclear density;
- calculate the four-momentum of the hadronic system: $W = p_1 + p_2 + q$;
- repeat steps 1. and 2. until the invariant hadron mass is larger than mass of two nucleons ($W^2 > (2M)^2$);

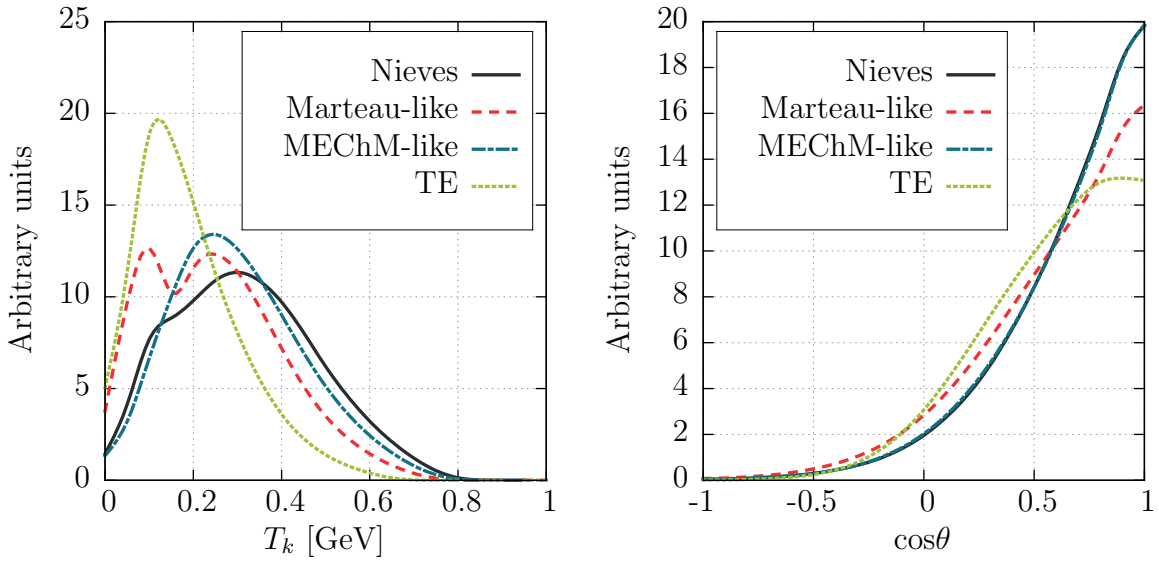

(a) Kinetic energy of the most energetic nucleon.

(b) Distribution of the most energetic nucleon angle (respect to neutrino beam).

Figure 2.7: The most energetic nucleon kinematics for the $np-nh$ contribution in the case of 1 GeV neutrino scattering off carbon.

- make the Lorentz boost to the hadronic center of mass system;
- isotropically select momenta of two final state nucleons;
- boost back to the laboratory frame.

Because of different distributions of the energy transfer (see Fig. 2.6), there is a large disagreement between the $np-nh$ models in the energy distributions of the final state nucleons (Fig. 2.7a). This may be very important in experiments with Cherenkov detectors. For example, the Cherenkov threshold for protons in water is $T_k \sim 480$ MeV. Nieves and MEChM models predict much more protons above this threshold than Marteau and TE. They also predict more forward directions of knock-out nucleons (see Fig. 2.7b).

2.2.5.2 Correlations

As it was mentioned in the previous subsection, the $np-nh$ models give only the inclusive cross section, not saying anything about final state nucleons. There are several possible channels for two-body current:

$$\nu + p + n \rightarrow l^- + p + p \quad (2.46)$$
$$\nu + n + n \rightarrow l^- + p + n \quad (2.47)$$
$$\overline{\nu} + p + n \rightarrow l^+ + n + n \quad (2.48)$$
$$\overline{\nu} + p + p \rightarrow l^+ + p + n \quad (2.49)$$
$$\nu(\overline{\nu}) + 2N \rightarrow \nu(\overline{\nu}) + 2N \quad (2.50)$$

The probability of the mixed isospin pair in the charged current interactions is defined in NuWro by arbitrary p_{CC} parameter, with the default value $p_{CC} = 0.6$. In the case of NC processes every isospin initial state pair is possible. To keep the same proportion between mixed and non-mixed pairs and assuming the same probability to have $n - n$ and $p - p$ pairs, the parameter $p_{NC} = (2/p_{CC} - 1)^{-1}$ is introduced, giving the likelihood of a mixed pair to be selected in a NC two-body current reaction.

It is not clear, what the value of p_{CC} parameter should be. Electron data suggests (see e.g. Ref. [70]), that about 20% of interactions occur on correlated pairs of nucleons, dominated by the ones with opposite isospin[5]. The estimation of the p_{CC} parameter is based on the assumption, that in 20% of cases there is always the mixed isospin pair and in other cases each pair is equally likely. Thus, the value of p_{CC} parameter is $p_{CC} = 0.2 + 0.8 * 0.5 = 0.6$. However, more studies is needed and for now p_{CC} is treated as a free parameter, which can be set in the *params.txt* file. More discussion about correlations can be found in 2.3.2.2.1.

2.2.6 Coherent pion production

In coherent pion production interaction occur on a whole nucleus ($\mathcal{N}$):

$$\nu + \mathcal{N} \rightarrow l^- + \pi^+ + \mathcal{N} \quad (2.51)$$
$$\overline{\nu} + \mathcal{N} \rightarrow l^+ + \pi^- + \mathcal{N} \quad (2.52)$$
$$\nu(\overline{\nu}) + \mathcal{N} \rightarrow \nu(\overline{\nu}) + \pi^0 + \mathcal{N} \quad (2.53)$$

NuWro uses the Rein-Sehgal model[6] (Ref. [71]) for COH reactions. Note, it is not the same model as used for RES. Estimation of the coherent π^0 cross section is based

[5] Is it the same for weak interactions?
[6] The same model is used in the most of MC generators.

on the Adler's PCAC formula (Ref. [72]), which describes the forward scattering:

$$\left(\frac{\mathrm{d}\sigma}{\mathrm{d}x\mathrm{d}y\mathrm{d}|t|}\right)^{NC\ COH}_{Q^2=0} = \frac{G^2 M E_\nu}{\pi^2}\frac{1}{2} f_\pi^2 (1-y) \left.\frac{\mathrm{d}\sigma\left(\pi^0\mathcal{N}\to\pi^0\mathcal{N}\right)}{\mathrm{d}|t|}\right|_{E_\pi=\nu} \tag{2.54}$$

where t is the Mandelstam variable ($t = -Q^2$), $y = \omega/E_\nu$, $f_\pi = 0.93 m_\pi$ is the pion decay constant. Non-forward directions ($Q^2 \neq 0$) are introduced by the following modification of the formula:

$$\left(\frac{\mathrm{d}\sigma}{\mathrm{d}x\mathrm{d}y\mathrm{d}|t|}\right)^{NC\ COH} = \left(\frac{\mathrm{d}\sigma}{\mathrm{d}x\mathrm{d}y\mathrm{d}|t|}\right)^{NC\ COH}_{Q^2=0} \left(\frac{1}{1+Q^2/1\ \mathrm{GeV}^2}\right)^2 \tag{2.55}$$

The $\pi\mathcal{N}$ differential cross section is expressed by:

$$\frac{\mathrm{d}\sigma\left(\pi^0 A\to\pi^0 A\right)}{\mathrm{d}t} = A^2 \left|F_\mathcal{N}(t)\right|^2 \left.\frac{\mathrm{d}\sigma\left(\pi^0 N\to\pi^0 N\right)}{\mathrm{d}t}\right|_{t=0} \tag{2.56}$$

where A in the atomic mass number. The pion-nucleon differential cross section in the forward direction is calculated within the optical theorem:

$$\left.\frac{\mathrm{d}\sigma\left(\pi^0 N\to\pi^0 N\right)}{\mathrm{d}t}\right|_{t=0} = \frac{1}{16\pi}\left[\sigma_{tot}^{\pi^0 N}\right]\left(1+r^2\right) \tag{2.57}$$

where r is the ratio of the real and imaginary parts of the scattering amplitude $r = \mathrm{Re}\, f_{\pi N}(0)/\,\mathrm{Im}\, f_{\pi N}(0) \approx 0.2$, the total cross section for neutral pion scattering off nucleon is assumed to be the average of the ones for charged pions (taken from tables from Ref. [73]):

$$\sigma_{tot}^{\pi^0 N} = \frac{1}{4}\left[\sigma_{tot}^{\pi^+ D} + \sigma_{tot}^{\pi^- D}\right] \tag{2.58}$$

The nuclear form factor with the inclusion of the absorption effects reads:

$$\begin{aligned} \left|F_\mathcal{N}(t)\right|^2 &= e^{-\frac{1}{3}R^2 t} F_{abs} \\ &= e^{-\frac{1}{3}R^2 t} \exp\left(-\frac{9A^{1/3}}{16\pi R_0^2}\sigma_{inel}^{\pi N}\right) \end{aligned} \tag{2.59}$$

where $R = R_0 A^{1/3}$ is the radius of the nucleus and $\sigma_{inel}^{\pi N}$ is taken from Ref. [73].

For high energy neutrino one can assume that the cross section for charged current coherent pion production is two times larger than for neutral current ($\sigma_{COH}^{CC} = 2\sigma_{COH}^{NC}$). However, for lower energies the mass of a lepton must be taken into account. The

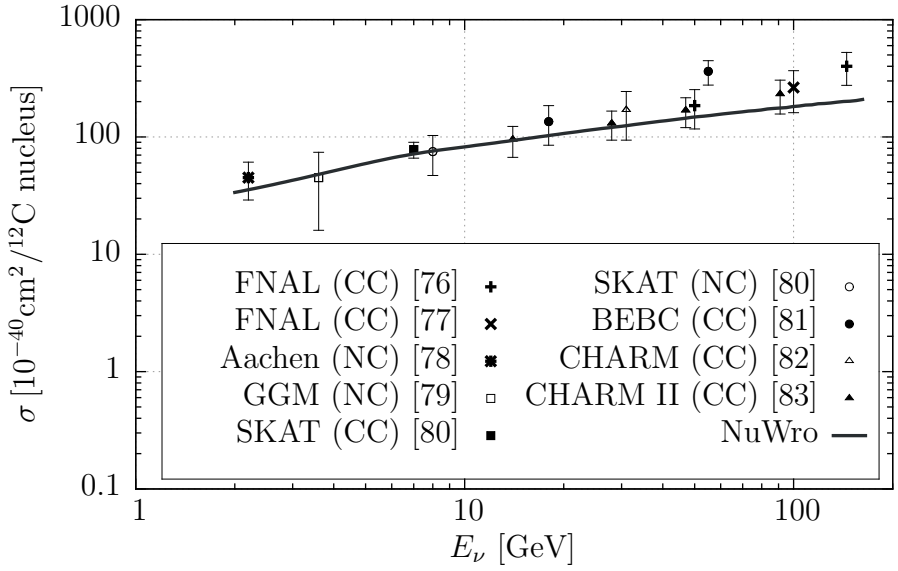

Figure 2.8: Total cross section for charged current coherent pion production. Data are scaled to ^{12}C assuming $A^{1/3}$ dependence. The data for neutral current are multiply by a factor 2 assuming the relation $\sigma^{CC}_{COH} = 2\sigma^{NC}_{COH}$.

correction is introduced as a multiplicative factor (Ref. [74]):

$$\mathcal{C} = \left[\left(1 - \frac{1}{2}\frac{Q^2_{min}}{Q^2 + m^2_\pi}\right)^2 + \frac{1}{4}y\frac{Q^2_{min}\,(Q^2 - Q^2_{min})}{(Q^2 + m^2_\pi)^2}\right]\theta(Q^2 - Q^2_{min})\theta(y - y_{min})\theta(y_{max} - y) \tag{2.60}$$

where $Q^2_{min} = m^2_l y/(1-y)$, $y_{min} = m_\pi/E_\nu$ and $y_{max} = 1 - m_l/E_\nu$.

NuWro predictions for the charged current coherent pion production cross section is presented in Fig. 2.8. Data are scaled to ^{12}C assuming $A^{1/3}$ dependence. The data for neutral current are multiplied by factor 2 assuming the relation $\sigma^{CC}_{COH} = 2\sigma^{NC}_{COH}$. The Rein-Sehgal model works well for higher energies, however, it is well known, that it fails for low neutrino energies (see e.g. Ref. [75]).

2.3 Nucleus models

Energy and momentum distribution of nucleons inside a nucleus can be described in the Fermi gas picture. It is a very easy and fast method used very often in MC simulations. However, there is also a much more reliable model, called spectral function. Cross section predictions obtained within the SF can differ by about 15% from the ones calculated with FG model. It may be significant in the oscillation analysis.

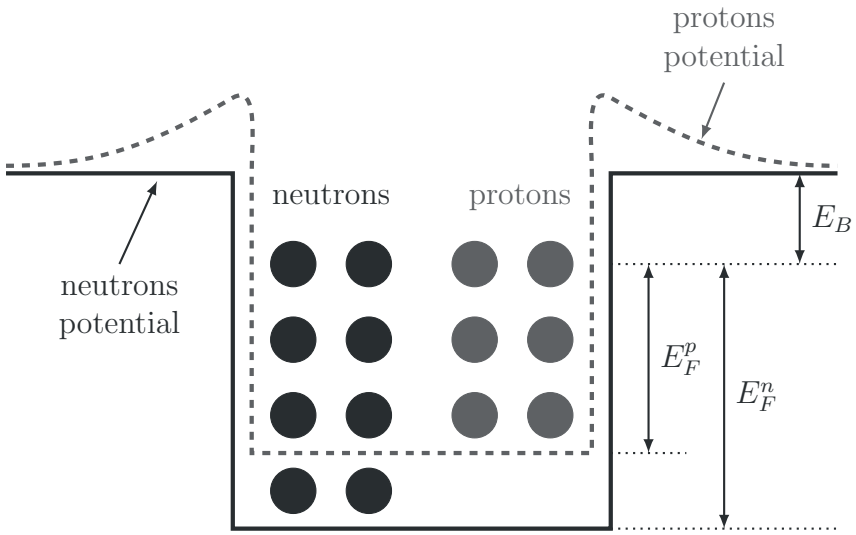

Figure 2.9: Nuclear potential wells for protons and neutrons. E_F^p, E_F^n are Fermi energies of protons and neutrons, and E_B is binding energy.

In the spectral function approach most of nucleons are described as occupying shell-model and moving in the mean-field (MF) potential. The shell orbits are modified by two- and three-nucleon interaction potentials. NN interactions also lead to pairs of strongly repulsive nucleons, so called short-range correlation (SRC) pairs, which can have large momenta.

In this section all nucleus models implemented in NuWro are presented. Global and local Fermi gas models are discussed in Subsec. 2.3.1. Subsec. 2.3.2 is devoted to spectral function. In Subsec. 2.3.3 Pauli blocking effect is introduced. Comparison of spectral function and Fermi gas models can be found in Subsec. 2.3.4.

2.3.1 Fermi gas

The theoretical concept of the Fermi gas model is applicable to systems of fermions. It may be used for a description of a nucleus, when one assumes no interactions between nucleons. The basic idea is to treat protons and neutrons independently and to assume they move freely (Fermi motion) within the nuclear volume in constant binding potential, generated by all nucleons (see Fig. 2.9).

Nucleons occupy all available energy states up to the maximum one, called Fermi energy (E_F). The binding potential is different for protons and neutrons. Each energy state is filled by two nucleons with the same isospin, but different spin projections. The difference between top of the potential well and Fermi level is called binding energy (E_B) - the energy needed to pull out a nucleon from the nuclear potential. Total binding

Nucleus	${}^{6}_{3}$Li	${}^{12}_{6}$C	${}^{24}_{12}$Mg	${}^{40}_{20}$Ca	${}^{58.7}_{28}$Ni	${}^{89}_{39}$Y	${}^{118.7}_{50}$Sn	${}^{181}_{73}$Ta	${}^{208}_{82}$Pb
p_F [MeV/c]	169	221	235	251	260	254	260	265	265

Table 2.1: Fermi momentum measured from electron scattering data (see Ref. [84]).

energy is defined as a difference between the total mass of all nucleons and the mass of nucleus (M_A):

$$E_B = [Z \cdot M_p + (A - Z) \cdot M_n - M_A] \cdot c^2 \tag{2.61}$$

The average value of E_B per nucleon is equal $7-9$ MeV. In NuWro E_B is controlled by the *kaskada_w* parameter (7 MeV by default).

According to Heisenberg's uncertainty principle, an elementary phase-space volume for a single particle is equal $h^3 = (2\pi\hbar)^3$. The number of particles in a phase space can be estimated as:

$$n = \frac{\int\int \mathrm{d}^3 r \mathrm{d}^3 p}{(2\pi\hbar)^3} \tag{2.62}$$

Assuming constant nuclear density, nucleus can be treated as a sphere with a radius $R = r_0 A^{1/3}$, where $r_0 = 1.25 \pm 0.20$ fm and A is atomic mass number. Nucleons occupy energy states from a sphere in momentum space, called Fermi sphere, with a radius being the Fermi momentum p_F. Taking into account that each energy state can be filled by two nucleons with the same isospin, one can obtain the relation between atomic numbers and Fermi momentum for protons and neutrons[7]:

$$\begin{aligned} p_F^{(p)} &= \left(\frac{9\pi Z}{4A}\right)^{1/3} \frac{\hbar}{r_0} \approx 310 \pm 50 \cdot \left(\frac{A}{Z}\right)^{1/3} \text{ MeV/c} \\ p_F^{(n)} &= \left(\frac{9\pi (A-Z)}{4A}\right)^{1/3} \frac{\hbar}{r_0} \approx 310 \pm 50 \cdot \left(\frac{A-Z}{A}\right)^{1/3} \text{ MeV/c} \end{aligned} \tag{2.63}$$

For nuclei with $Z = A/2$, one gets $p_F \approx 246 \pm 40$ MeV/c. This estimation is in quite good agreement with experimental data (see Tab. 2.1).

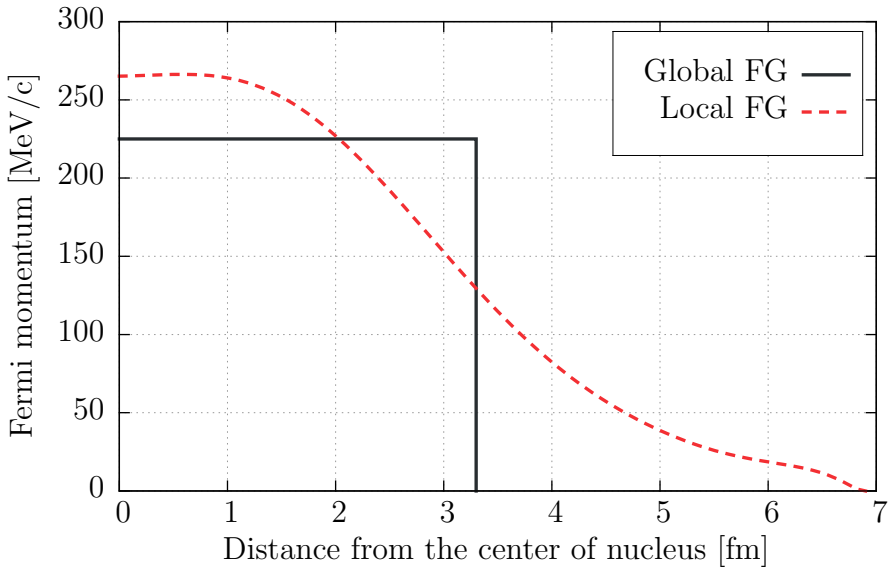

Figure 2.10: The comparison of the Fermi momentum for global and local Fermi gas in the case of carbon.

2.3.1.1 Local Fermi gas

So far, the nucleus was defined as a perfect sphere with a constant nuclear density. As a consequence, the nuclear binding potential and Fermi level are constant in the whole nucleus. The FG model, based on this assumptions, is called global Fermi gas.

The alternative way to describe the nucleus in the FG picture is to use local density approximation (LDA) (Refs. [85], [86]). In this approach nuclear matter density is described by the distribution $\rho(r)$, known from the electron scattering data (Ref. [27]), and, accordingly, it affects the binding potential, and so the Fermi level. The FG model, based on the LDA, is called local Fermi gas (LFG).

The local Fermi momentum is assumed to depend on $\rho(r)$ (where r is a distance from the center of the nucleus) in the following way:

$$\begin{aligned} p_F^{(p)}(r) &= \hbar \left((3\pi^2 \rho(r) \frac{Z}{A} \right)^{1/3} \\ p_F^{(n)}(r) &= \hbar \left(3\pi^2 \rho(r) \frac{A-Z}{A} \right)^{1/3} \end{aligned} \tag{2.64}$$

Note, that in the case of constant density the distribution $\rho(r) = A \left(\frac{4}{3}\pi R^3\right)^{-1}$ and above equations simplify to Eq. 2.63. The comparison of local Fermi momentum for

[7] The errors are taken from the calculation with extreme values of r_0

global and local FG is presented in Fig. 2.10.

Using the local instead of global Fermi gas model affects the final state nucleons energy distribution (Ref. [87]). It may have also an influence on inclusive cross sections, due to Pauli blocking effect (see Subsec. 2.3.3).

2.3.2 Spectral function

The Fermi gas model is still used in many analysis. Despite its simplicity, it reconstructs sufficiently well many experimental data. However, it is well known from the electron scattering data, that NN interactions significantly affects the nucleon momentum distribution inside nucleus (see e.g. Ref. [88] or [89]). Spectral function, based on shell-model with SRC included, gives more accurate description of nuclei.

In general, SF gives the probability distribution of removing a nucleon with the momentum $\vec{p}$ and leaving the residual nucleus with the excitation energy E. It can be expressed by the following equation[8]:

$$P(\vec{p}, E) = \sum_n \left| \left\langle \Psi_n^{A-1} \right| a_p \left| \Psi_0^A \right\rangle \right|^2 \delta\left(E + E_0 - E_n\right) \tag{2.65}$$

where Ψ_0^A is the initial state of A nucleons with energy E_0 and a_p is the annihilation operator. SF is sum over all possible final states of $A-1$ nucleons Ψ_n^{A-1}. The integration over removal energy E leads to the nucleon momentum distribution:

$$\begin{aligned} \int P(\vec{p}, E)\mathrm{d}E &= \int \mathrm{d}E \sum_n \left\langle \Psi_0^A \right| a_{p'}^\dagger \left| \Psi_n^{A-1} \right\rangle \left\langle \Psi_n^{A-1} \right| a_p \left| \Psi_0^A \right\rangle \delta\left(E + E_0 - E_n\right) \\ &= \left\langle \Psi_0^A \right| a_p^\dagger a_p \left| \Psi_0^A \right\rangle = n(\vec{p}) \end{aligned} \tag{2.66}$$

where $n(\vec{p})$ is normalized to the number of nucleons:

$$\int n(\vec{p})\mathrm{d}^3p = A \tag{2.67}$$

The study of (e, e'), $(e, e'p)$ and $(e, e'pN)$ data suggests, that about 80% of interactions occur on a single nucleon moving in a mean field potential (see e.g. Ref. [70]). However, one out of five processes happens on a correlated nucleon (via SRC). The second nucleon, usually with opposite isospin, is a spectator, but it can also be knocked-out from the nucleus. Commonly, one introduces mean field and correlation

[8] In general, one needs separate spectral functions for protons and neutrons. To simplify notations the isospin index is skipped.

parts for spectral function:

$$P(\vec{p}, E) = P_{MF}(\vec{p}, E) + P_{corr}(\vec{p}, E) \tag{2.68}$$

2.3.2.1 Mean field part

In the case of independent nucleons, moving in a mean field potential, within the shell model picture, spectral function (Eq. 2.65) simplifies to:

$$P_{SM}(\vec{p}, E) = \sum_n |\phi_n(\vec{p})|^2 \, \delta\left(E - E_n\right) \tag{2.69}$$

where sum is over all occupied states from Fermi sea. ϕ_n is the momentum-space wave function (normalized to 1) associated with the single particle shell model state n.

Measurements of the energy spectrum of knock-out nucleons (by electrons or hadrons) indicate, that the independent particle model does not describe properly nuclear dynamics. In fact, nucleon correlations, induced by strong forces, modify shell orbits and give a rise to nucleons with momenta above Fermi level. The realistic theoretical calculation of nuclear dynamics can be done within non-relativistic many body theory with two- and three-nucleon interaction potentials. However, it is impossible to find exactly the wave function, so the results are combined with experimental data.

Spectral function part, corresponding to the removal of nucleon from the shell model, can be parametrized in the following way (Ref. [90]):

$$P_{MF}(\vec{p}, E) = \sum_n Z_n \, |\phi_n(\vec{p})|^2 \, F_n\left(E - E_n\right) \tag{2.70}$$

where the F_n function is the width of n shell state (e.g. Gaussian or Breit-Wigner distribution) and $Z_n < 1$ is called spectroscopic factor, which normalizes the nth state. Z_n factors are obtained from the normalization requirement:

$$\int \mathrm{d}^3 p \mathrm{d}E P(\vec{p}, E) = 1 \tag{2.71}$$

2.3.2.2 Correlation part

It is known from the studies of knock-out protons by electrons (Ref. [91]) or protons (Ref. [92]), that correlations, which produce pairs of nucleons with relative large momenta (with opposite directions), dominate among all SRC. Moreover, these are pairs of nucleons with opposite isospin (Ref. [93]). Therefore, SRC give a rise to high-momentum

tail in the nucleon momentum distribution (see Fig. 2.13a). The impact of this tail on the results is discussed in Subsec. 2.3.4.

The estimation of the correlation part of spectral function can be done in local density approximation:

$$P_{corr}(\vec{p}, E) = \int \mathrm{d}^3 r \rho_A(\vec{r}) P^{NM}_{corr}(\vec{p}, E; \rho = \rho_A(\vec{r})) \tag{2.72}$$

where ρ_A is the nuclear density distribution and P^{NM}_{corr} is the correlation part of spectral function of uniform nuclear matter at density ρ. The calculation of P^{NM}_{corr} can be found in Ref. [94].

2.3.2.2.1 SRC and two-body current

Including SRC in one-body current interactions leads to $2p2h$ final states, which can interfere with the ones produced via two-body current (Subsec. 2.2.5). In general, the probability of a transition from an initial state of A nucleons $|i\rangle$ to one of possible final state $|f\rangle$ is given by the following formula:

$$P = \sum_f \left| \langle f | \hat{J} | i \rangle \right|^2 \tag{2.73}$$

where $\hat{J}$ is the nuclear electroweak current and the P is summed up over all the possible final states. When one- and two-body current contributions are taken into account, $\hat{J}$ can be expressed as the sum of them $\hat{J} = \hat{J}_{1p1h} + \hat{J}_{2p2h}$ and the probability reads:

$$\begin{aligned} P &= \sum_f \left| \langle f | \hat{J}_{1p1h} | i \rangle \right|^2 + \sum_f \left| \langle f | \hat{J}_{2p2h} | i \rangle \right|^2 && (2.74) \\ &+ \sum_f \langle i | \hat{J}_{1p1h} | f \rangle \langle f | \hat{J}_{2p2h} | i \rangle + \sum_f \langle i | \hat{J}_{2p2h} | f \rangle \langle f | \hat{J}_{1p1h} | i \rangle && (2.75) \end{aligned}$$

Without SRC one-body current reaction leads to a final states of $(A-1)$ spectators and one knock-out nucleon with four-momentum p:

$$|f\rangle_{1p1h} = |A-1\rangle \otimes |p\rangle \tag{2.76}$$

while interactions via two-body current produce a final states of $(A-2)$ spectators and two knock-out nucleons with four-momenta p and p':

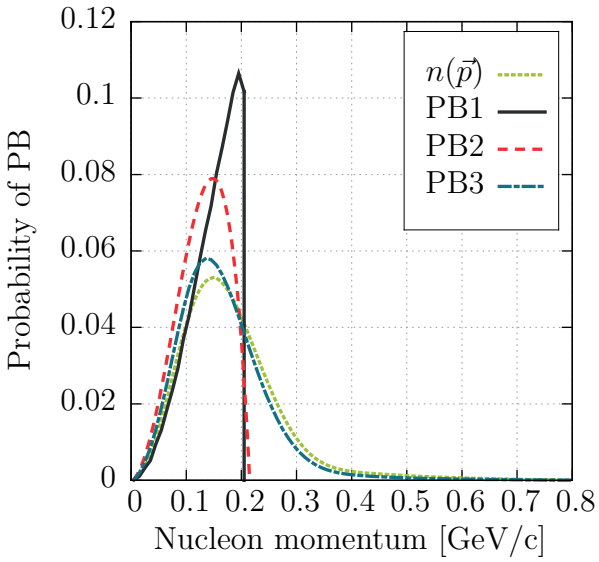

(a) The probability of Pauli blocking as a function of the initial nucleon momentum distribution $n(\vec{p})$.

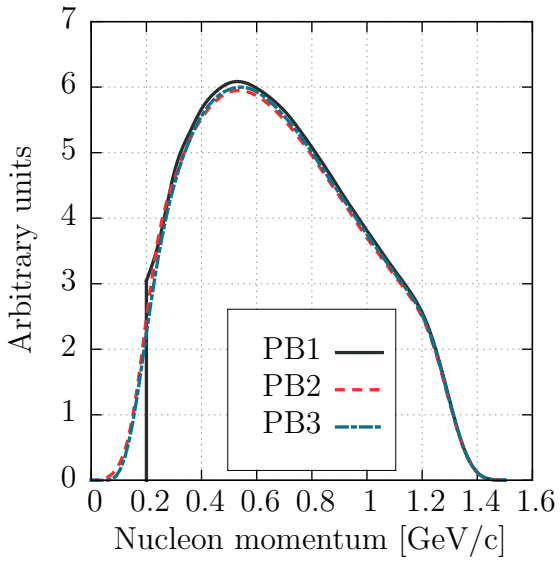

(b) The final nucleon momentum distribution in the case of QEL scattering off carbon ($E_\nu = 1$ GeV).

Figure 2.11: The comparison of different approaches to Pauli blocking for spectral function.

$$|f\rangle_{2p2h} = |A-2\rangle \otimes |p\rangle \otimes |p'\rangle \tag{2.77}$$

The contraction of $|f\rangle_{1p1h}$ and $|f\rangle_{2p2h}$ vanishes and there is no interference terms in Eq. 2.75. However, one-body current interactions on correlated nucleons lead to $2p2h$ final states:

$$|f\rangle_{1p1h+SRC} = |A-1\rangle \otimes |p\rangle + |A-2\rangle \otimes |p\rangle \otimes |p'\rangle \tag{2.78}$$

giving a rise to the interference between one- and two-body currents, which is not included in current models. The size of the effect is now extensively studied (see e.g. Refs. [95, 96]).

2.3.3 Pauli blocking

Pauli principle forbids fermions to be in the same quantum state. As a consequence, interactions leading to a final nucleon in already occupied state are not allowed. The effect is called Pauli blocking.

In the Fermi gas model all states up to Fermi level are occupied. In this case PB

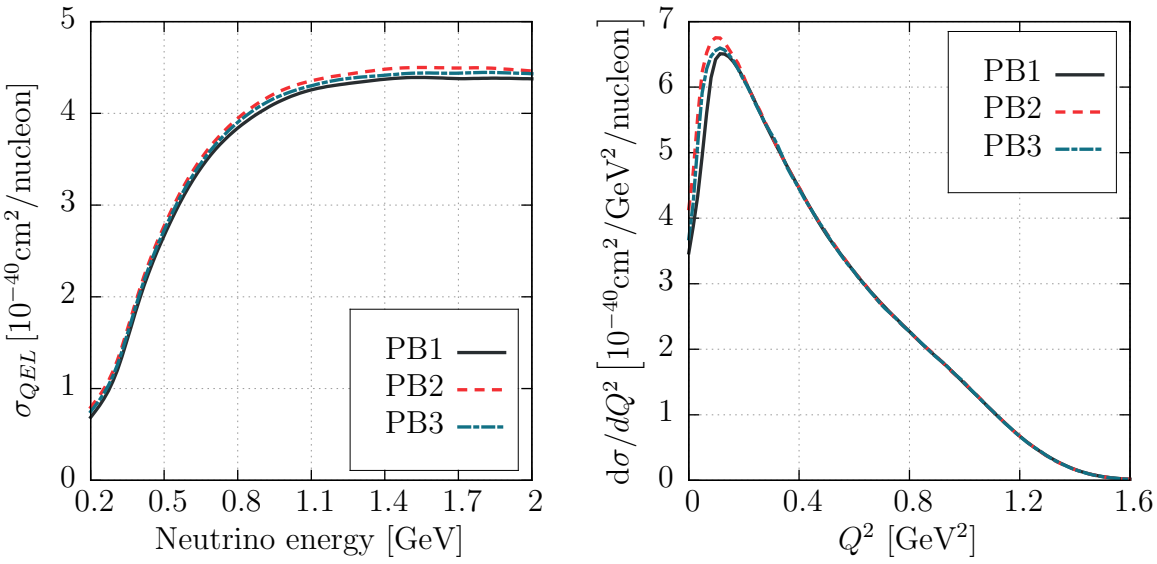

(a) The total cross section.

(b) The differential cross section (E_ν = 1 GeV).

Figure 2.12: The total and differential cross sections for QEL scattering off carbon obtained using different approaches to PB for spectral function.

means that the cross section for all interactions with a final state nucleon with a momentum smaller than p_F is equal to zero. There is a significant difference between PB in FG and LFG. The latter one has a Fermi level, which depends on the nuclear density, so the effect of PB is larger around the center of a nucleus than at the edge.

2.3.3.1 Pauli blocking for spectral function

In the case of spectral function not all states up to Fermi level are occupied, so it is not obvious how to apply Pauli blocking. Usually one calculates the average Fermi momentum $\tilde{p}_F$ and modifies spectral function as following (PB1):

$$P(\vec{p}, E) \rightarrow \Theta(\tilde{p}_F - |\vec{p}_{final}|)P(\vec{p}, E) \tag{2.79}$$

The disadvantage of this approach is an unphysical cut for low energy final state nucleons (see Fig. 2.11). It may be revised by using local Fermi momentum instead of the average one (PB2):

$$P(\vec{p}, E) \rightarrow \Theta(p_F(r) - |\vec{p}_{final}|)P(\vec{p}, E) \tag{2.80}$$

The alternative way is to look at the momentum distribution (Eq. 2.66) and use the

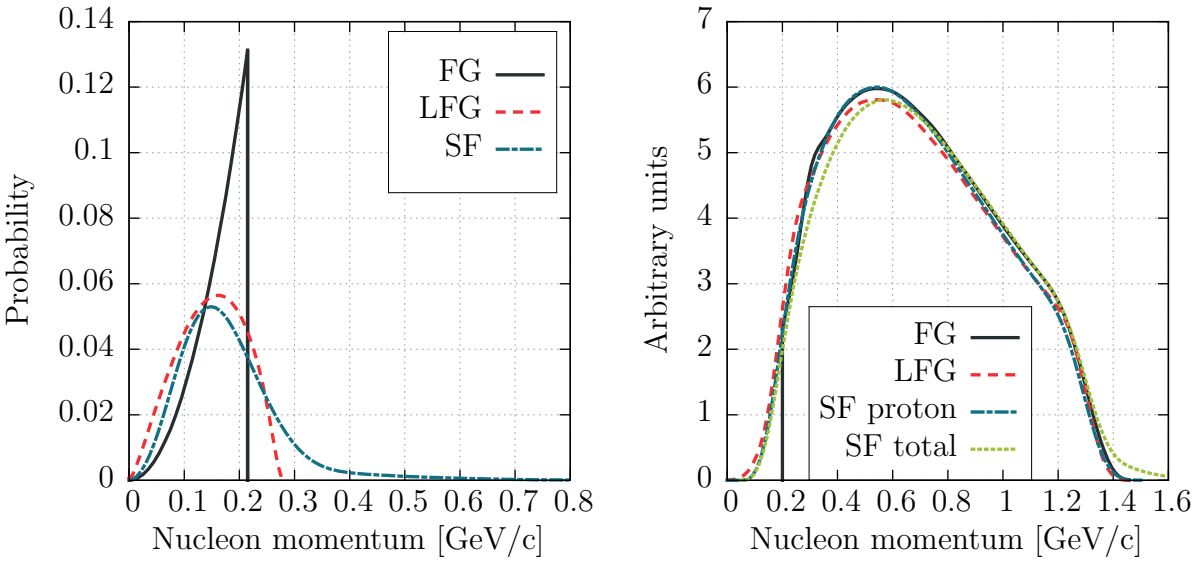

(a) The initial nucleon momentum distribution $n(\vec{p})$.

(b) The final nucleon momentum distribution for QEL scattering off carbon ($E_\nu = 1$ GeV).

Figure 2.13: The comparison of nucleon momentum distributions for spectral function and Fermi gas models.

Monte Carlo method to decide if the chosen momentum is already occupied (PB3):

$$P(\vec{p}, E) \to \Theta(n(\vec{p}_{final}) - \text{random}[0,1])P(\vec{p}, E) \tag{2.81}$$

Intuitively, the distribution of final nucleons momenta for blocked events should more or less reconstruct $n(\vec{p})$ (Eq. 2.66). As shown in Fig. 2.11a this is only true in the case of the last PB model. Using global Fermi momentum produces an unphysical cut for low energy final nucleons (see Fig. 2.11b), while two other models give a smooth tail in the low momenta region. The choice of the approach for Pauli blocking does not affect the cross section in a significant way though (see Fig. 2.12).

2.3.4 Summary

Short-range correlations produce pairs of high energetic nucleons (usually with opposite isospins), absent in the Fermi gas picture. In Fig. 2.13a a probability of finding a nucleon with given momentum for spectral function, local and global Fermi gas is shown. In the case of FG there is an unphysical cut for a momentum higher than p_F. If LDA is applied, the probability distribution is closer to the one obtained by spectral function. However, the high-momentum tail is still missing. The influence of choosing the model

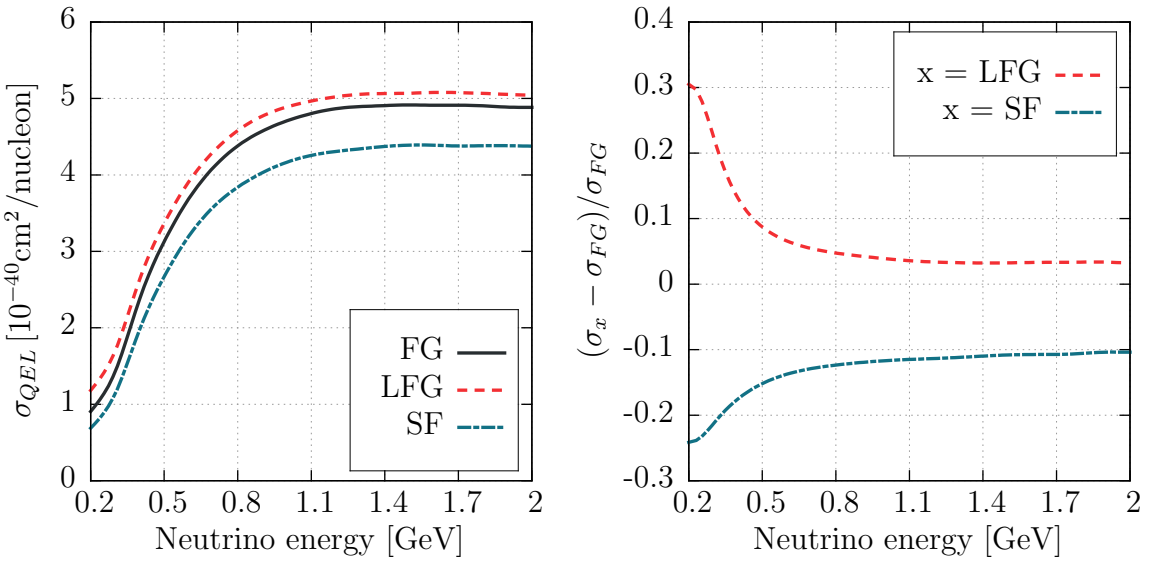

(a) The total cross section.

(b) The ratio of LFG and SF to FG cross sections.

Figure 2.14: The total cross section for QEL scattering off carbon obtained using spectral function and Fermi gas models ($M_A = 1.2$ GeV).

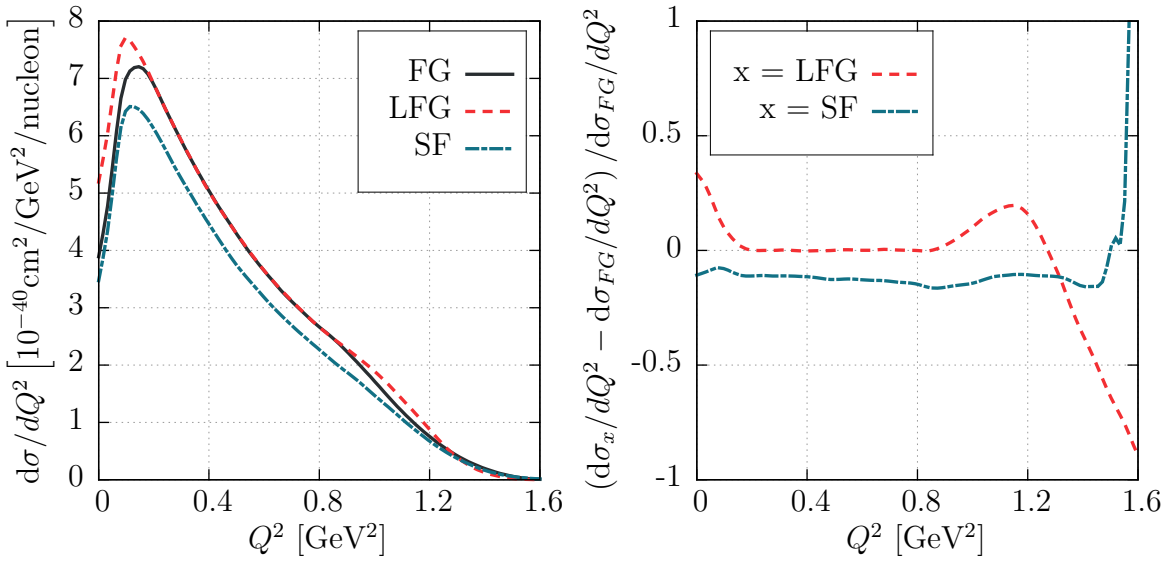

(a) The differential cross section.

(b) The ratio of LFG and SF to FG differential cross sections.

Figure 2.15: The differential cross section for QEL scattering off carbon for neutrino energy $E_\nu = 1$ GeV obtained using spectral function and Fermi gas models ($M_A = 1.2$ GeV).

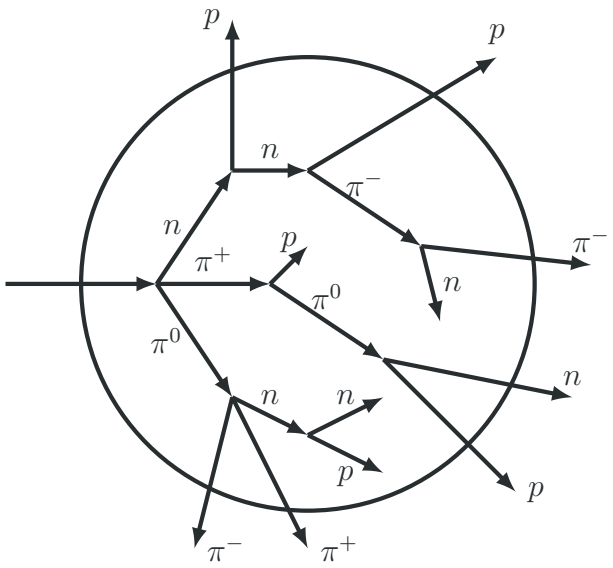

Figure 2.16: Possible scenario of final state interactions.

on the final proton momentum is negligible (see Fig. 2.13b). However, if one looks also at correlated nucleon (in the case of SF), the total momentum distribution of all final state nucleons is shifted to the higher energies.

Usually, in MC generators Fermi gas is used. It is well known from electron scattering data that cross section predictions obtained using spectral function are much closer to the data (see e.g. Ref. [90]). For many purposes FG is a good approximation. However, one must be aware that it affects significantly the cross section prediction (see Fig. 2.14). For the neutrino energy $E_\nu \sim 1$ GeV the difference is about 10%. The disagreement between global and local FG models is caused by the Pauli blocking - the effect of PB is lower for LFG. Besides the normalization, the shape of the differential cross section is also affected around the pick (see Fig. 2.15), but in this region IA is doubtful anyway. There is also a disagreement at high Q^2.

2.4 Final state interactions

Final state interactions describe the propagation of particles created in the primary vertex through the nuclear matter (see Fig. 2.16). It is necessary, when one assumes Impulse Approximation. Secondary processes affect observed distributions (only particles which left the nucleus are visible in a detector). A good control of FSI effects is needed to analyze experimental data.

In NuWro FSI are described in terms of the intranuclear cascade (INC) model (Ref. [97, 98]), used in most of MC generators. Note, that the alternative approach is proposed

in GIBUU (Ref. [99]). FSI are performed by solving the Boltzmann-Uehling-Uhlenbeck equation.

The general scheme of the INC model in NuWro is described in Subsec. 2.4.1. The details of nucleon and pion cascade models can be found in Subsecs 2.4.2 and 2.4.3. The last subsection (2.4.4) is devoted to the formation zone effect.

2.4.1 Intranuclear cascade algorithm

In the intranuclear cascade model particles are assumed to be classical and move along straight lines between collisions. In general, the probability of passing a distance λ (small enough to assume constant nuclear density ρ) without any interaction with a nucleon is given by:

$$P(\lambda) = e^{-\lambda/\tilde{\lambda}} \tag{2.82}$$

where $\tilde{\lambda} = (\sigma\rho)^{-1}$ is the mean free path and σ - the total cross section. The problem of a propagation through nuclear matter is difficult to solve analytically, because ρ is changing during the path of a particle. However, it is easy to handle using Monte Carlo methods.

The NuWro algorithm for INC is presented in Fig. 2.17. Before the main loop starts, formation zone (see Subsec. 2.4.4) can be applied for all hadrons from the primary vertex. During the procedure all particles are stored in a queue. The cascade loop is stopped when the queue is empty or there are no more nucleons inside a nucleus.

In each step of the loop the mean free path of the particle is calculated from:

$$\tilde{\lambda} = [\sigma_p\rho_p(r) + \sigma_n\rho_n(r)]^{-1} \tag{2.83}$$

where indexes p and n refer to proton and neutron, respectively, r is the distance from the center of a nucleus. The free path λ is calculated from Eq. 2.82 using MC methods and assuming constant nuclear density:

$$\lambda = -\tilde{\lambda} \cdot \ln(\text{rand}[0,1]) \tag{2.84}$$

To satisfy the assumption of constant ρ, the nuclear density is probed in intervals not exceeding λ_{max} (defined by *step* parameter from *params.txt*, 0.2 fm by default, see App. A). It means, that the particle is always propagated by the distance $\min(\lambda, \lambda_{max})$ and the interaction happens only if $\lambda < \lambda_{max}$. Numerous tests show, that further decreasing λ_{max} does not affect final results.

The particle are assumed to be outside the nucleus if their distance from the center is larger then R. In the case of global Fermi gas $R = r_0 A^{1/3}$ with $r_0 = 1.25$ fm. For local Fermi gas R is defined as the distance from the center, where the density is smaller by factor of 10^6 than the maximum one. When nucleons leave nucleus, the nuclear potential (V) is subtracted from their kinetic energy (E_k). If it is not possible ($E_k < V$), they are assumed to be absorbed.

If the interaction happens, the choice of the type of the process (i) is done using Monte Carlo methods based on the cross sections ratio: if rand$[0, 1] < \sigma_i/\sigma_{total}$, the ith kind of the interaction is assumed to have happened. The target nucleon momentum is set randomly from the Fermi ball and the kinematics is generated.

If Pauli blocking occurs, the interaction is withdrawn and the particle is reinserted to the queue. In the other case all final particles are put to the queue and the nuclear matter density is reduced (but the shape of the density profile is assumed to be unchanged).

2.4.2 Nucleon cascade

The nucleons cascade model is based on Ref. [97, 98]. Elastic scattering, single and double pion production processes are considered. The total cross section (σ) is extracted from available experimental data. The fraction of pion production processes is described by f_{inel} parameters, while f_π gives a contribution coming from single pion production to all inelastic scattering interactions. The numbers adopted in NuWro are presented in Tab. 2.2. Between energy points the parameters are assumed to be constant and the cross section is assumed to change in a linear manner. For kinetic energies lower than 335 MeV the following formulas are used:

$$\sigma_{ii} = \left(\frac{10.63}{\beta^2} - \frac{29.92}{\beta} + 42.9\right) \text{ [mb]} \tag{2.85}$$

$$\sigma_{ij} = \left(\frac{34.10}{\beta^2} - \frac{82.20}{\beta} + 82.2\right) \text{ [mb]} \tag{2.86}$$

where β is the particle velocity in the units of velocity of light, ii (ij) denotes the interaction with nucleon with the same (opposite) isospin. For energies above 3900 MeV the cross section is assumed to be constant.

The procedure for choosing the type of the interaction is presented in Fig. 2.18. At the beginning the relative kinetic energy to a nucleon from nucleus is introduced to obtain effective scattering parameters. A decision about the interaction type is made using MC method. If the chosen inelastic process cannot be done (because of insufficient

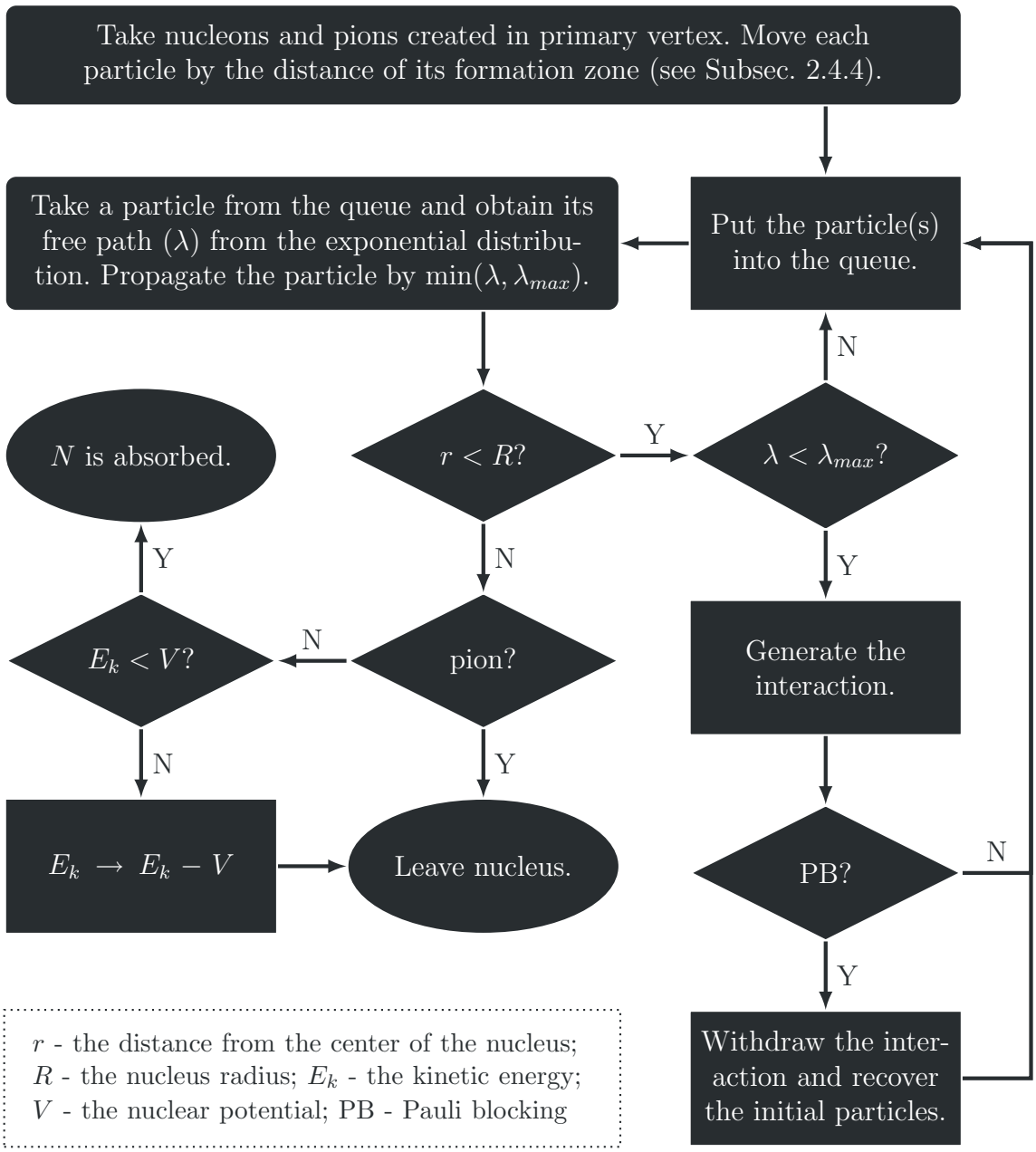

Figure 2.17: A block diagram of the NuWro INC algorithm.

amount of energy), the "less" inelastic one is proceeded.

In the single pion production channel, neutral pions are assumed to be produced in 11% of events in the case of ii interaction and 43% for ij. In double pion production, 60% of cases is taken as producing two π^0 and 20% for a $\pi^+\pi^-$ combination.

For all processes the kinematics of final state particle is obtained in the center-of-mass system (CMS), followed by the boost to the laboratory frame. In the case of elastic scattering the angular distribution is given by the following formula:

T_k [MeV]	335	410	510	660	840	1160	1780	3900
σ_{ii} [mb]	24.5	26.4	30.4	41.2	47.2	48.0	44.2	41.0
σ_{ij} [mb]	33.0	34.0	35.1	36.5	37.9	40.2	42.7	42.0
f_{inel}^{ii}	0.07	0.20	0.31	0.43	0.58	0.65	0.69	0.69
f_{inel}^{ij}	0.04	0.07	0.15	0.27	0.37	0.36	0.35	0.35
f_π	1.0	1.0	1.0	1.0	0.97	0.80	0.44	0.44
A_{ii}	0.1	0.9	2.7	9.0	14.3	19.2	∞	∞
B_{ii}	0	0	0	0	0	0	0	0
A_{ij}	2.2	1.8	2.3	8.8	15.0	29.4	∞	∞
B_{ij}	-1.0	-1.1	-0.7	-0.2	0	0	0	0

Table 2.2: Total cross section (σ) for nucleon-nucleon collisions, parameters used for inelastic processes (f_{inel} and f_π) and coefficients for the angular distribution (A and B). T_k stands for the nucleon kinetic energy. ii (ij) denotes the interaction on a nucleon with the same (opposite) isospin.

$$\frac{\mathrm{d}\sigma}{\mathrm{d}\Omega} \sim A\cos^4\theta + B\cos^3\theta + 1 \tag{2.87}$$

where values A and B are fit to the experimental data. For inelastic processes momenta are distributed uniformly.

Nucleons propagated through nuclear matter are assumed to be on-shell. The Pauli blocking effect is included as described in Subsec. 2.3.3. The effective nuclear potential is introduced as a sum of binding and Fermi energy (see Fig. 2.9):

$$V(r) = E_F(r) + E_B \tag{2.88}$$

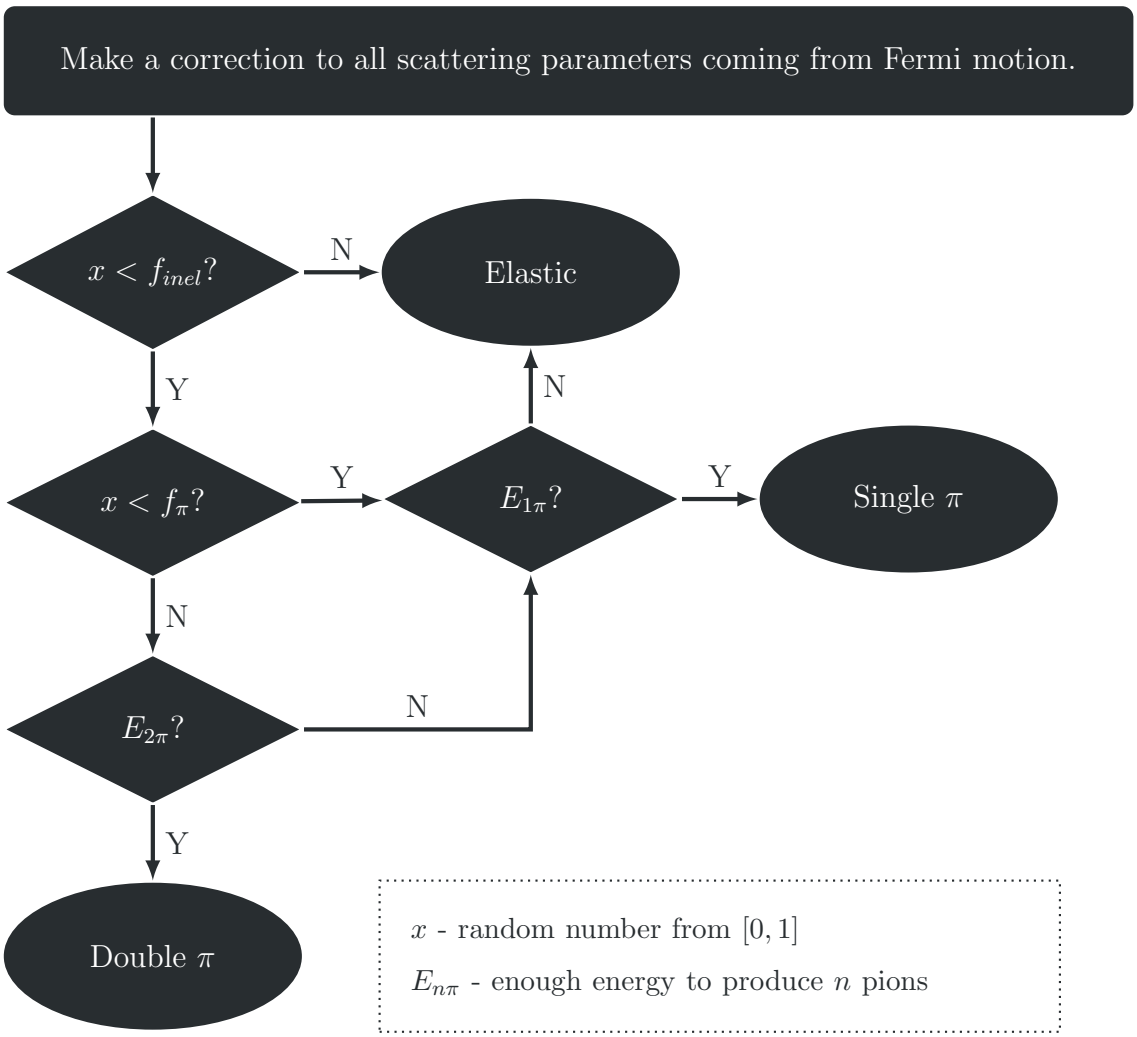

Figure 2.18: A block diagram of the algorithm for "Generate the interaction" from Fig. 2.17 in the case of nucleon-nucleon scattering.

2.4.2.1 Modification of Metropolis et al. model

New parametrization of the f_{inel} and f_π parameters from Tab. 2.2 is introduced in NuWro, based on experimental data[9]. f_π is now given separately for ii and ij scattering types. The changes are done for high energy bins, as presented in Tab. 2.3. All other parameters are unchanged.

Recently, the in medium modification of the NN cross section, based on Ref. [100], was introduced.

T_k [MeV]	660	840	1160	1780	2500
f_{inel}^{ii}	0.43	0.48	0.51	0.62	0.70
f_{inel}^{ij}	0.37	0.37	0.51	0.55	0.65
f_{π}^{ii}	1	1	0.90	0.73	0.50
f_{π}^{ij}	1	0.87	0.55	0.46	0.30

Table 2.3: The modification of the original Metropolis et al. parameters from Fig. 2.2.

2.4.2.2 Results

The results of nucleon INC in the case of scattering off carbon are presented in Fig. 2.19. In Fig. 2.19a there is the prediction for the total cross section together with contributions coming from different channels: events without any pion, with one or two pions in the final state. Please note, that the result may be affected by the pion cascade, described in details in Subsec. 2.4.3. In Fig. 2.19b the angular distributions in the case of elastic scattering are presented for different incident nucleon energy ranges.

2.4.3 Pion cascade

Final state interactions of pions are essential in the analysis of neutrino data. For the energies around 1 GeV there is a significant contribution coming from resonance pion production processes (see Fig. 2.1). If the pion is absorbed in the nuclear matter, the event is indistinguishable from elastic scattering (very important in the oscillation analysis). To estimate this background, it is necessary to have a good theoretical model for both, pion production in the primary vertex and FSI.

There are two models of the pions cascade in NuWro. The first one is taken from Ref. [97, 98]. The second one (default) uses a microscopic calculation done in Ref. [101] for low energy pions and a phenomenological approach for the higher energies.

2.4.3.1 Metropolis et al. model

The following interaction types are considered in the model:

- elastic scattering;

[9] The original Metropolis et al. table can be still used, if *xsec = 0* is selected (see App. A for details).

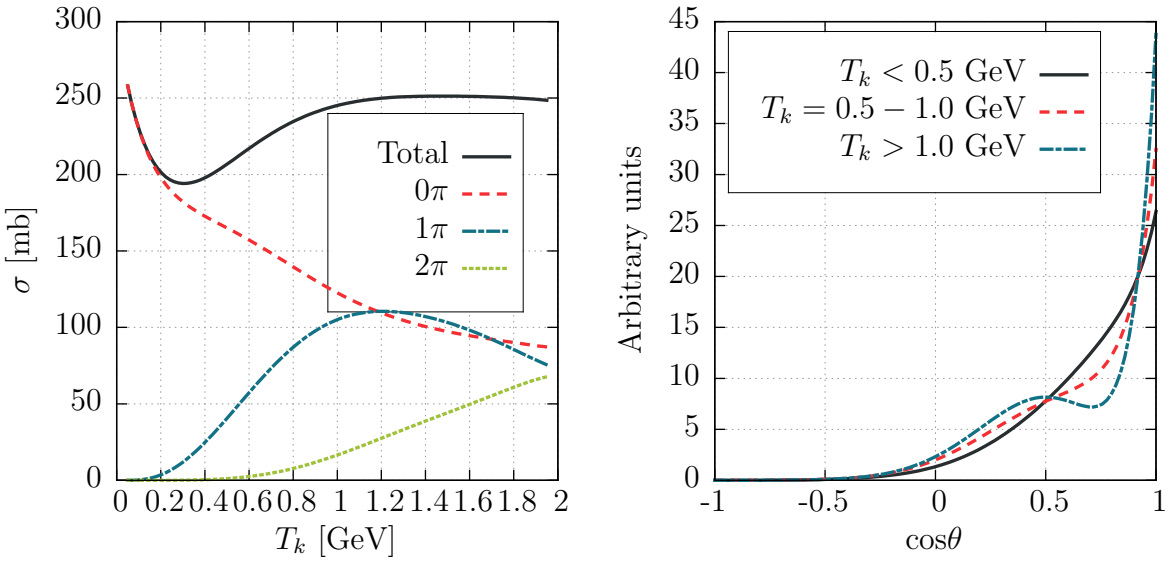

(a) The total cross section together with contributions coming from events with 0, 1, or 2 pions in the final state.

(b) The scattering angle (θ) distribution in LAB frame for elastic scattering. Results are normalized to the same area.

Figure 2.19: The total cross section and the scattering angle distribution for proton-carbon scattering.

- charge exchange (CEX);
- single and double pion production;
- absorption.

Parameters used in the model can be found in Tabs 2.4 and 2.5. σ_{ii} is the cross section (excluding absorption processes) for $\pi^+ p$ or $\pi^- n$ scattering, while σ_{ij} for $\pi^+ n$ and $\pi^- p$. The cross section for π^0-nucleon collisions is taken to be an average: $\sigma_0 = \frac{1}{2}(\sigma_{ii} + \sigma_{ij})$. The effective absorption cross section for ij channel is σ_{abs}, while for π^0 mesons is assumed to be $\frac{1}{2}\sigma_{abs}$. The cross section is assumed to change between energy points in a linear manner. For pion kinetic energies lower than 49 MeV the following formulas are used:

$$\sigma_{ii} = 3.7 + 286\,(\gamma - 1)^3 \quad (2.89)$$

$$\sigma_{ij} = 6.5 + 23.9\,(\gamma - 1) \quad (2.90)$$

$$\sigma_{abs} = 16.4\left(0.14 + \eta^2\right)/\eta \quad (2.91)$$

T_k [MeV]	49	85	128	184	250	350	540	1300
σ_{ii} [mb]	16	50	114	200	110	51	20	30
σ_{ij} [mb]	15	21	43	66	44	23	22	30
σ_{abs} [mb]	20	32	45	36	18	0	0	0
f^{ii}_{inel}	0	0	0	0.03	0.06	0.16	0.30	0.88
f^{ii}_{CEX}	0	0	0	0	0	0	0	0
f^{ij}_{inel}	0.45	0.57	0.62	0.64	0.62	0.56	0.58	0.94
f^{ij}_{CEX}	1.0	1.0	1.0	0.95	0.89	0.72	0.51	0.06
f^{0}_{inel}	0.42	0.36	0.36	0.37	0.40	0.50	0.59	0.94
f^{0}_{CEX}	1.0	1.0	1.0	0.90	0.84	0.67	0.50	0.05
f_{π}	1.0	1.0	1.0	1.0	1.0	0.98	0.91	0.24
A_{ii}	3.2	2.2	1.9	2.2	2.6	3.0	3.0	3.0
B_{ii}	-1.8	-2.1	-1.5	-0.3	2.0	4.0	4.0	4.0
A_{ij}	1.1	1.9	2.2	2.2	2.0	2.7	3.0	3.0
B_{ij}	0.8	0.7	0.8	1.0	1.4	2.6	3.6	4.0
A_0	3.4	2.1	1.9	2.1	2.5	3.0	3.0	3.0
B_0	-1.8	-2.0	-1.4	0	1.7	4.0	4.0	4.0

Table 2.4: Cross section (σ) for pion-nucleon scattering, parameters used for inelastic processes (f_{inel}, f_{CEX} and f_{π}) and coefficients for the angular distribution (A and B). T_k stands for the pion kinetic energy. ii (ij) denotes π^+p and π^-n (π^+n and π^-p) scattering. Index 0 is for neutral pion interactions.

where γ is the total energy in units of $m_{\pi^0}c^2$ and η is momentum in units of $m_{\pi^0}c$. For the energies above 1300 MeV the cross section is assumed to be constant.

Collision type	ii	ij	0	CEX
A	2.5	2.5	3.0	1.5
B	-3.5	3.5	-2.0	-2.5

Table 2.5: Coefficients for the angular distribution of pion-nucleon interactions below 51 MeV.

A fraction of inelastic processes (including CEX) is described by f_{inel} parameter. f_{CEX} gives the fraction of inelastic events that are charge exchange. A fraction of single pion production among all pion production processes is defined by f_{π}.

Fig. 2.20 presents the interaction type selection algorithm. The procedure starts with calculating a relative velocity of an incident particle respect to a target nucleon. Then, the effective cross sections and parameters are established. The scattering type is chosen using MC methods. If a process cannot be done for kinematics reasons, the next one is tried.

In the single pion production channel, neutral pions are assumed to be produced in 55% of events in the case of ii type and 45% for ij and π^0 collisions. In double pion production, 18.75% of cases is taken as producing of two π^0, and 6.25% of a $\pi^+\pi^-$ combination.

The angular distribution in CMS for elastic and charge exchange scattering is defined by Eq. 2.87. For energies above 49 MeV the coefficients A and B for CEX are assumed to be the same as for ii scattering type. For other processes momenta are distributed uniformly in CMS.

2.4.3.2 Oset et al. model

This model describes pion-nucleon interactions in the pion kinetic energy range $T_k = 85 - 350$ MeV. Quasi-elastic scattering, charge exchange processes and pion absorption are considered. The calculations are based on Ref. [102], where the pion-nucleon optical potential (V_{opt}) coming from the p-wave contribution in infinite nuclear matter is calculated. Additionally, the s-wave contribution and the modification of Δ width in nuclear medium (by the Δ self-energy) are considered. The finite range effects are introduced by using local density approximation.

Oset et al. model is also used in NEUT. It was later modified by the parameters, tuned to the experimental data (Ref. [103]).

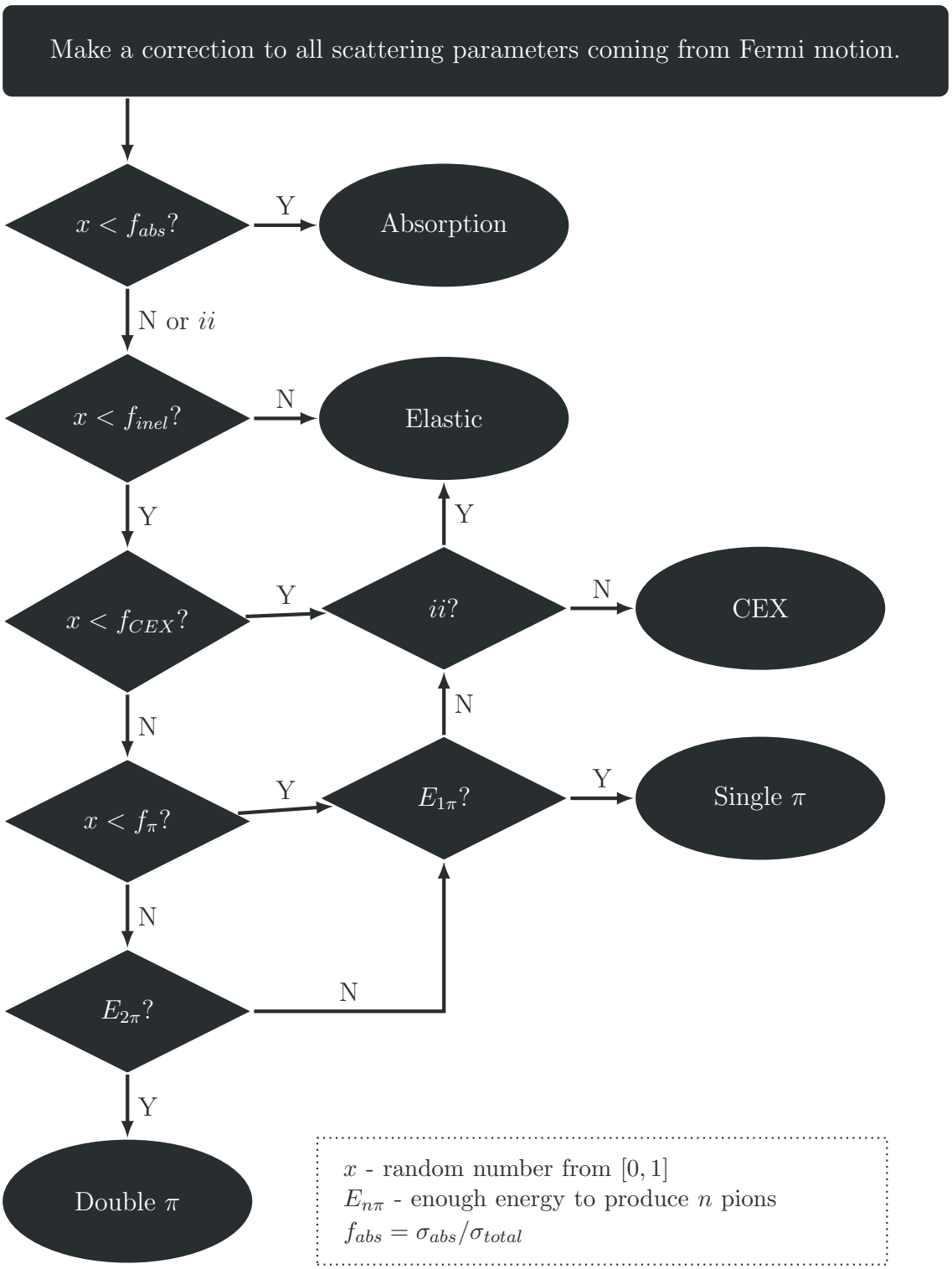

Figure 2.20: A block diagram of the algorithm for "Generate the interaction" from Fig. 2.17 in the case of pion-nucleon scattering.

2.4.3.2.1 Quasi-elastic and charge exchange scattering

In general, the probability per unit time for $\pi^{\lambda}N \rightarrow \pi^{\lambda'}N$ ($\lambda = 1, 0, -1$ for π^+, π^0, π^- respectively) can be expressed in the following form:

$$P_{\lambda\lambda'} = \frac{1}{9}P \begin{pmatrix} 5-4\chi & 1-\chi & 0 \\ 1+\chi & 4 & 1-\chi \\ 0 & 1+\chi & 5+4\chi \end{pmatrix} \tag{2.92}$$

where $\chi = (N-Z)/A$ and P is given by

$$P = \frac{1}{E}\int \frac{\mathrm{d}^3k}{(2\pi)^3} n(\vec{k}) \frac{2}{3} \left(\frac{f^*}{m_\pi}\right)^2 |\vec{p}_{CMS}|^2 |G_\Delta(p+k)|^2 \frac{1}{2}\tilde{\Gamma}\left(p+k\right) \tag{2.93}$$

In the above equation $n(\vec{k})$ stands for the average density of protons and neutrons (normalized to $\rho = \rho_p + \rho_n$), f^* is the $\pi N\Delta$ coupling constant $f^{*2}/4\pi = 0.36$, $p = (E, \vec{p})$ is the pion four-momentum, $\vec{p}_{CMS}$ is pion momentum in center-of-mass system, G_Δ is the Δ propagator:

$$G_\Delta(p+k) = \frac{1}{\sqrt{s} - M_\Delta + \frac{1}{2}i\tilde{\Gamma}\left(p+k\right)} \tag{2.94}$$

where $s = (p+k)^2$ and $\tilde{\Gamma}$ is a reduced (due to Pauli blocking) Δ width:

$$\frac{1}{2}\tilde{\Gamma}(p+k) = \frac{1}{2}\Gamma(p+k) \times \frac{1}{4}\left(\mu^3 + \mu + 2\right) \tag{2.95}$$

$$= \frac{1}{12\pi}\left(\frac{f^*}{m_\pi}\right)^2 \frac{M}{\sqrt{s}} |\vec{p}_{CMS}|^3 \times \frac{1}{4}\left(\mu^3 + \mu + 2\right) \tag{2.96}$$

with M being the average mass of a nucleon and the μ parameter calculated to be:

$$\mu = \begin{cases} -1 & \text{if} \quad \mu^0 < -1 \\ \mu^0 & \text{if} \quad -1 \leqslant \mu^0 \leqslant 1 \\ 1 & \text{if} \quad \mu^0 > 1 \end{cases} \tag{2.97}$$

where $\mu^0 = (E_\Delta E_{CMS} - E_F\sqrt{s})/|\vec{p} + \vec{k}||\vec{p}_{CMS}|$. Setting constant $\mu = 1$ disables Pauli blocking.

2.4.3.2.2 Absorption

Absorption processes are included into the model by introducing the Δ self-energy (Σ_Δ), which modifies the Δ width in nuclear medium:

$$\frac{1}{2}\tilde{\Gamma} \rightarrow \frac{1}{2}\tilde{\Gamma} - \mathrm{Im}\,\Sigma_\Delta \tag{2.98}$$

It affects both, the probability formula (Eq. 2.93) and the Δ propagator (Eq. 2.94). Δ self-energy can be expressed in the following way:

$$\mathrm{Im}\,\Sigma_\Delta(E_\pi) = -\left[C_Q(\rho/\rho_0)^\alpha + C_{A2}(\rho/\rho_0)^\beta + C_{A3}(\rho/\rho_0)^\gamma\right] \tag{2.99}$$

where C_Q, C_{A2}, C_{A3}, α, β, γ are functions of the pion energy (their parametrization can be found in Ref. [67]), ρ is nuclear density, and ρ_0 stands for density in the center of the nucleus. C_Q corresponds to the higher order quasi-elastic cross section, but it is provided only globally (without further distinction of its source), so it is taken into account in G_Δ (Eq. 2.94), but not in the probability formula (Eq. 2.93) - to avoid the double counting. Contributions proportional to C_{A2} and C_{A3} are related to two- and three-body absorption.

Note, that the same Δ width parametrization is used in Nieves and Marteau models for two-body current interactions (Subsec. 2.2.5).

2.4.3.2.3 πN s-wave contribution

For the quasi-elastic and charge exchange scattering the effective s-wave contribution parametrization is introduced by the following formula:

$$P^{(s)}_{\lambda\lambda'} = P^{(s)} \begin{pmatrix} A - \chi B & (1-\chi)C & 0 \\ (1+\chi)C & D & (1-\chi)C \\ 0 & (1+\chi)C & A + \chi B \end{pmatrix} \tag{2.100}$$

In general, the probability per time unit is related to the cross section through the

equation:

$$P^{(s)} = \frac{|\vec{p}|}{E}\rho(\vec{r})\sigma^{(s)} \tag{2.101}$$

The coefficients A, B, C, D (dimensionless) and $\sigma^{(s)}$ (in pion mass units) are parameterized as a function of the variable $\xi \equiv \sqrt{s} - M - m_\pi$ (in pion mass units):

$$\begin{aligned}
A &= \frac{1}{2}(1+D) && (2.102)\\
C &= \frac{1}{2}(1-D) && (2.103)\\
D &= -0.03130 + 0.37062\xi - 0.08229\xi^2 && (2.104)\\
B &= 0.21972 + 0.06602\xi - 0.01866\xi^2 && (2.105)\\
\sigma^{(s)} &= 0.19753 + 0.06899\xi - 0.01334\xi^2 && (2.106)
\end{aligned}$$

This parametrization is valid in the energy range considered in the model. The s-wave contribution to the absorption probability is given by:

$$P^{(s)}_{abs} = \frac{4\pi}{E}\left(1 + \frac{E}{2M}\right)\mathrm{Im}\, B_0^{(abs)}\rho^2(\vec{r}) \tag{2.107}$$

with $\mathrm{Im}\, B_0^{(abs)} \approx 0.035 m_\pi^{-4}$.

2.4.3.2.4 The implementation

To keep the general cascade scheme used in the model described in 2.4.3.1, the Metropolis-like tables are introduced in NuWro. The σ_{ii}, σ_{ij}, σ_{abs}, f_{inel}, and f_{CEX} parameters from Tab. 2.4 are calculated based on corresponding probability formulas. Separate tables are done in $0.1\rho/\rho_0$ intervals for several values of ρ. Parameters are assumed to change in a linear manner between intervals.

For the angle distributions in CMS in the case of quasi-elastic or charge exchange scattering the following formula is used:

$$\frac{\mathrm{d}\sigma}{\mathrm{d}\Omega} \sim \sum_{i=0}^{7} a_i \cos^i\theta \tag{2.108}$$

where a_i parameters are extracted from the SAID model (Ref. [104]). For each channel (ii, ij, 0 and CEX) the a_i coefficients are fitted to SAID distributions for 70 different ranges of pion kinetic energy, up to 10 GeV.

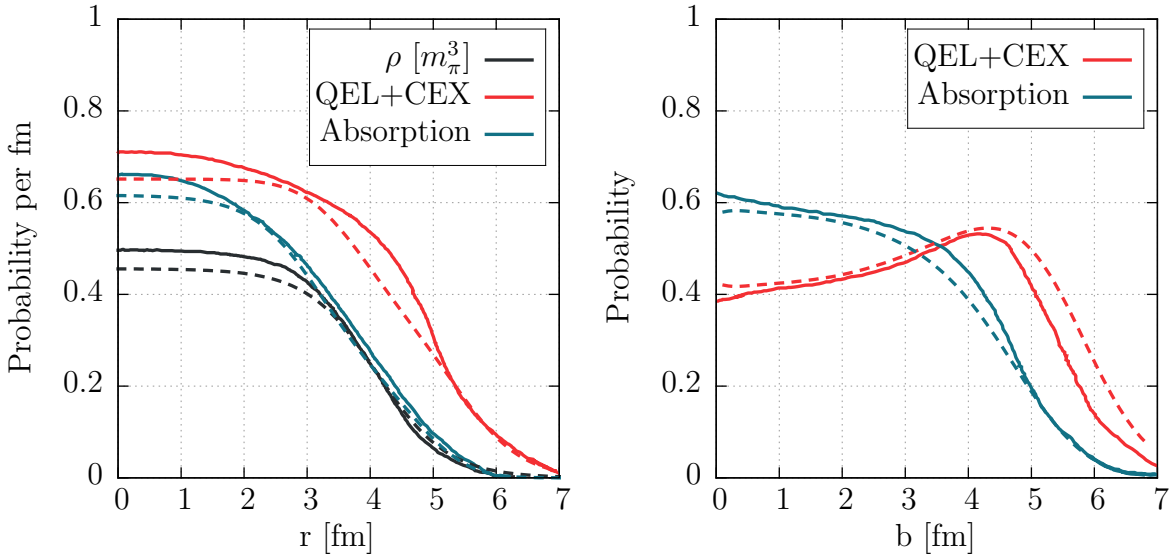

(a) The probability of an interaction per fm as a function of a distance from the center of a nucleus in the case of pion scattering off iron ($T_k = 165$ MeV).

(b) The probability of QEL+CEX and absorption events as a function of the impact parameter of the initial pion in the case of pion scattering off calcium ($T_k = 180$ MeV).

Figure 2.21: The comparison of the original Oset et al. calculations from Ref. [101] (solid lines) and NuWro implementation (dashed lines).

		$T_k = 85$ MeV			$T_k = 245$ MeV			
		$n = 1$	$n = 2$	$n = 3$	$n = 1$	$n = 2$	$n = 3$	$n = 4$
$P_n^{(qel)}$	Oset et al.	0.90	0.09	0.01	0.69	0.25	0.05	0.01
	NuWro	0.89	0.10	0.01	0.67	0.24	0.07	0.02
		$n = 0$	$n = 1$	$n = 2$	$n = 0$	$n = 1$	$n = 2$	$n = 3$
$P_n^{(abs)}$	Oset et al.	0.81	0.17	0.02	0.37	0.41	0.17	0.04
	NuWro	0.87	0.12	0.01	0.41	0.37	0.16	0.05

Table 2.6: The probability that the QEL/CEX scatterings proceeds through n collisions ($P_n^{(qel)}$) and the probability that pion absorption occurs after nth QEL/CEX scatterings ($P_n^{(abs)}$) in the case of pion scattering off calcium.

The comparison of the original predictions of the Oset et al. model (taken from Ref. [101]) and NuWro's implementation is presented in Fig. 2.21 and in Tab. 2.6. In Fig. 2.21a there is a probability of an interaction per fm as a function of a distance from the center of a nucleus for quasi-elastic or charge exchange scattering and for absorption, together with the density profile. Fig. 2.21b presents the probability of QEL/CEX[10] and absorption[11] events. As expected, absorption is more likely to occur in the high density region (small impact parameter b). Tab. 2.6 presents how many collisions take part in QEL/CEX events or precede absorption for two different pion kinetic energies. For higher T_k pions usually undergo more collisions. It is also more likely that high energy pion is scattered before absorption.

2.4.3.2.5 High-energy extension

The Oset et al. model is valid for pion kinetic energy below 350 MeV. For higher energies the Metropolis-like table, based on the experimental data is prepared (Tab. 2.7). Triple pion production is introduced to the model by the new $f_{2\pi}$ parameter, which gives the fraction of double pion production among all non-single pion production processes.

In the single pion production channel the following charge fragmentation is used:

$$ii: \quad \pi^+ p \ (\pi^- n) \ \rightarrow \begin{cases} 75\% & p\pi^+\pi^0 \ (n\pi^-\pi^0) \\ 25\% & n\pi^+\pi^+ \ (p\pi^-\pi^-) \end{cases} \tag{2.109}$$

$$ij: \quad \pi^- p \ (\pi^+ n) \ \rightarrow \begin{cases} 65\% & n\pi^+\pi^- \ (p\pi^+\pi^-) \\ 25\% & p\pi^-\pi^0 \ (n\pi^+\pi^0) \\ 10\% & n\pi^0\pi^0 \ (p\pi^0\pi^0) \end{cases} \tag{2.110}$$

In the double pion production ii channel half of events is assumed to be without neutral pions. In all other cases all possibilities are equally likely.

[10] At least one quasi-elastic or charge exchange scattering, no absorption.
[11] Absorption occurs after any number of QEL/CEX scatterings.

T_k [MeV]	350	540	900	1300	2000	3000
σ_{ii} [mb]	-	16	25	41	29	28
σ_{ij} [mb]	-	25	41	29	28	28
f^{ii}_{inel}	0.05	0.50	0.60	0.65	0.80	0.80
f^{ii}_{CEX}	0	0	0	0	0	0
f^{ii}_{π}	1	1	0.90	0.65	0.30	0.20
f^{ij}_{inel}	0.60	0.60	0.70	0.75	0.75	0.80
f^{ij}_{CEX}	0.65	0.20	0.10	0.05	0.025	0.01
f^{ij}_{π}	1	1	0.75	0.65	0.40	0.30
f^{0}_{inel}	0.325	0.55	0.65	0.70	0.775	0.80
f^{0}_{CEX}	0.325	0.10	0.05	0.025	0.0125	0.005
f^{0}_{π}	1	1	0.825	0.65	0.35	0.25
$f^{ii,ij,0}_{2\pi}$	1	1	1	0.90	0.75	0.60

Table 2.7: The Metropolis-like table for the high-energy extension.

2.4.3.3 The comparison of pion cascade models

The comparison of Metropolis et al. and Oset et al. models with experimental data is presented in Fig. 2.22. The positive pion scattering off carbon is considered. Three channels are defined:

abs - if there is no pion in the final state;

CE - if there is one π^0 in the final state;

inel - all other interactions.

The cross section measurement of the charge current and absorption processes is straightforward, while the inelastic cross section is obtained in an indirect way as:

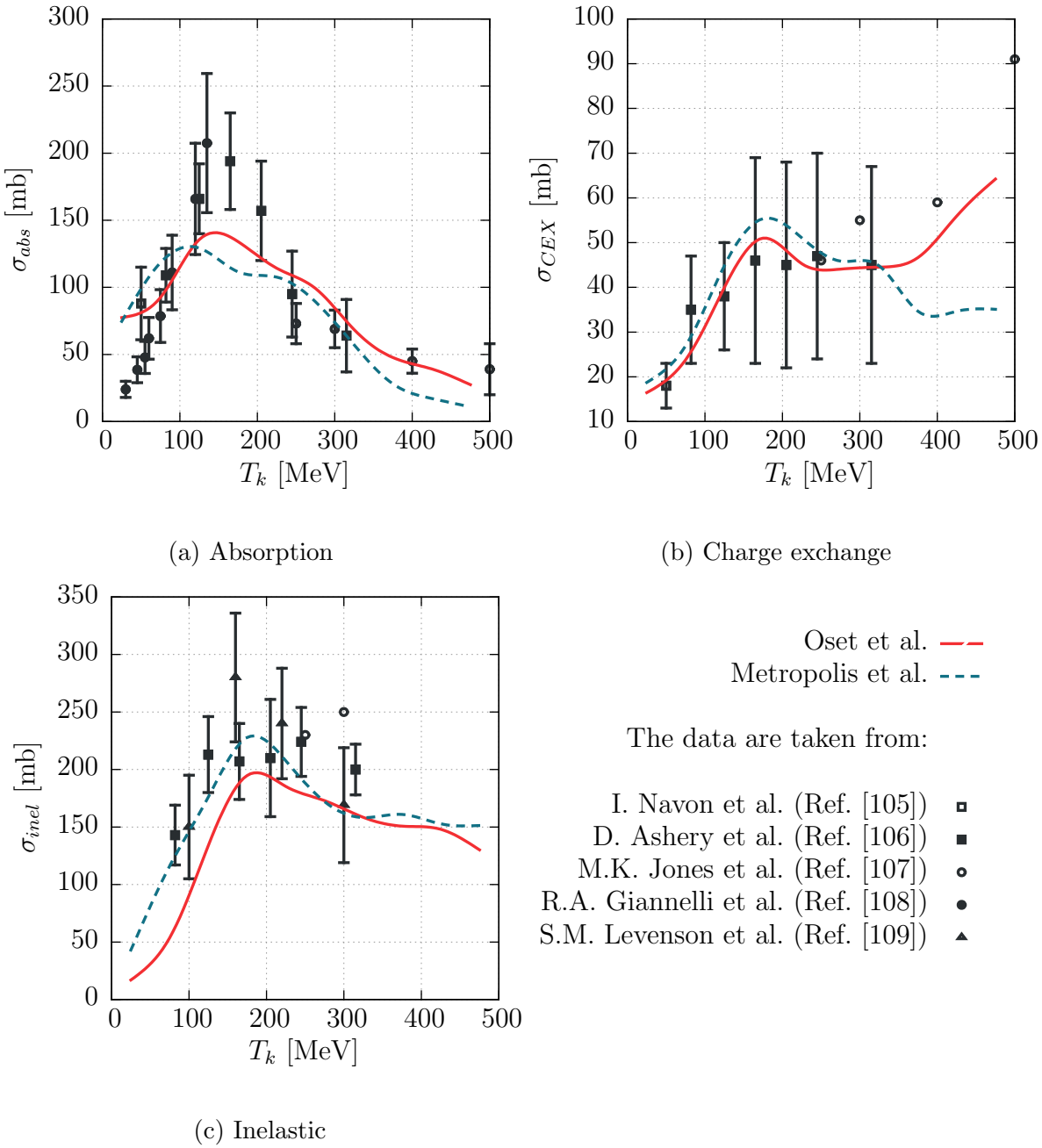

(a) Absorption

(b) Charge exchange

(c) Inelastic

Figure 2.22: The comparison of Metropolis et al. and Oset et al. models with experimental data for three different channels (explained in the text).

$$\sigma_{inel} = \sigma_{total} - \sigma_{elastic} - (\sigma_{abs} + \sigma_{CE}) \tag{2.111}$$

with the elastic pion-nucleus cross section contribution evaluated based on theoretical and experimental arguments (see Ref. [106]). The NuWro prediction are obtained in the standard way by arranging a homogeneous flux of pions and counting the particles

in the final state assuming that at least one interaction took place:

- put π^+ with given T_k on the edge of a nucleus and run cascade (N times);
- count the number of events N_i (i = abs, CE, inel) with the final state as defined above;
- calculate cross sections using the formula:

$$\sigma_i = \frac{N_i}{N}\pi R^2$$

where R is the radius of the nucleus. In the simulations the impact parameter is limited to $b < 6.5$ fm. Taking larger b does not affect the results.

Both models are in a good agreement with the data. The Metropolis et al. model prediction for inelastic scattering is closer to the experimental observation, while Oset et al. model gives a better estimation for absorption and CE processes.

Note, that each model underestimates the cross section for absorption. In Oset et al. model pion absorption is described in terms of Δ resonance. It was expected, that Δ reactions dominate among absorption processes from the studies of π^+ scattering on deuteron (Ref. [110]) or on ^3He (Ref. [111]). However, further investigation of pion-nucleus interactions suggests, that there is a large contribution coming from multi-nucleon absorption. The data published by LADS collaboration (Ref. [112]) indicate that about 25% of pion absorption on ^3He occurs on all three nucleons. In the case of heavier nuclei this fraction is expected to be larger (Ref. [113]). It is clear, that more theoretical studies are needed to understand the pion absorption mechanism.

There are preliminary results for proton multiplicity from the ArgoNeuT experiment (Refs [114, 115]). Liquid Argon Time Projection Chamber technique allows to measure protons with kinetic energy $T_k > 22 \pm 3$ MeV. Only events with no pion are investigated. The fractions of events with muon and 0, 1, 2, 3 or more protons in the final state are presented in Tab. 2.8. The main sources of multi-proton events are two-body current interactions and pion absorption processes. There is good agreement between data and NuWro predictions.

2.4.4 Formation zone

The concept of formation zone / formation time (FZ/FT) was introduced by Landau and Pomeranchuk (Ref. [116]) in the context of multiple scattering of electrons passing

	ν mode		$\overline{\nu}$ mode	
No. of protons	Data	NuWro	Data	NuWro
0	14	15.4	67.7	64.9
1	48	50.8	23.7	22.7
2	26	17.8	6.4	8.0
3	12	9.6	1.4	2.8
more	0	6.3	1.0	1.6

Table 2.8: Fractions of events with μ, N protons and no pion in the final state. The ArgoNeuT preliminary results are taken from Refs [114, 115]. The experimental errors are of the order of 20%.

through a layer of material (see Par. 2.4.4.1 for details). The FZ effect decreases the probability of re-interactions.

The idea of FZ was applied to hadron production by Stodolsky (Ref. [117]), who considered the production of mesons by protons passing through a nucleus. Several parameterizations of his formula was done to use in various MC generators (see Par. 2.4.4.2).

On the most fundamental level the FT is related to Quantum Chromodynamics phenomenon called color transparency (CT), proposed by Brodsky and Mueller (Refs [118, 119]). For high enough four-momentum transfers a quark system is created with a small transverse size (Point-Like Configuration - PLC) which is supposed to suppress hadrons re-interactions. As the typical size of the PLC is of the order of $1/|Q|$ (Ref. [120]), the CT effects are expected to be seen mostly at higher energies. Moreover, two-quark systems are more likely to create PLC than three-quark ones so the effect is expected to be larger for pions, than for nucleons.

The formation time occurrence for lower energies is controversial. In MC generators FZ is a useful handle to control the size of FSI effects. However, it is not clear, if it is a true physical effect or just a way to tune the FSI model.

(a) Electron passing through a layer of material undergo multiple scatterings, which lead to production of photons.

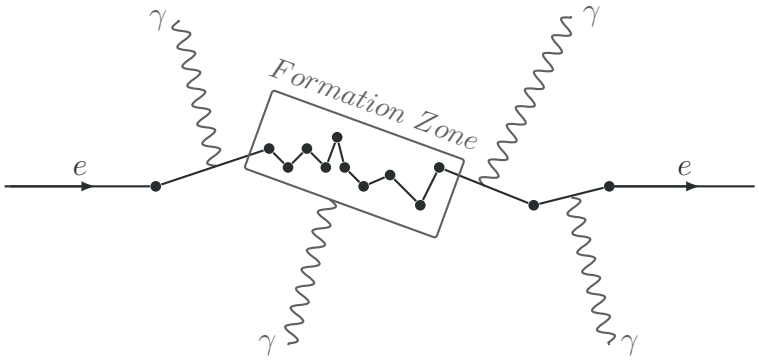

(b) Some of photons are produced coherently over entire length of formation zone.

Figure 2.23: An illustration of the Landau-Pomeranchuk effect.

2.4.4.1 Landau-Pomeranchuk effect

Electrons passing through a layer of material undergo multiple scatterings, which lead to production of photons (see Fig. 2.23). The energy radiated in such process is estimated as:

$$\frac{\mathrm{d}I}{\mathrm{d}^3k} \sim \left| \int_{-\infty}^{\infty} \vec{j}(\vec{x},t) e^{i\left(\omega t - \vec{k}\vec{x}(t)\right)} \mathrm{d}^3x \mathrm{d}t \right|^2 \tag{2.112}$$

where $\vec{x}(t)$ describes the trajectory of an electron, ω and $\vec{k}$ stand for the energy and momentum of the emitted photon. If there is no interference between scatterings on different atoms, one can take the average radiation emitted in one collision and multiply by the number of collisions. It turns out that this procedure does not work for higher energies.

Assuming the electron trajectory to be a series of straight lines, the current density

$j(\vec{x},t) \sim \delta^3(\vec{x}-\vec{v}t)$, with $\vec{v}$ being the velocity of the electron, and the radiation integral from Eq. 2.112 becomes:

$$\sim \int_{path} e^{i(\vec{k}\vec{v}-\omega)t} \mathrm{d}t \tag{2.113}$$

When the exponential varies rapidly enough, collisions at different points have random relative phase factors destroying any interference effects. It happens when:

$$t >> \frac{1}{\omega - \vec{k}\vec{v}} \equiv t_f \tag{2.114}$$

On the other hand, if the time between collisions is much smaller than formation time (t_f), a photon is produced coherently over entire length of formation zone (see Fig. 2.23b), which reduces *the bremsstrahlung*.

The expression for formation time can be rewritten in the following form:

$$t_f = \frac{1}{\omega - \vec{k}\vec{v}} = \frac{E_e}{kp} = \frac{E_e}{m_e}\frac{1}{\omega_{r.f.}} = \gamma T_{r.f.} \tag{2.115}$$

where k, p are electron and photon four-momenta, and $\omega_{r.f.}$ is the photon frequency in the rest frame of the electron. Formation time can be interpreted as the "creation time" of a photon in the electron rest frame.

2.4.4.2 Formation zone for hadrons

A straightforward translation of formation zone to the hadron production was done by Stodolsky (Ref. [117]) by replacing the electron and the photon in Eq. 2.115 with projectile and produced hadrons, respectively, with the following four-momenta:

$$p_0 = (E_0, 0, 0, \sqrt{E_0^2 - M_0^2}) \tag{2.116}$$

$$p = (E, \vec{p}_\perp, \sqrt{E^2 - \mu_\perp^2}) \tag{2.117}$$

where $\mu_\perp$ is the transverse mass defined as $\mu_\perp^2 \equiv |\vec{p}_\perp|^2 + M^2$. The formation time formula can be rewritten in the following form:

$$t_f = \frac{E_0}{p_0 p} = \frac{E_0}{E E_0 - \sqrt{E^2 - \mu_\perp^2}\sqrt{E_0^2 - M_0^2}} \tag{2.118}$$

$$= \frac{1}{E\left(1 - \sqrt{1 - \frac{\mu_\perp^2}{E^2}}\sqrt{1 - \frac{M_0^2}{E_0^2}}\right)} \tag{2.119}$$

For energies high enough to assume $\frac{M_0}{E_0} << 1$ and $\frac{\mu_\perp}{E} << 1$, square roots in the above equation can be expanded into the Taylor's series:

$$t_f \approx \frac{1}{E\left(1 - \left(1 - \frac{1}{2}\frac{\mu_\perp^2}{E^2}\right)\left(1 - \frac{1}{2}\frac{M_0^2}{E_0^2}\right)\right)} \tag{2.120}$$

$$\approx \frac{1}{E\left(\frac{1}{2}\frac{\mu_\perp^2}{E^2} + \frac{1}{2}\frac{M_0^2}{E_0^2}\right)} \tag{2.121}$$

$$= \frac{2E}{(Mx)^2 + \mu_\perp^2} \tag{2.122}$$

where $x \equiv \frac{E}{E_0}$. The above equation is a base for many parametrizations used in the neutrino-nucleus scattering.

Ranft argued (see Ref. [121]) that a further simplification $x \approx 0$ is usually well justified and finally in the LAB frame:

$$t_f \approx \frac{2E}{\mu_\perp^2} \tag{2.123}$$

and in the hadron rest frame:

$$t_{f,r.f.} \approx \frac{2M}{\mu_\perp^2} \tag{2.124}$$

Inspired by this expression Ranft postulated another formula for FT in the hadron rest frame. He kept the basic relativistic character of FT, but introduced arbitrary τ_0 parameter to control its size:

$$t_{f,r.f} = \tau_0 \frac{M^2}{\mu_\perp^2} \tag{2.125}$$

The above equation was implemented in the MC event generator DPMJET (Ref. [122]), which later became a part of the FLUKA code and was used by the NOMAD collaboration (Ref. [123]). In the DPMJET cascade model FT is applied to hadrons

resulting from all the primary interactions (QEL, RES, DIS). Following the ideas of Bialas (Ref. [124]) the values of FT are sampled from the exponential distribution.

In the above estimations of the FT effect several assumptions were made, which are not necessarily valid at lower energies. This is taken into account in the more recent low energy FLUKA cascade model, called PEANUT (Ref. [125]). For QEL reactions FT was replaced by the concept of coherence length (CL).

Derivation of CL is based on the uncertainty principle arguments. Let p be the outgoing nucleon four-momentum and q - the four-momentum transfer (both in LAB frame). Because $p \cdot q$ is a Lorentz scalar, one can calculate easily the energy transfer in the rest frame of the nucleon ($\omega_{r.f.}$):

$$|p \cdot q| = |p_{r.f.} \cdot q_{r.f.}| = |\omega_{r.f.} M| \Rightarrow |\omega_{r.f.}| = \frac{|p \cdot q|}{M} \tag{2.126}$$

From the uncertainty principle $\omega_{r.f.}$ can be used to estimate the reaction time in the nucleon's rest frame:

$$t_{CL,r.f.} = \frac{M}{|p \cdot q|} \tag{2.127}$$

Within that time the nucleon is assumed to be unable to re-interact. Going to the LAB frame, the Landau-Pomeranchuk formula (Eq. 2.115) is reproduced:

$$t_{CL} = \gamma t_{CL,r.f.} = \frac{E}{|p \cdot q|} \tag{2.128}$$

Among other approaches to give a quantitative evaluation of FT one should mention the SKAT parametrization (Ref. [126]):

$$t_f = \frac{E}{\mu^2} \tag{2.129}$$

with μ^2 being the free parameter, estimated to be $\mu^2 = 0.08 \pm 0.04$ GeV^2 based on the experimental data for the protons multiplicity. In SKAT parametrization FZ is identical for pions and nucleons with the same momentum. At $|\vec{p}| \sim 1$ GeV formation length is expected to be ~ 2.5 fm, which is of the size of the carbon nucleus.

In the case of pions produced through the Δ excitation there is another way to model the FT-like effect. In the INC picture one can treat Δ (like in GiBUU approach, Ref. [99]) as a real particle propagating some distance before it decays. The Δ lifetime in its rest frame is equal $\frac{1}{\Gamma}$, with $\Gamma \approx 120$ MeV, so in the LAB frame one obtains:

$$t_\Delta = \frac{E_\Delta}{M_\Delta \Gamma} \tag{2.130}$$

MC generator	QEL	RES	DIS
NEUT	-	SKAT (Eq. 2.129)	SKAT (Eq. 2.129)
FLUKA	CL (Eq. 2.128)	Ranft (Eq. 2.125)	Ranft (Eq. 2.125)
GENIE	-	-	Ranft (Eq. 2.125 with $\|\vec{p}_\perp\| = 0$)
NUANCE	1 fm	1 fm	1 fm

Table 2.9: Formation time models in various Monte Carlo event generators. Note that every MC has its own definition of what does the RES and DIS terms mean.

where E_Δ is the LAB frame Δ energy and $\frac{1}{\Gamma}$ is sampled from the exponential distribution.

2.4.4.2.1 Formation zone in MC generators

All models described in 2.4.4.2 are implemented in NuWro. However, as default, the formation zone effects is described:

- as coherence length (Eq. 2.128) for quasi-elastic scatterings;
- as Δ propagation (Eq. 2.130) for RES interactions;
- using Ranft formula (Eq. 2.125) for DIS.

with the smooth transition between the last two models at invariant mass $W \sim$ 1.6 GeV. For the $np - nh$ events the formation time is assumed to be zero, because there is no clear physical motivation to introduce it. The FZ models used in other MC generators are presented in Tab. 2.9.

In Fig. 2.24 there is the comparison of FZ models used in different MC generators for nucleons and pions. In the case of NuWro formation time depends on the interaction type and neutrino energy. The results show an average formation length for $E_\nu = 1$ GeV. GENIE use the Ranft formula (Eq. 2.125) assuming $|\vec{p}_\perp| = 0$. The τ_0 parameter is chosen, so the SKAT parametrization with $\mu^2 = 0.08$ GeV^2 is reproduced for pions.

2.4.4.3 The impact of FZ on the results

In the context of the intranuclear cascade formation zone is applied just after the primary vertex, as presented in Fig. 2.25. For each particle the corresponding formation

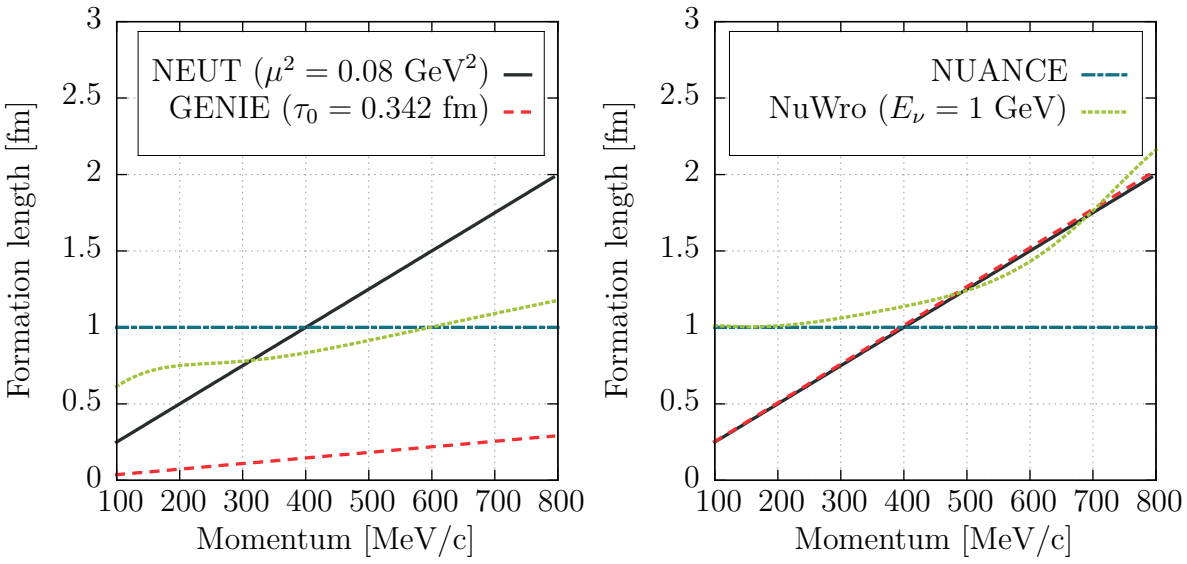

(a) Nucleons (b) Pions

Figure 2.24: The comparison of FZ models in various MC generators.

length is calculated and the particle is moved according to its momentum direction. FZ decreases the probability of the re-interaction, affecting the final results. Below various results with and without the FZ effect are compared to the data.

2.4.4.3.1 Nuclear transparency for protons

The appropriate observable to qualitatively estimate the FSI model is nuclear transparency (T). It is defined as the ratio of the measured cross section (σ_{exp}) to the theoretical prediction without FSI (σ_{th}): $T = \sigma_{exp}/\sigma_{th}$. In other words, T gives the probability that a particle created in the primary vertex leaves a nucleus without an interaction.

The study of the transparency for protons are based on quasifree $(e, e'p)$ reactions (Refs [127, 128]). The measurement is done for fixed kinematics (Tabs 2.10 and 2.11). To reconstruct the data the following procedure is used:

- put the proton in a random (respect to the density profile) position in the nucleus;
- apply formation zone;
- start a propagation;
- check if there was an interaction.

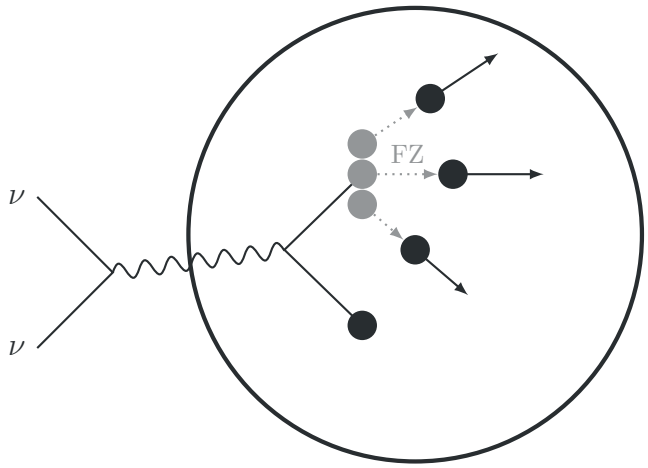

Figure 2.25: An illustration of the formation zone effect in INC. The particles created in the primary vertex are not allowed to interact over a length of formation zone.

T_p [MeV]	E_e [GeV]	Q^2 [GeV^2]	θ_e	θ_p
350	2.445	0.6	20.5	35.4, 39.4, 43.4, 47.4, 51.4, 55.4, 59.4, 63.4, 67.4, 71.4, 75.4
700	2.445	1.3	32.0	31.0, 35.0, 39.0, 43.0, 47.0, 51.0, 55.0
970	3.245	1.8	28.6	33.5, 37.5, 40.5, 44.5, 48.5, 52.5
1800	3.245	3.3	50.0	25.1, 27.6, 30.1

Table 2.10: The measurement kinematics from Ref. [127]. T_p stands for the kinetic energy of the knockout proton; E_e is the energy of the incident electron; θ_e, θ_p are scattering angles for the electron and the proton, respectively, in the LAB frame.

E_e [MeV]	E'_e [GeV]	Q^2 [GeV^2]	θ_e	θ_p
2.015	1.39	1.04	35.5	43.4, 46.2, 49.0, 51.8, 54.6
3.188	1.47	3.06	47.7	27.7, 30.5, 33.3
4.212	1.47	53.4	5.00	20.9, 22.6
5.120	1.47	6.77	56.6	15.9, 16.7, 17.3

Table 2.11: The measurement kinematics from Ref. [128]. E_e, E'_e stand for the energy of the initial and final, respectively, electron; θ_e, θ_p are scattering angles for electron and proton, respectively, in the LAB frame.

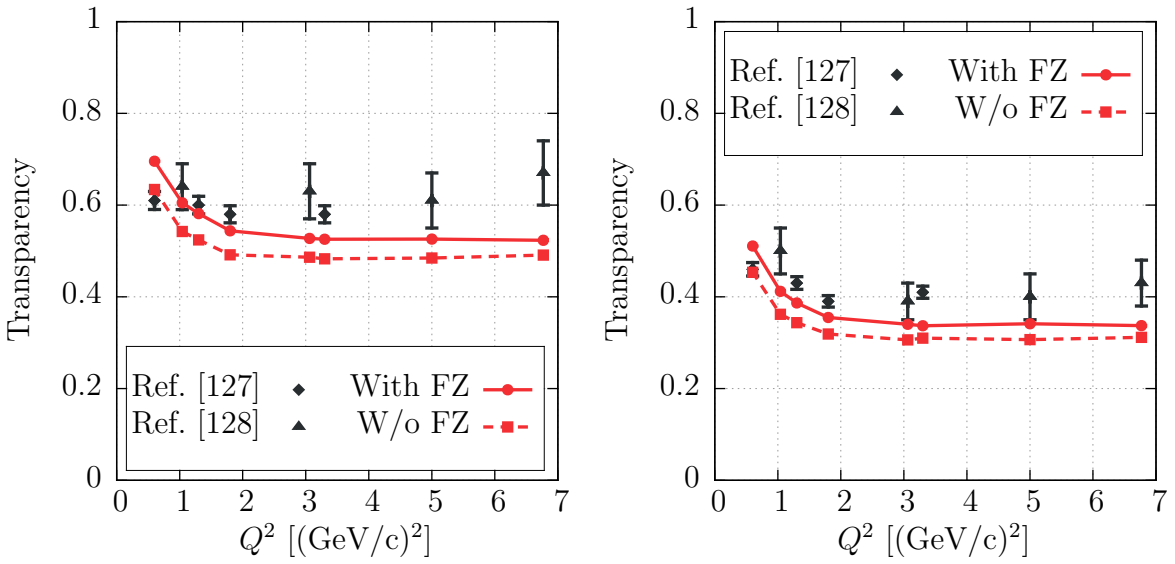

(a) Carbon (b) Iron

Figure 2.26: Nuclear transparency for protons.

Nuclear transparency is defined as the ratio of the number of events without an interaction (N_{noFSI}) to the number of all events (N): $T = N_{noFSI}/N$. In this case, coherence length is used as formation zone model. Neglecting Fermi motion (justified for this electron energy range), Eq. 2.128 can be written in the following form:

$$t_f = \frac{E}{|p \cdot q|} = \frac{E}{|p \cdot (p - p_0)|} \approx \frac{E}{|M^2 - EM|} = \frac{E}{MT_p} = \frac{2(T_p + M)}{Q^2} \tag{2.131}$$

where T_p and Q^2 are taken from Tabs 2.10 and 2.11. In the case of data from Ref. [128] the kinetic energy of final proton is assumed to be $T_p = E_e - E'_e$. The results for carbon and iron are presented in Fig. 2.26. The impact of FZ is small, as expected for QEL reactions, but it makes the prediction closer to the data.

2.4.4.3.2 Nuclear transparency for pions

The study of nuclear transparency for pions is based on $(e, e'\pi^+)$ reactions (Ref. [129]). The measurement is done for fixed kinematics (Tab. 2.12), chosen to avoid the resonance region - invariant mass is of order $W \sim 2.2$ GeV. The simulation procedure is the same as for protons. However, the Ranft formula (Eq. 2.125) is now used as formation zone model:

E_e [GeV]	E'_e [GeV]	Q^2 [GeV^2]	θ_e	p_π [Gev/c]	θ_π
4.021	1.190	1.10	27.76	2.793	10.58
5.012	1.730	2.15	28.85	3.187	13.44
5.012	1.430	3.00	37.77	3.418	12.74
5.767	1.423	3.91	40.38	4.077	11.53
5.767	1.034	4.69	52.67	4.412	9.09

Table 2.12: The measurement kinematics from Ref. [129]. E_e, E'_e stand for the energy of the initial and final, respectively, electron; θ_e, θ_π are scattering angles for the electron and the pion, respectively, in the LAB frame, and p_π is the pion momentum.

$$t_f = \tau_0 \frac{E_\pi m_\pi}{\mu_T^2} = \tau_0 \frac{m_\pi \sqrt{p_\pi^2 + m_\pi^2}}{p_\pi^2 \sin^2\theta_\pi + m_\pi^2} \tag{2.132}$$

where p_π and θ_π are taken from Tab. 2.12. The NuWro prediction for carbon and copper for various values of τ_0 are presented in Fig. 2.27. It is clear, that the data are very sensitive to FT. The best agreement with the data is for τ_0 of order $0.025 - 0.05$ fm/c.

2.4.4.3.3 Backward moving pions

Formation zone for deep inelastic scattering is tuned to the NOMAD experimental data (Ref. [123]). The average neutrino energy is $\langle E_\nu \rangle = 24$ GeV, so DIS is a dominant channel. The target composition is dominated by carbon (64.30%) and oxygen (22.13%) with small additions of other elements.

The investigated observable is the average number of backward moving ($\cos\theta_{LAB} < 0$) negative pions Bπ^- with the momentum between 350 and 800 MeV/c. Bπ^- appear mainly due to nuclear re-interactions, so the observable is very sensitive to final state interactions. Formation time decreases the effect of FSI, making the number of backward moving pions smaller.

Simulations made for various values of τ_0 (see Eq. 2.125) lead to the conclusion that a good agreement with the data is obtained with $\tau_0 \sim 8$ fm/c, which is consistent with the one suggested by Ranft ($\tau_0 \sim 5 - 10$ fm/c) in Ref. [121]. However, the study of nuclear transparency for pion (see 2.4.4.3.2) indicates much lower value of τ_0. Should τ_0

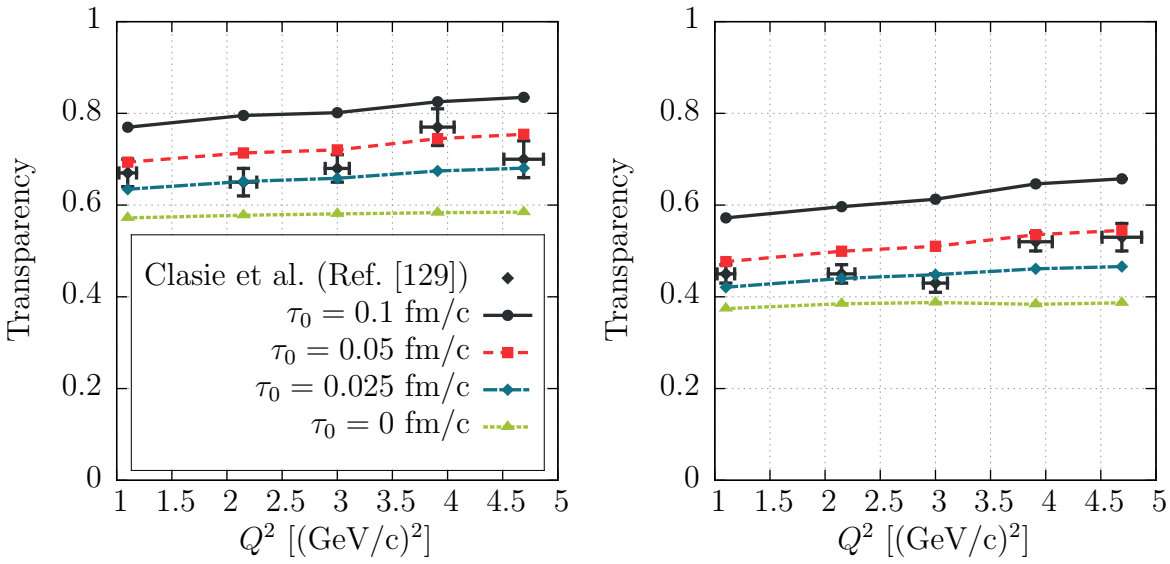

(a) Carbon

(b) Copper

Figure 2.27: Nuclear transparency for pions.

parameter be dependent on lepton energy / energy transfer or is there another physics involved?

Fig. 2.28 shows the average number of backward moving π^- reported by the NOMAD collaboration, and predicted by NuWro, with and without FZ, as a function of Q^2. As expected, in this energy region formation zone must be taken into account in order to have an agreement with the data. In order to better understand the NuWro performance, various ways in which Bπ^- appear were analyzed:

1. pions are created in the primary vertex and undergo quasi-elastic scatterings;
2. pions are created in FSI pion-nucleon interactions:
   (a) single pion production;
   (b) double pion production;
   (c) triple pion production;
3. pions are created in FSI nucleon-nucleon interactions;
4. there are more FSI pion production processes.

Contributions from the above scenarios are listed in Tab. 2.13. One can see that FZ decreases the probability for pion production during cascade. This is due to the fact

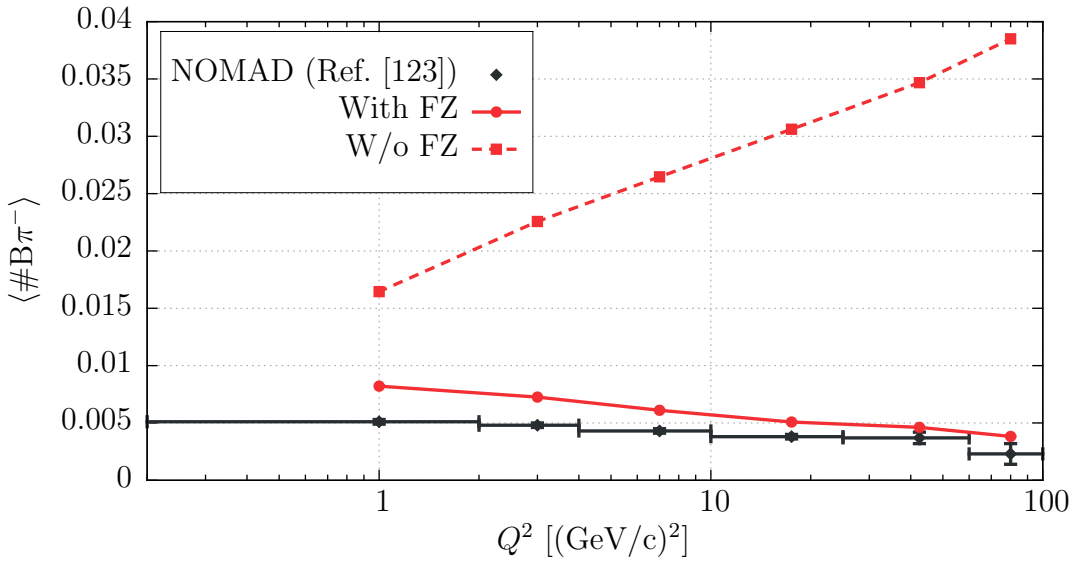

Figure 2.28: The average number of backward going π^- as a function of Q^2.

Scenario	1	2	2a	2b	2c	3	4
W/o FZ	37.2%	43.4%	22.0%	15.6%	5.8%	2.7%	16.7%
With FZ	83.7%	15.5%	8.1%	7.4%	0%	0.7%	0.1%

Table 2.13: The contribution to the sample of events with backward moving π^- from different scenarios (explained in the text). The results with FZ are obtained using $\tau_0 = 8$ fm/c.

that formation time, as well as the cross section for inelastic scattering increase with the hadron energy.

The number of events as a function of the multiplicity of backward negative pions is presented in Tab. 2.14. The NOMAD result suggests that $\sim$ 3.7% of events with backward π^- contains in fact two of them, while NuWro predicts that this is only 1.6% or 0.1% cases (with and without FZ, respectively).

2.4.4.3.4 NC π^0 production

Recent experimental data for neutral current π^0 production come from three experiments. Basic information about them is summarized in Tab. 2.15[12]. In the K2K and MiniBooNE experiments the signal is defined as exactly one π^0 leaving the nucleus

[12]Please note, that simulations are done for full neutrino flux, not the averaged.

$B\pi^-$	NOMAD	W/o FZ	With FZ
0	939617	921048	937883
1	4238	22590	6126
2	164	375	8

Table 2.14: The number of events as a function of the multiplicity of backward negative pions.

Experiment	Beam	$\langle E_\nu \rangle$ [GeV]	Target	Measurement
K2K (Ref. [130])	ν_μ	1.30	H_2O	$\mathrm{d}N/\mathrm{d}T_\pi$
MB (Ref. [131])	ν_μ	0.81	CH_2	$\mathrm{d}\sigma/\mathrm{d}T_\pi$, $\mathrm{d}\sigma/\mathrm{d}\cos\theta_\pi$
MB (Ref. [131])	$\overline{\nu}_\mu$	0.66	CH_2	$\mathrm{d}\sigma/\mathrm{d}T_\pi$, $\mathrm{d}\sigma/\mathrm{d}\cos\theta_\pi$
SciB (Ref. [132])	ν_μ	0.81	C_8H_8	$\mathrm{d}N/\mathrm{d}T_\pi$, $\mathrm{d}N/\mathrm{d}\cos\theta_\pi$

Table 2.15: Recent NC π^0 production measurements.

target and no other mesons, nor a charged lepton in the final state. In the case of SciBooNE (SciB) events with at least π^0 (with possible other pions as well) are taken into account.

From the theoretical perspective the experimental signal for $1\pi^0$ production comes from[13]:

- single π^0 production in the primary vertex in the single pion production reaction;
- π^0 produced in the double pion production reaction with the other pion being absorbed;
- single $\pi^\pm$ production with the charge exchange reaction $\pi^\pm \to \pi^0$ afterwards;
- primary quasi-elastic scattering with π^0 produced in FSI.

According to NuWro, most of the $1\pi^0$ signal events come from the initial RES single pion production reactions, see Tab. 2.16. This is expected, as SPP is the dominant

[13]For the SciB signal the number of possibilities becomes larger.

Channel	K2K	MB ν	MB $\overline{\nu}$
$1\pi^0 \rightarrow 1\pi^0$	93.1% (84.5%)	93.0% (88.3%)	94.8% (92.4%)
no $\pi \rightarrow 1\pi^0$	2.0% (3.2%)	1.8% (2.4%)	1.2% (1.6%)
$1\pi^{\pm} \rightarrow 1\pi^0$	3.7% (6.8%)	4.2% (5.8%)	3.2% (3.9%)
more $\pi \rightarrow 1\pi^0$	1.2% (5.5%)	1.0% (3.5%)	0.7% (2.1%)

Table 2.16: The origin of the events with $1\pi^0$ in the final state. Values in brackets refer to results without FZ.

Channel	K2K	MB ν	MB $\overline{\nu}$
$1\pi^0 \rightarrow 1\pi^0$	81.6% (64.0%)	79.1% (66.9%)	83.0% (74.5%)
$1\pi^0 \rightarrow$ no π^0	5.9% (19.3%)	7.2% (19.2%)	6.4% (15.9%)
$1\pi^0 \rightarrow \pi^{\pm}$	10.1% (11.0%)	10.2% (10.1%)	9.6% (7.8%)
$1\pi^0 \rightarrow$ more π	2.4% (5.7%)	2.0% (3.7%)	1.0% (1.8%)

Table 2.17: The impact of FSI effects on the events with $1\pi^0$ in the primary vertex. Values in brackets refer to results without FZ.

channel in the neutrino energy around 1 GeV. Note, that also in the channel $1\pi^0 \rightarrow 1\pi^0$ FSI can affect momentum and angular distributions of the neutral pion.

FSI effects are more apparent when one looks at what happens to π^0 created in the primary vertex (Tab. 2.17). Absorption, as well as charge exchange processes, reduces the number of NC $1\pi^0$ events. However, one can see that the influence of formation zone on the latter is smaller. This is because for low energy pions, for which FT is small, CE scatterings are more likely than absorption.

Tab. 2.18 shows the composition of the π^0 signal in the SciBooNE experiment as it is understood by NuWro. The second column contains the values reported by the SciB collaboration obtained from their Monte Carlo generator.

K2K and SciBooNE collaborations did not publish the normalized differential cross section. However, flux averaged ratios of NCπ^0 and total CC cross sections were given. In Tab. 2.19 both values are compared to the NuWro results.

Channel	SciB MC	NuWro (with FZ)	NuWro (w/o FZ)
$1\pi^0$	85%	82%	80%
$1\pi^0 + \pi^\pm$	11%	14%	16%
$2\pi^0$	4%	4%	4%

Table 2.18: Predictions of contributions to π^0 channel from SciBooNE MC and NuWro.

Experiment	Data	NuWro (with FZ)	NuWro (w/o FZ)
K2K	0.064±0.008	0.079	0.070
SciB	0.077±0.010	0.077	0.071

Table 2.19: The ratio of NCπ^0/CC cross sections.

Fig. 2.29 shows the MiniBooNE, K2K and SciBooNE data together with the NuWro predictions for the π^0 momentum distributions. In the case of normalized cross section the main effect of the introduction of FZ is to increase the cross section in the pion absorption peak region. The effect can be estimated to be $10-15\%$. In the case of K2K measurement the use of FZ also moves the peak of the pion momentum distribution to larger values by about 50 MeV/c, resulting in better agreement with the data.

Both MB and SciB experiments provide distributions of events versus the cosine of the angle between neutrino flux and π^0 momenta[14]. The NuWro predictions together with the data are presented in Fig. 2.30. The backward directions are investigated, as an important impact of FZ is expected in this kinematic region. Figs 2.30a and 2.30b show that FZ increases the π^0 in the backward directions, but the effect is rather small. The reason is that at lower neutrino energies there are many backward moving π^0 in the primary vertex. FSI becomes the main source of Bπ^0 for larger Q^2 and then FZ reduces their number.

In the case of SciBooNE experiment (Figs 2.30c and 2.30d) the NuWro results are normalized to the number of π^0. In this case FZ makes the number of backward moving π^0 little smaller. As it was mentioned before, FZ increases the cross section, but when only the shapes are compared, distributions are shifted to higher energies and more

[14]In the case of SciB, if there were two neutral pions in the event, the more energetic was taken into account.

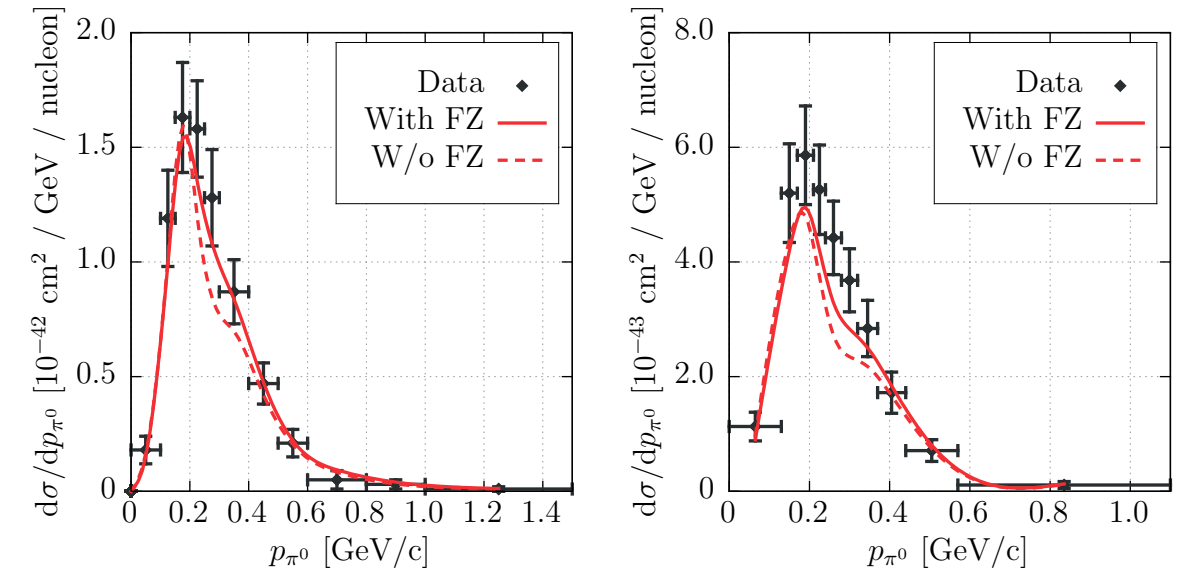

(a) MiniBooNE ν mode

(b) MiniBooNE $\bar{\nu}$ mode

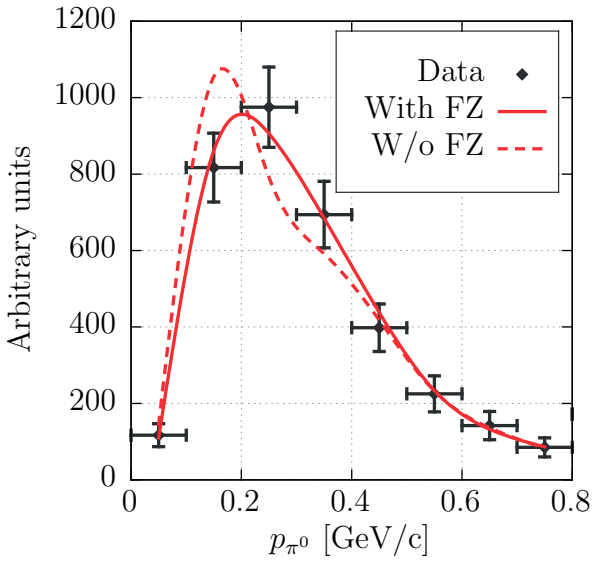

(c) K2K

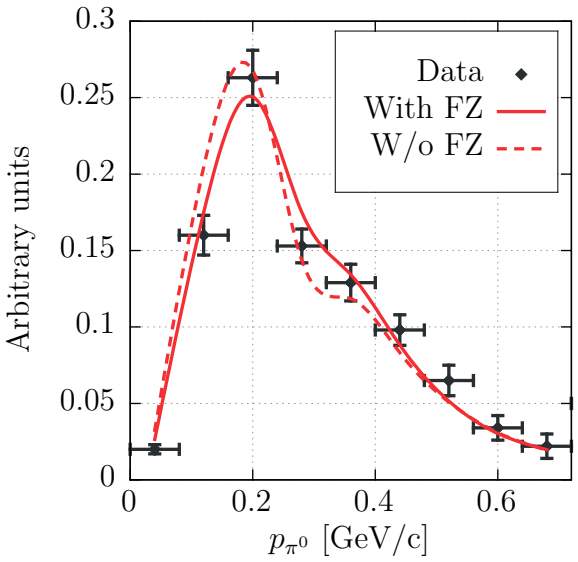

(d) SciBooNE

Figure 2.29: NCπ^0 production as a function of π^0 momentum. In the case of K2K and SciB data NuWro predictions are normalized to the same area.

forward directions.

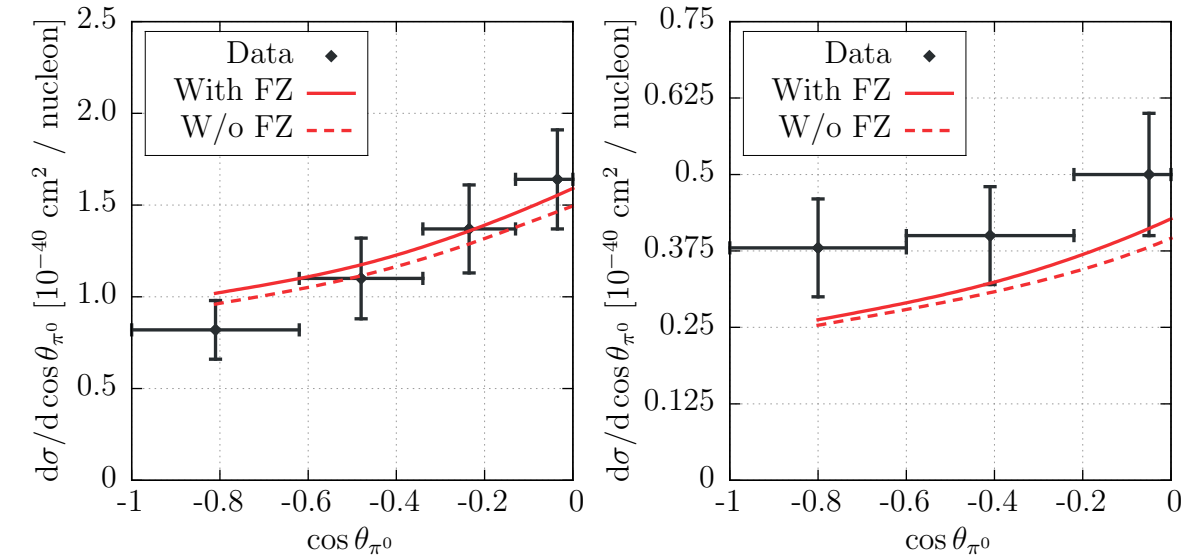

(a) MiniBooNE ν mode

(b) MiniBooNE $\overline{\nu}$ mode

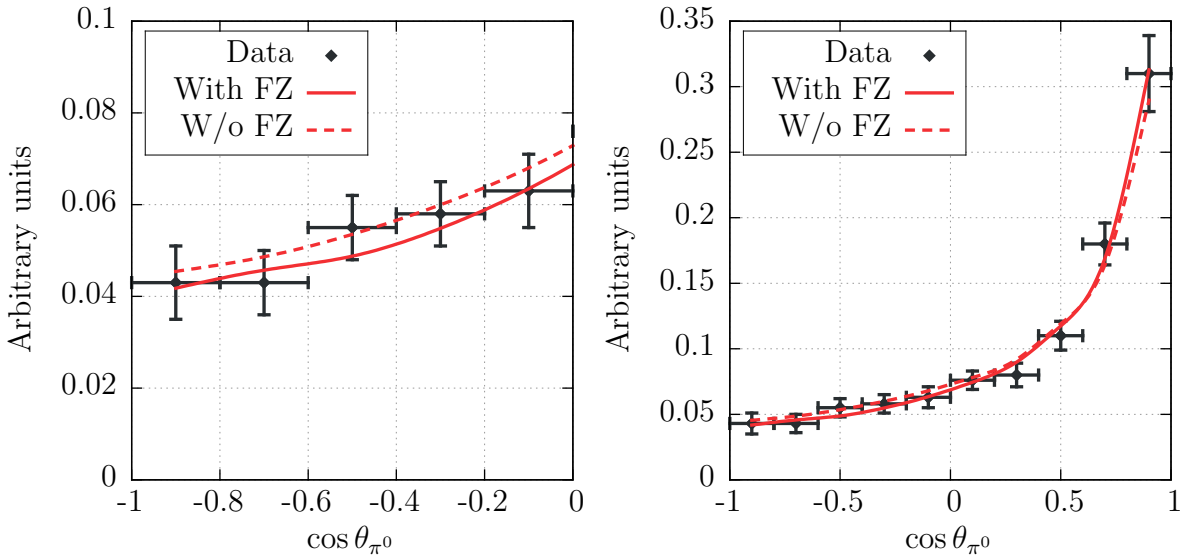

(c) SciBooNE

(d) SciBooNE (full range)

Figure 2.30: The angular distribution of π^0. SciBooNE data and NuWro predictions are normalized to the same area (over the whole $\cos\theta_{\pi^0}$ range).

Chapter 3

The comparison of MC generators

Monte Carlo generators are important tools in the investigation of neutrino measurements. Regardless of the measurement method used in an experiment, particles seen in a detector are the ones produced in a neutrino-nucleus scattering, usually affected by the final state interactions. To interpret correctly the observation one needs reliable MC simulations.

There are several MC neutrino event generators and they share many common features. However, despite of the similarities, their results can differ significantly on the level of both, primary vertex and final state interactions (see e.g. [7]). A short summary of each generator discussed in this chapter can be found in Sec. 3.1.

The best way to test them is to compare their predictions with the available data. In Sec. 3.3 there is a comparison of GENIE, NEUT and NuWro predictions to CC pion production MiniBooNE data.

Because there is a limited set of neutrino data, comparisons just between generators are also very useful. Such approach has an extra advantage of freedom in defining the observables, which may be not easily measurable, but still are useful in crosschecking the generators. The various distributions obtained using GENIE, NEUT, NUANCE and NuWro are presented in Sec. 3.4.

In Sec. 3.2 the study of pion production in neutrino-oxygen interactions is discussed. Considered generators are: FLUKA (Ref. [133]), GENIE, NEUT and NuWro.

3.1 MC generators

The general scheme in all MC generators is the same. At the beginning neutrino flavor and momentum, as well as nucleus type are determined. The total cross section is calculated (or read from tables) as the sum of cross sections for each channel:

$$\sigma_{total} = \sum_i \sigma_i \tag{3.1}$$

The interaction type i is chosen with the probability $\frac{\sigma_i}{\sigma_{tot}}$. In the MC algorithm the kinematics of the process is obtained from the cross section σ_i model, usually affected by nuclear effects like Fermi motion or Pauli blocking. Finally, the hadrons are propagated through nucleus.

Each generator uses a different set of models for primary neutrino-nucleon interactions. Each one has also its own approach to describe nuclear effects. Some of them are tuned to experimental data[1]. All this affects the final results.

This section contains basic informations about models used in FLUKA (Subsec. 3.1.1), GENIE (Subsec. 3.1.2), NEUT (Subsec. 3.1.3) and NUANCE (Subsec. 3.1.4).

3.1.1 FLUKA

The FLUKA event generator is well known from its hadron-nucleon interactions and nuclear effects model, called PEANUT (Ref. [134]). It has been used for over twenty years in many various aspects of particle physics (Ref. [122]). Neutrino-nucleon QEL scattering was introduced into FLUKA in 1997, while DIS interactions (NunDIS) and Δ production (NunRES) development started in 2005 (Ref. [135]). For the resonance pion production the Rein-Sehgal model (Ref. [51]) is used. A non-resonant contribution is obtained from NunDIS, with a smooth linear transition in invariant mass from the resonance region to DIS. FLUKA routines are used for hadronization. Coherence length is applied for a final nucleon in QEL processes, while the Ranft formula (Ref. [121]) is used for inelastic scattering.

3.1.2 GENIE

GENIE is a neutrino event generator that evolved from the NEUGEN package (Ref. [136]). Nuclei are modeled within the Fermi gas picture with Bodek-Ritchie modification (Ref. [137]). The Llewellyn-Smith formalism (Ref. [42]) with the latest BBBA form factors parametrization (Ref. [138]) is used for QEL cross section calculations. Resonance production is described by the Rein-Sehgal model up to the hadronic invariant mass $W = 1.7$ GeV. However, resonances are added incoherently and their interference is neglected. For higher W the Bodek-Young model (Ref. [139]) is used. The transition region from RES to DIS is tuned using the experimental data (Ref.

[1]Most of these data are model-dependent, is not it vicious circle?

[136]). Coherent pion production is described within Rein-Sehgal model (Ref. [71]). Hadronization is done using the AGKY model (Ref. [140]) for low W and PYTHIA library for higher invariant masses, with a smooth transition between them. The effective approach to FSI (INTRANUKE) is applied, preceded by formation zone described by the SKAT parametrization (Ref. [126]). INTRANUKE is tuned to hadron-nucleus data (Ref. [141]). Recently, the two-body current contribution has been implemented, based on Dytman model (Ref. [68]). GENIE is currently used by many collaborations, including T2K, MINOS, MINERvA, NoVA, LBNE.

3.1.3 NEUT

The NEUT generator was developed for Kamiokande experiment. It has been used by SuperK, K2K, T2K collaborations. The general set of cross section models is similar to the one used in GENIE: the Llewellyn-Smith formalism for QEL, the Rein-Sehgal models for RES and COH, and the Bodek-Young model for DIS. However, the RES cut is set on $W = 2$ GeV and the lepton mass effect (see e.g. [142]) is included in coherent Rein-Sehgal model. Hadronization is performed using PYTHIA routines. The INC model is applied for FSI. The SKAT parametrization is used for formation time. Fermi gas, as well as spectral function, can be used for a description of nucleus. NEUT has a pion-less Δ decays effect implemented. However, it has been turned off after the inclusion of two-body current interactions into the generator. $np - nh$ processes implementation is based on the Nieves model (Ref. [63]) with the high-energy extension (Ref. [64]).

3.1.4 NUANCE

NUANCE uses similar cross section models as NEUT and GENIE. Hadronization is handled by PYTHIA, however, a KNO-based hadronization scheme is also included. Fermi gas with κ-parametrization (Ref. [143]) is used for nuclear model. The INC is applied for FSI. NUANCE uses constant value of formation length, equal to 1 fm. The generator was used by MiniBooNE collaboration.

3.2 Pion production in neutrino-oxygen interactions

During the 45th Karpacz Winter School in Theoretical Physics in 2009 (Ref. [144]) students were investigating pion production in various MC generators. Results are collected

	FLUKA	GENIE	NEUT	NuWro
0π	54.0% (64.5%)	52.6% (61.9%)	66.9% (74.2%)	58.1% (68.5%)
1π	45.1% (34.6%)	46.0% (36.8%)	29.7% (23.6%)	40.1% (29.6%)
$1\pi^0$	11.6% (9.8%)	8.8% (8.1%)	5.1% (5.2%)	7.1% (6.8%)
$1\pi^+$	33.5% (24.3%)	37.2% (28.5%)	24.6% (17.6%)	33.0% (21.5%)
$1\pi^-$	0% (0.5%)	0% (0.2%)	0% (0.8%)	0% (1.3%)
$> 1\pi$	0.9% (0.9%)	1.4% (1.3%)	3.4% (2.2%)	1.8% (1.9%)

Table 3.1: The percent of events without π, exactly one π or more π's in the final state. Values in brackets refer to results after FSI.

in Ref. [7]. In this section the summary of these results is presented. The predictions were prepared over 5 years ago and each generator has been updated since then.

The general idea was to look at the distributions of primary and final state pion topologies. The number of events with given number of neutral and charge pion in the final state was extracted from 500k events samples of 1 GeV ν_μ CC interactions on ^{16}O, before and after FSI.

Tab. 3.1 is based on the results from Ref. [7]. It presents the fraction of events with no pion, with exactly one pion and with more pions in the final state, before and after FSI. FLUKA and GENIE predicted about 1.5 times more single pion production processes than NEUT. Note, that there is no coherent pion production in FLUKA. The NuWro prediction were somewhere in the middle.

In about 25% of SPP neutral pion was produced in the case of FLUKA. For GENIE it was about 20%. NEUT and NuWro predicted that one of the six SPP events contains π^0. However, all the generators, but FLUKA, had the same fraction of single π^0 events among all SPP in the sample (about 22%), when FSI is applied.

The effect of FSI in events with single pion in the primary vertex is presented in Tab. 3.2. Pion are more likely to interact in the nuclear matter in NEUT and NuWro. In GENIE the probability of re-interactions was exactly the same for neutral and charged pion. Other generators predicted nuclear matter to be more transparent for charged pion, then neutral one.

These studies showed the inconsistency of MC generators on the level of both -

	FLUKA	GENIE	NEUT	NuWro
$\pi^0 \rightarrow \pi^0$	67%	75%	57%	50%
$\pi^0 \rightarrow 0\pi's$	24%	20%	28%	29%
$\pi^0 \rightarrow \pi^+$	5%	2%	7%	9%
$\pi^0 \rightarrow \pi^-$	3%	2%	6%	8%
$\pi^+ \rightarrow \pi^+$	69%	75%	65%	59%
$\pi^+ \rightarrow 0\pi's$	25%	20%	27%	30%
$\pi^+ \rightarrow \pi^0$	5%	4%	6%	8%

Table 3.2: The percent of events with single pion or no pion in the final state if there was single pion in the initial state.

primary vertex and FSI. As it was mentioned, these calculations were performed in 2009. Many updates were done in MC generators in the last few years.

3.3 MC generators vs MiniBooNE data for CC single pion production

There is a lot of interest in single pion production processes in neutrino-nucleus interactions, coming from the oscillation experiments and the demand to better constrain the systematic errors. Both $\nu_\mu \rightarrow \nu_e$ appearance and $\nu_\mu \rightarrow \nu_\mu$ disappearance signals are contaminated with these processes and better understanding of them is needed.

The MiniBooNE collaboration provided the datasets for high-statistic cross sections measurements for charged current single π^+ and π^- production (Refs [145, 146]). In both cases the signal is defined as a muon, exactly one π. The contributions to such events come from various scenarios, discussed in 2.4.4.3.4.

In this section the MB data is compared to GENIE, NEUT and NuWro predictions. The results depend on the nucleon-level cross section, as well as on the final state interactions, handled differently in each generator. Both GENIE and NEUT use the Rein-Sehgal model [51], the former up to the hadronic invariant mass $W = 1.7$ GeV, while the latter up to $W = 2$ GeV. In NuWro only the Δ resonance is included along

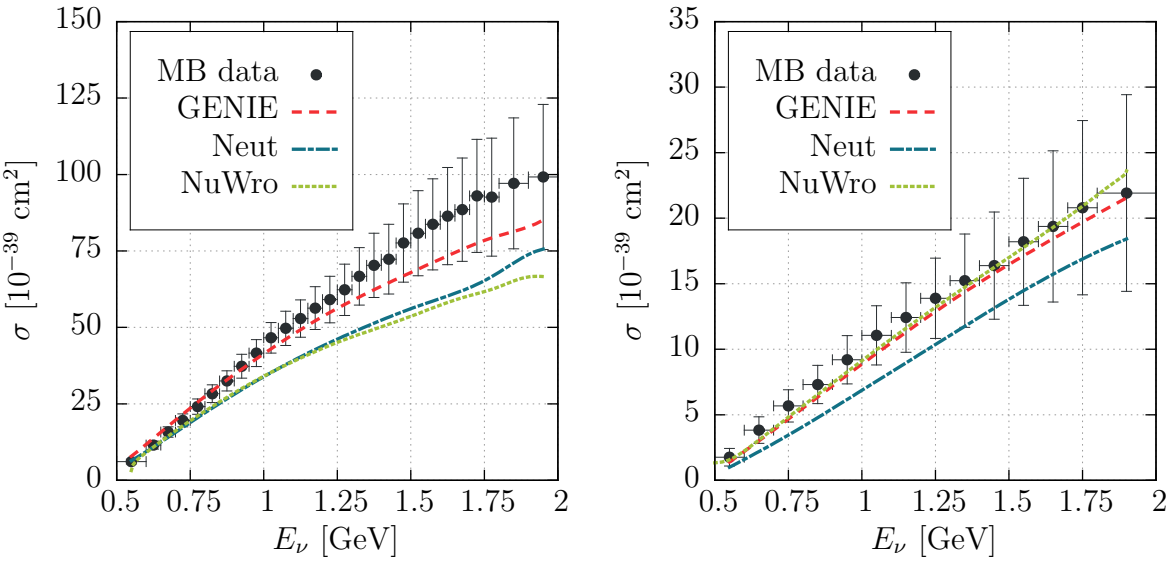

(a) $1\pi^+$ production

(b) $1\pi^0$ production

Figure 3.1: The total CC cross section for single pion production.

with the non-resonant background calculated from the DIS formalism. NEUT uses intra-nuclear cascade based on the Oset model tuned to the experimental data. Final state interactions in GENIE comes from fits to πA and pA data.

In Fig. 3.1 the total cross section as a function of neutrino energy is shown. All generators are in a good agreement for π^0 production (Fig. 3.1b). However, in the case of charged pion (Fig. 3.1a) the cross section is underestimated. Despite the fact that GENIE and NEUT have similar models for pion production in primary vertex, their results differ significantly, which is probably caused by different approach to FSI.

Figs 3.2 - 3.4 shows the differential cross sections over Q^2, muon kinetic energy and pion kinetic energy or momentum. Ignoring the normalization, the shape agreement in Q^2 and T_μ variables is quite good (see Ref. [147] for more detailed analysis). The largest discrepancy between generators is found, when one looks at pion momentum / energy distributions (Fig. 3.4). Both, kinematics of primary vertex, as well as FSI model for pion, may be a reason for that.

The pion angle distribution for neutral pion production is presented in Fig. 3.5. The shape is exactly the same for GENIE and NEUT, while NuWro predicts more forward going pions.

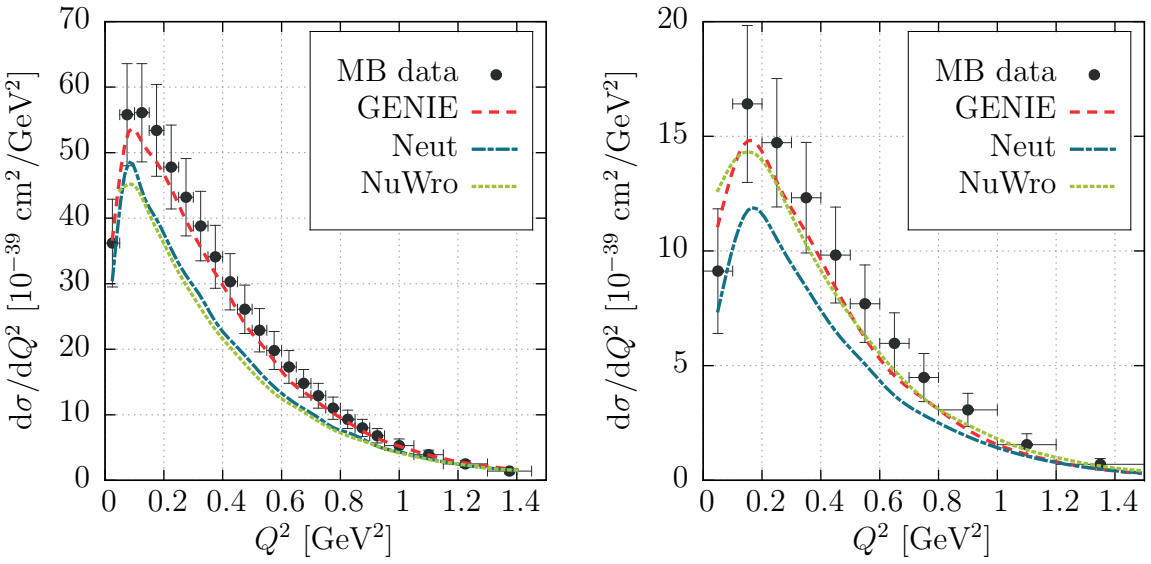

(a) $1\pi^+$ production

(b) $1\pi^0$ production

Figure 3.2: The differential CC cross section over Q^2 for single pion production.

3.4 Other MC comparisons

In this section the predictions of GENIE, NEUT, NUANCE and NuWro for other observables, suggested by physicists from several neutrino experiments, are considered.

The first observable is protons (with $T_k > 50$ MeV) multiplicity in neutrino-argon CC interactions for two values of incident neutrino energy: $E_\nu = 1$ GeV and $E_\nu = 3$ GeV (see Fig. 3.6). The predictions depend mainly on the nucleons cascade model. However, a relevant impact comes also from the model of pion absorption, giving a significant contribution to multi-nucleon events.

The differences between MC predictions are quite large. In the case of $E_\nu = 3$ GeV NuWro produces more events with only one proton in the final state than other generators[2]. Most likely the reason for that lies in the treatment of the formation zone effect, which decreases a probability of re-interactions. FZ is smaller for lower energies, so the difference at $E_\nu = 1$ GeV is also smaller. GENIE and NEUT have a relatively good agreement with each other, while NUANCE produces more multi-proton events than other generators. Note, the preliminary results for protons multiplicity from the ArgoNeuT experiment discussed in 2.4.3.3.

Total visible energy, defined as the sum of kinetic energies of all protons and total

[2]Note, that recently, the in medium modification of the NN cross section, based on Ref. [100], was introduced in NuWro. It may change the nucleon multiplicity.

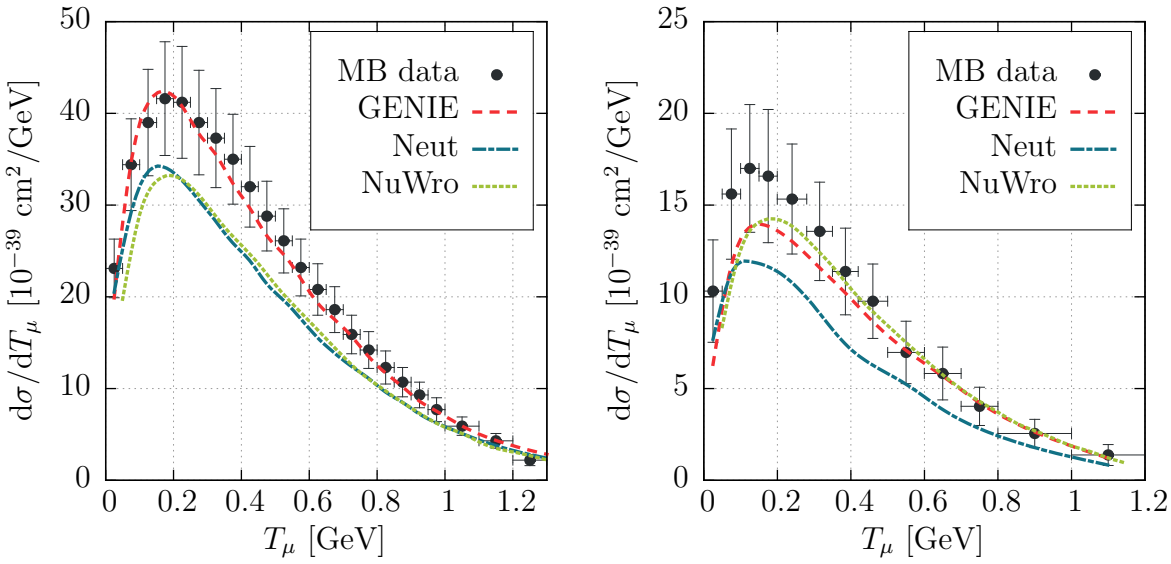

(a) $1\pi^+$ production

(b) $1\pi^0$ production

Figure 3.3: The differential CC cross section over muon kinetic energy for single pion production.

energies of all mesons and charged lepton, for neutrino energy $E_\nu = 3$ GeV, in the case of neutrino-argon CC scattering is presented in Fig. 3.7. The loss of the initial energy is related to the number of neutrons in the final state and the treatment of losing energy by nucleons due to FSI effects. The predictions, again, are not satisfactorily consistent.

As it was mentioned, NuWro uses a model of FZ with a dependence of the effect on the incident neutrino energy. For $E_\nu = 3$ GeV it significantly decreases the number of re-interactions and it results in lower energy loss, comparing to other generators. The highest energy loss is predicted by NEUT.

Having in mind the protons multiplicity disagreement, one can assume the same situation to hold true also for neutrons. This is probably the main reason of the difference in the MC results. It would be also interesting to investigate the total energy carried by all particles in the final state to check the size of the difference in modeling nuclear potential in MC generators.

The next presented observable is the momentum of the most energetic proton in neutrino-argon CC interactions for $E_\nu = 1$ GeV (see Fig. 3.8). Only events with no meson in the final state are taken into account. The MC predictions are shown for four cases: events with only one, two, three or more protons in the final state. Together they are all normalized to 100 events. A cut on the proton kinetic energy $T_k > 50$ MeV is applied. Opposite to protons multiplicity (Fig. 3.6) these results depend not only on

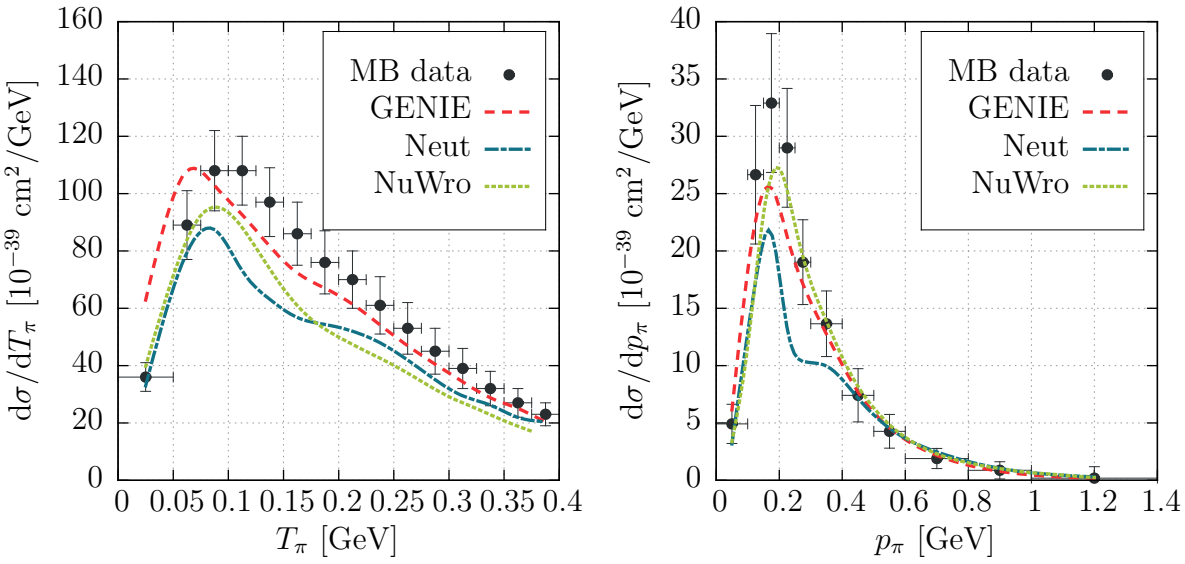

(a) $1\pi^+$ production

(b) $1\pi^0$ production

Figure 3.4: The differential CC cross section over pion kinetic energy/momentum for single pion production.

the cross sections model used in nucleons cascade, but also on kinematics.

There is quite good agreement for all MC generators in the case of events with only one proton in the final state. When the protons number becomes larger (the effect of FSI), the differences in predictions start to increase, both in shape and in normalization. The kinematics of the elastic nucleon-nucleon scattering and the pion absorption process have the crucial impact on the distributions for multi-proton events. A treatment of the nuclear potential influence on the nucleons energy may also be important.

Two-dimensional distribution of π^+ energy vs cosine of scattering angle (respect to the neutrino beam) in the case of 5 GeV neutrino CC scattering off carbon is presented in Fig. 3.9. Only events with single π^+ (and no other mesons) in the final state are considered.

One can see much better agreement between predictions as for nucleon observables. This is a result of intensive studies on pion cascade models made over last few years in the MC generators community, which were triggered by the need for a better estimation of backgrounds for QEL scattering processes, coming from events with a single pion produced in the primary vertex and absorbed during FSI.

GENIE and NuWro results are very similar, but GENIE predicts larger smearing of the distribution. NEUT has a sharp peak around $T_k \sim 0.5$ GeV for forward directions. The distribution is sensitive to both: single pion production process in the primary

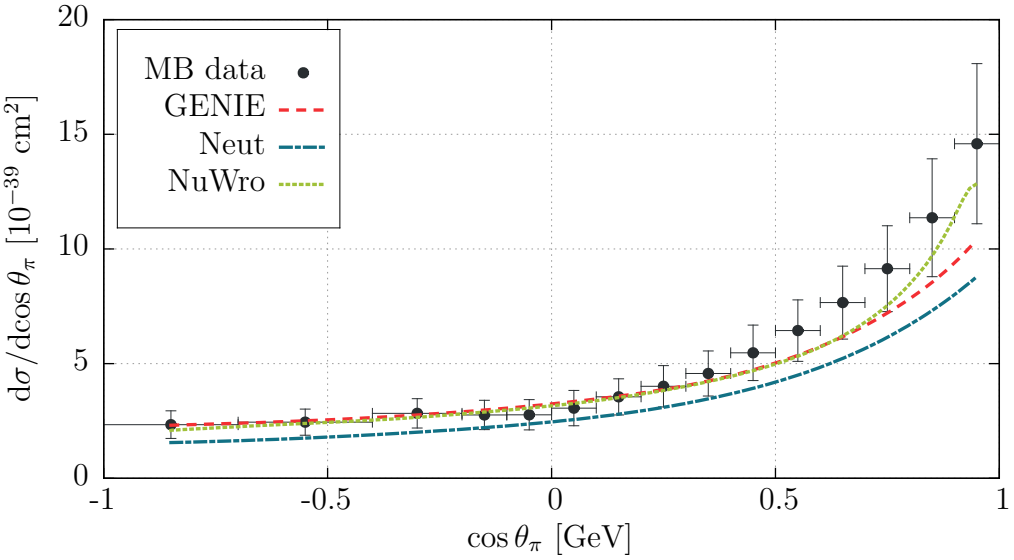

Figure 3.5: The pion scattering angle distribution for CC $1\pi^0$ production.

vertex and the FSI model.

It is clearly seen from the results presented in this section, that FSI for nucleons was not studied as intensively as for pions. The disagreement in simple observables like proton multiplicity or total visible energy is disturbing and motivates further studies on nucleon cascade models.

Predictions for GENIE, NEUT and NUANCE were provided by Hugh Gallagher, Yoshinari Hayato and Sam Zeller, respectively. More comparisons can be found in Ref. [148].

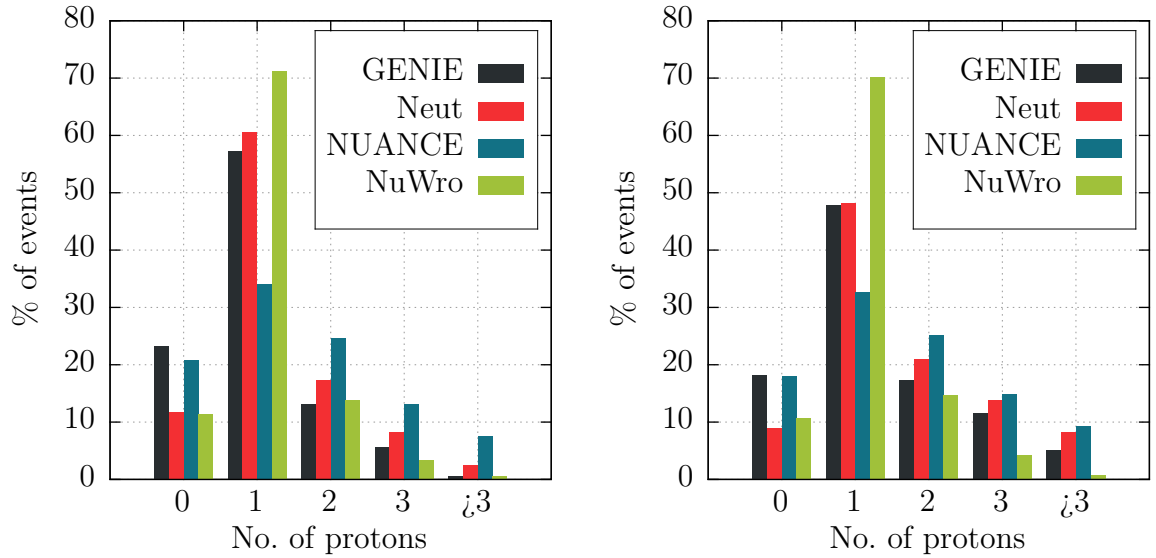

(a) $E_\nu = 1$ GeV (b) $E_\nu = 3$ GeV

Figure 3.6: Protons with $T_k > 50$ MeV multiplicity in the neutrino-argon CC interaction with no meson in the final state.

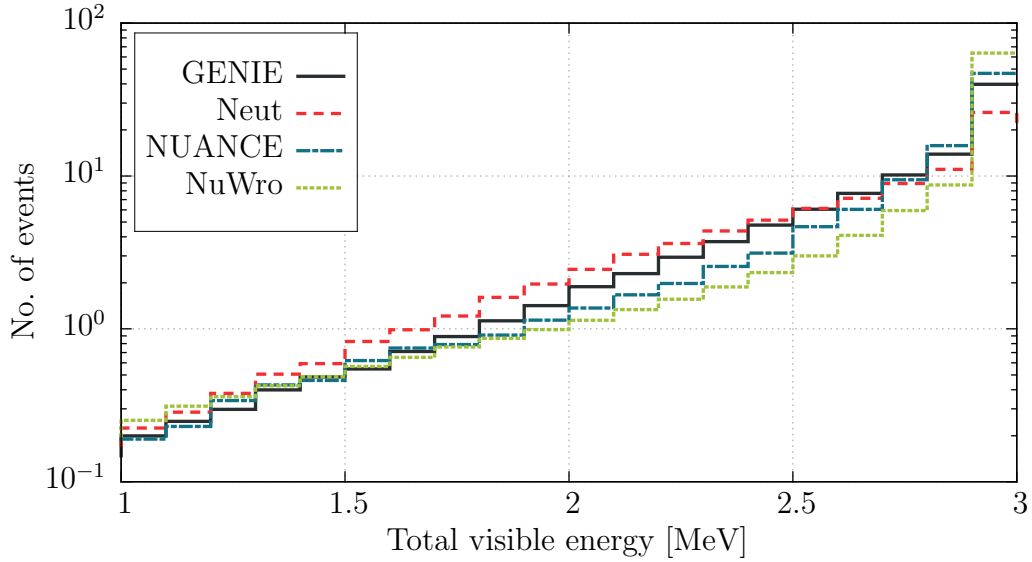

Figure 3.7: Total visible energy (the sum of kinetic energies of protons and total energies of mesons and charged leptons) in the neutrino-argon CC interactions for the neutrino energy $E_\nu = 3$ GeV.

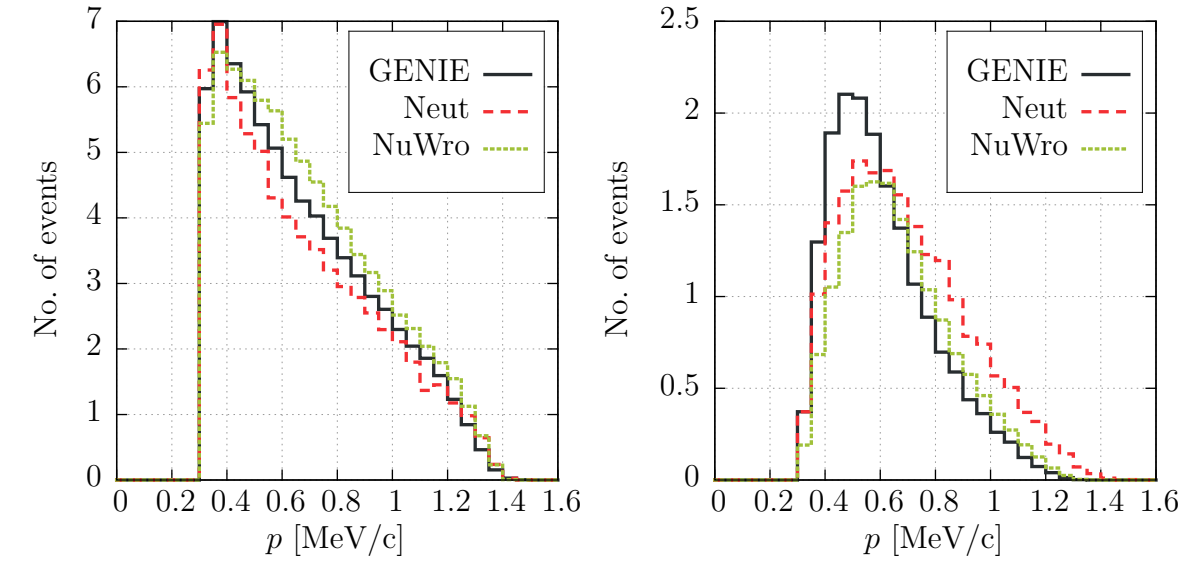

(a) Events with 1 proton

(b) Events with two protons

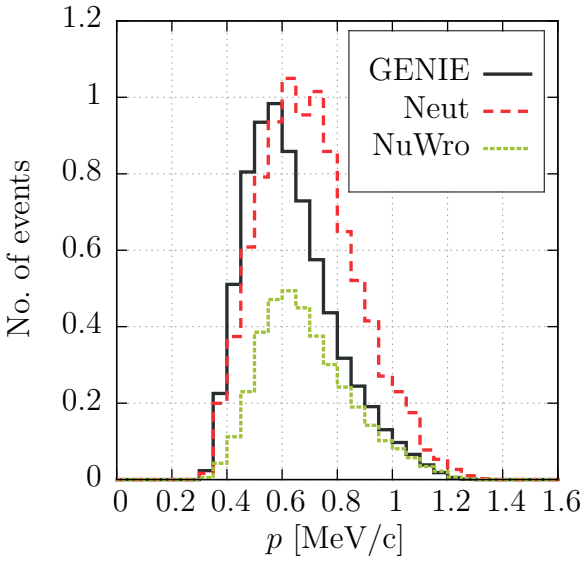

(c) Events with 3 protons

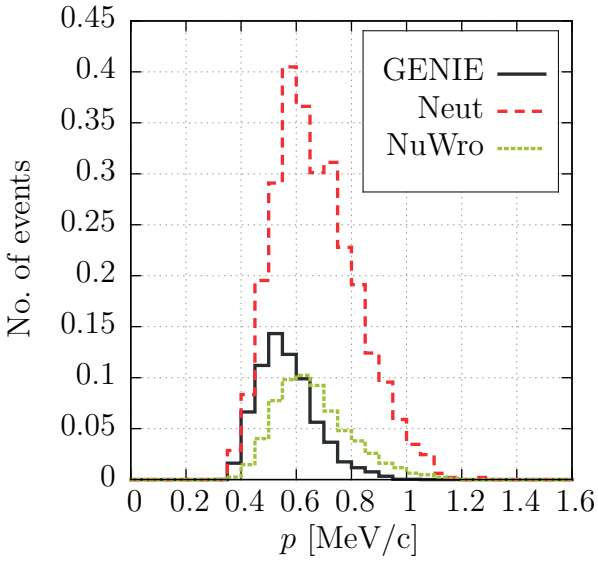

(d) Events with more than 3 protons

Figure 3.8: The most energetic proton momentum in the neutrino-argon CC interactions with no meson in the final state for neutrino energy $E_\nu = 1$ GeV. Only protons with $T_k > 50$ MeV are taken into account.

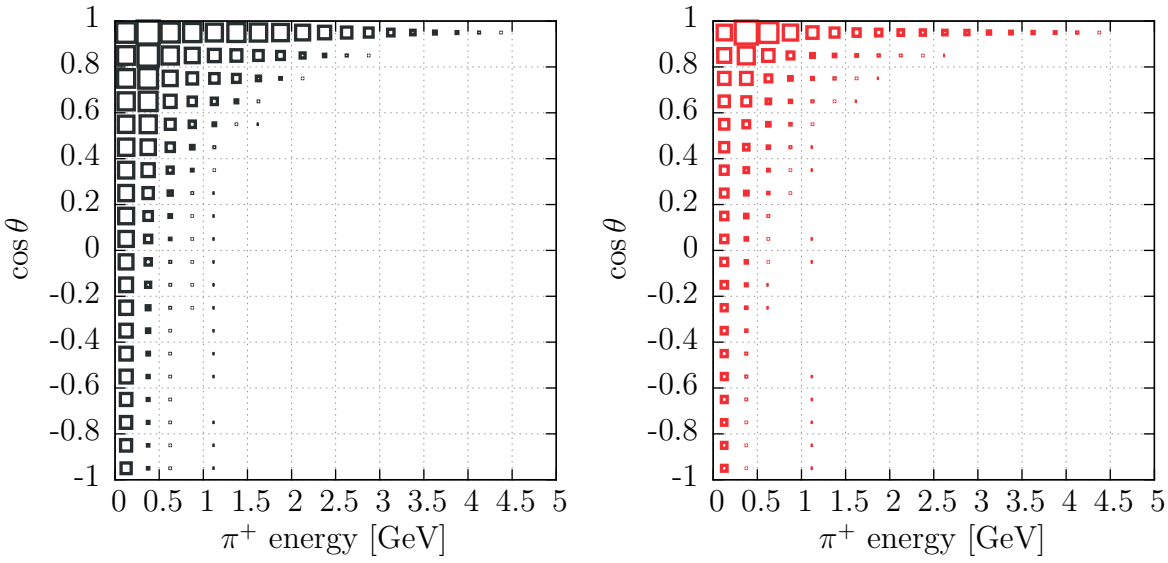

(a) GENIE

(b) Neut

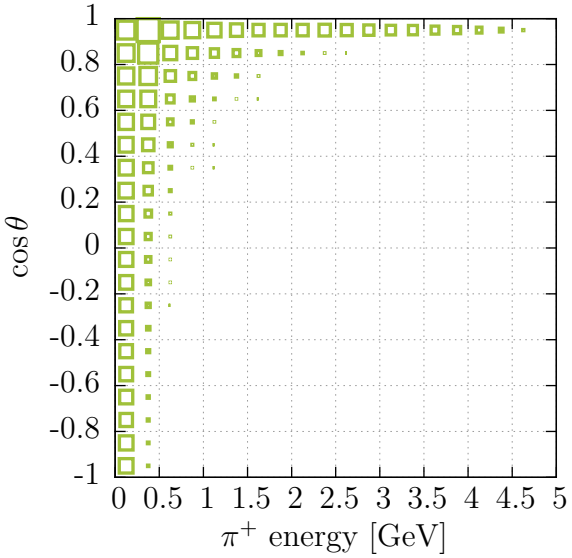

(c) NuWro

Figure 3.9: π^+ total energy vs cosine of the scattering angle distribution in the case of 5 GeV neutrino-carbon CC interaction. Only events with single π^+ (and no other mesons) are taken into account. The fields of the boxes are proportional to the cross section.

Chapter 4

The analysis of the MiniBooNE data for NC elastic scattering

The MiniBooNE collaboration measured the flux averaged NCEL differential cross section on the CH_2 target. Two observables were considered. The first one is the distribution of events in the total reconstructed kinetic energy of the final state nucleons. This measurement is based on the MB detector ability to analyze scintillation light in the absence of Cherenkov light from the final state muon. In the second observable a proton enriched sample of events with the kinetic energies above the Cherenkov radiation threshold is analyzed. This observable is defined as the ratio of the cross section for the proton enriched sample to the total NCEL-like (events with no pions in the final state) cross section.

The MB collaboration made two separate parameter extractions. Assuming $g_A^s = 0$ (see Eq. 2.17) the value of $M_A^{eff} = 1.39 \pm 0.11$ GeV was obtained from the first observable. Taking the value $M_A^{eff} = 1.35$ GeV from the CCQE analysis (Ref. [41]), $g_A^s = 0.08 \pm 0.26$ from the proton enriched sample of events was found. The description of both data samples in terms of $M_A^{eff} \sim 1.35$ GeV and $g_A^s \sim 0$ is consistent. The MB collaboration did not attempt to make a simultaneous extraction of both parameters (it was only discussed in Ref. [149]).

In the MB analysis the values of M_A used in modeling scattering off carbon and off free protons were different. For protons the M_A was fixed to be 1.13 GeV. For carbon the axial mass value was treated as a free parameter. A large *effective* M_A value is expected to account for the $np - nh$ contribution present in the neutrino-carbon scattering but absent in the scattering off proton.

In this chapter the analysis of the MB NCEL data using NuWro is presented. An important difference respect to the previous studies (see e.g. Refs [150–152]) is the

inclusion of the two-body current contribution. Moreover, the NuWro predictions are compared to the quantities (visible energy) that are directly observable, so this study do not rely on the NUANCE[1] FSI model.

In the absence of other two-body current models for NC, TE model is used in the analysis. As it was discussed in Subsec. 2.2.5, TE model does not properly describe the energy transfer to two-nucleon system. It affects the final nucleon energy distribution, which is discussed in Subsec. 4.3.2.

This chapter is organized as follows: the unfolding procedure is described in Sec. 4.1 and the NuWro-based analysis without and with the $np-nh$ contribution is presented in Secs 4.2 and 4.3, respectively.

4.1 The unfolding procedure

Two data samples provided by the MB collaboration are discussed. The first one (the NCEL sample) contains the distribution of the total reconstructed kinetic energy of all nucleons in the final state, normalized to the number of events seen in the detector.

The second data sample (the NCEL high energy sample) is provided in a form of the ratio:

$$\eta = \frac{\tilde{X}(\nu p \to \nu p)}{X(\nu N \to \nu N)} \tag{4.1}$$

where $\tilde{X}$ denotes a contribution from the special class of events, called single proton or proton enriched. Those are events with visible Cherenkov light and the proton scattering angle $\theta < 60^0$. In the MC simulations the largest contribution to those events comes from the NCEL scattering on protons, which then do not undergo re-interactions. In the case of multiple proton events, the energy of an individual proton is in general too low to produce Cherenkov light. Even if a high energy proton appears in the multiple proton event, it has typically larger scattering angle than protons unaffected by FSI. The denominator (X) denotes the contribution from all the NCEL-like (no charged lepton nor pion in the final state) interactions.

Both data samples are presented as a function of reconstructed energy[2] (ν), measured in the detector. To compare this data with the theoretical predictions given in terms of the true kinetic energy (μ), one needs the unfolding procedure, allowing a passage from μ to ν.

[1] NUANCE was used by the MB collaboration in the data analysis.
[2] The original notations from Ref. [149] is kept.

In Subsec. 4.1.1 the original MB unfolding procedure is described. The treatment of $np-nh$ events, not considered in the MB analysis, is discussed in Subsec. 4.1.2.

4.1.1 MiniBooNE unfolding procedure

For all but $np-nh$ events the approach proposed by Perevalov (Ref. [149]) is used. For both data samples the unfolding procedure is similar. Five types of events giving the contribution to the final distributions are considered:

1. NCEL on hydrogen;
2. NCEL on a proton from carbon unaffected by FSI;
3. NCEL on a proton from carbon affected by FSI;
4. NCEL on a neutron from carbon;
5. irreducible background (pions produced in the primary vertex and absorbed due to FSI effects).

For each type of the signal events, $k = 1, 2, ..., 5$, there is a response matrix ($R^{(k)}$) provided in Ref. [153], which simulates the energy smearing, the detector efficiency and defines a relation between true and reconstructed energy distributions:

$$\nu_j^{(k)} = \sum_i R_{ij}^{(k)} \mu_i^{(k)} \tag{4.2}$$

$R^{(k)}$ are either 51x51 or 30x30 matrices for the two data samples, respectively. The columns of matrices label the true kinetic energy bins and rows label the reconstructed kinetic energy. There are 50 bins starting from 0 MeV up to 900 MeV plus an extra overflow bin for the NCEL sample in the true kinetic energy. For NCEL high energy sample there are 28 bins, starting from 300 MeV up to 900 MeV plus underflow and overflow bins. The graphical representation of the response matrices can be found in App. B.

To obtain the reconstructed kinetic energy distribution and compare with the data one goes through the following steps:

1. use a theoretical model and calculate the flux-averaged distributions for five different signal events using the same bins as in the response matrices;
2. use the proper response matrices to translate each histogram to the reconstructed kinetic energy distribution;

3. sum all the histograms and add the background events (ν^{BKG} contains dirt, beam-unrelated, and other background provided by the MB collaboration in Ref. [153]) to get the total reconstructed energy spectrum:

$$\nu_j^{MC} = \sum_k \nu_j^{(k)} + \nu_j^{BKG} \tag{4.3}$$

4. use the provided error matrices (M_{ij}) to calculate χ^2:

$$\chi^2 = \sum_i \sum_j \left(\nu_i^{DATA} - \nu_i^{MC}\right) M_{ij}^{-1} \left(\nu_j^{DATA} - \nu_j^{MC}\right) \tag{4.4}$$

Unlike the CCQE MB data published in Ref. [41] the flux normalization error is already included in the error matrices.

4.1.2 Alternative unfolding procedure

An alternative way to convert the true kinetic energy to the reconstructed one is to translate it on the event by event basis. For each value of the true kinetic energy the corresponding column in the response matrix gives a probability distribution with the information how the given true energy value is smeared out in the detector, normalized to the efficiency. To obtain the reconstructed kinetic energy distribution one proceeds as follows:

1. for each event calculate the total true kinetic energy of all nucleons in the final states (μ) and get a bin number j;
2. find the type of signal (k), see Subsec. 4.1.1;
3. choose j-th column of the $R^{(k)}$ response matrix as the probability distribution;
4. use the MC method to decide if the event is accepted (according to the efficiency) and what energy is visible in the detector.

4.1.2.1 The unfolding procedure for the two-body current events

In the $np-nh$ events there are typically two hit nucleons after a primary interaction and both propagate through a nucleus. In the MB analysis there are no $np-nh$ events included and no response matrices were prepared for them. To take two-body current events into account, they must be expressed in terms of five signals defined in Subsec. 4.1.1.

A naive interpretation may suggest a treatment of each nucleon from the $np-nh$ events separately. However, it would be incorrect. The signal is recorded by photomultiplier tubes (PMT), which absorb the light emitted in the scintillator (and also the Cherenkov radiation). The event is accepted if there is a sufficient number of PMT hits. Any of two individual nucleons may have too low energy to generate enough PMT hits, but together the can make it (Ref. [154]).

In this analysis both nucleons from a two-body current event are treated together and the kinetic energies of all nucleon in the final state are summed up as if they come from only one nucleon. In the detector $np-nh$ events are seen as multiple protons events, so as signals (3) - NCEL on proton from carbon affected by FSI and (4) - NCEL on neutron from carbon.

One expects events without proton in the final state to be more smeared out in the detector, so the response matrix for the signal (4) is applied, if there are two neutrons in the primary vertex or for the signal (3) in other cases (Ref. [154]). If there is a proton in a $np-nh$ event with the scattering angle $\theta < 60^0$, its energy is translated to the reconstructed one to check if the Cherenkov light is produced and the event gives contribution to the numerator of the ratio η (Eq. 4.1).

However, in $np-nh$ events the energy transfered to the hadronic system is shared by two nucleons, and it is unlikely that there will be a proton with energy large enough to produce Cherenkov light. Thus, the $np-nh$ events usually contribute only to the numerator of the ratio η, making it smaller.

4.2 The analysis without the two-body current contribution

The numerical procedure was checked by making the analysis without $np-nh$ events and compared to the MB results.

The fixed value of axial mass for hydrogen $M_A = 1.03$ GeV was assumed and χ^2 function was minimized for the effective axial mass for carbon (M_A^{eff}) using the data for the reconstructed energy distribution. Following the MB procedure the value $g_A^s = 0$ was assumed.

The value $M_A^{eff} = 1.47 \pm 0.10$ GeV was obtained with $\chi^2_{min}/DOF = 23.6/50$ (confidence level (CL) = 99%, see Fig. 4.2a). This value is larger than the one reported by the MB collaboration ($M_A^{eff} = 1.39 \pm 0.11$ GeV), but consistent within the 1σ error bars. The discrepancy is probably caused by the presence of the pion-less Δ resonance decays

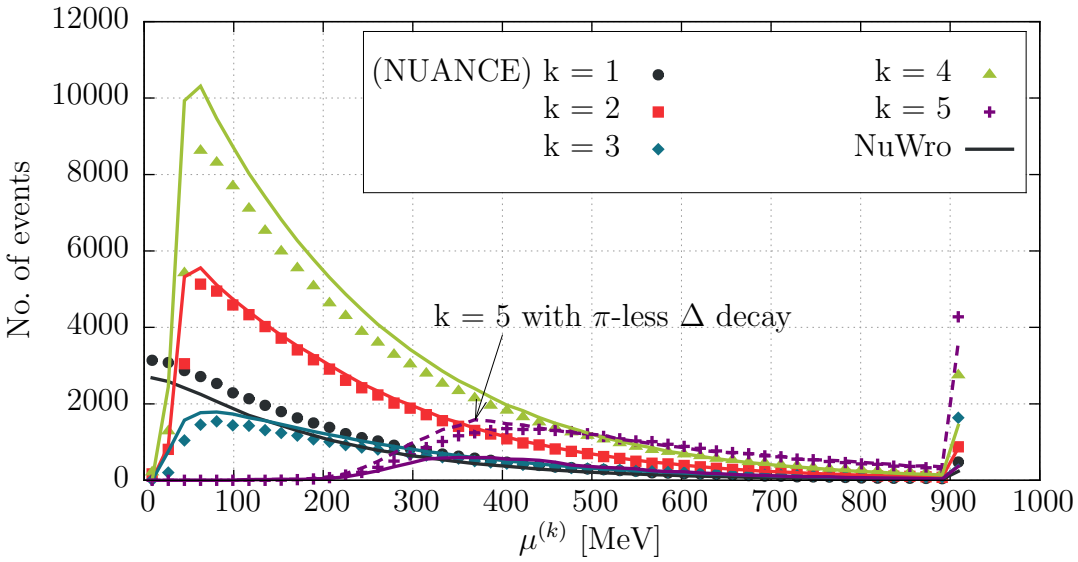

Figure 4.1: The comparison of the NUANCE (points) and NuWro (lines) predictions for the true kinetic energy distributions for each signal defined in Subsec. 4.1.1.

in the NUANCE, but not in NuWro. π-less decays is the effective in-medium modification of the Δ width, realized by the assumption that 20% of Δ decay without any pion. Fig. 4.1 shows the NUANCE and NuWro predictions for the true kinetic energy distributions for each signal defined in Subsec. 4.1.1. For all but irreducible background there is a good agreement between generators.

To investigate a possible impact of the choice of the electromagnetic form factors parametrization on the final results, the computations was repeated using the form factors corrected by a two-photon exchange (Refs [155, 156]) and almost identical results were obtained.

Using the data for the ratio η (Eq. 4.1) the strange quark contribution to the NCEL cross sections was examined. Fixed values of the axial mass values were assumed: 1.03 GeV for hydrogen and effective value 1.47 GeV for carbon. The strange quark contribution was found to be $g_A^s = 0.24 \pm 0.46$ with $\chi^2_{min}/DOF = 26.7/29$ (CL = 58.8%, see Fig. 4.2b). This result is consistent with the value published by the MB collaboration.

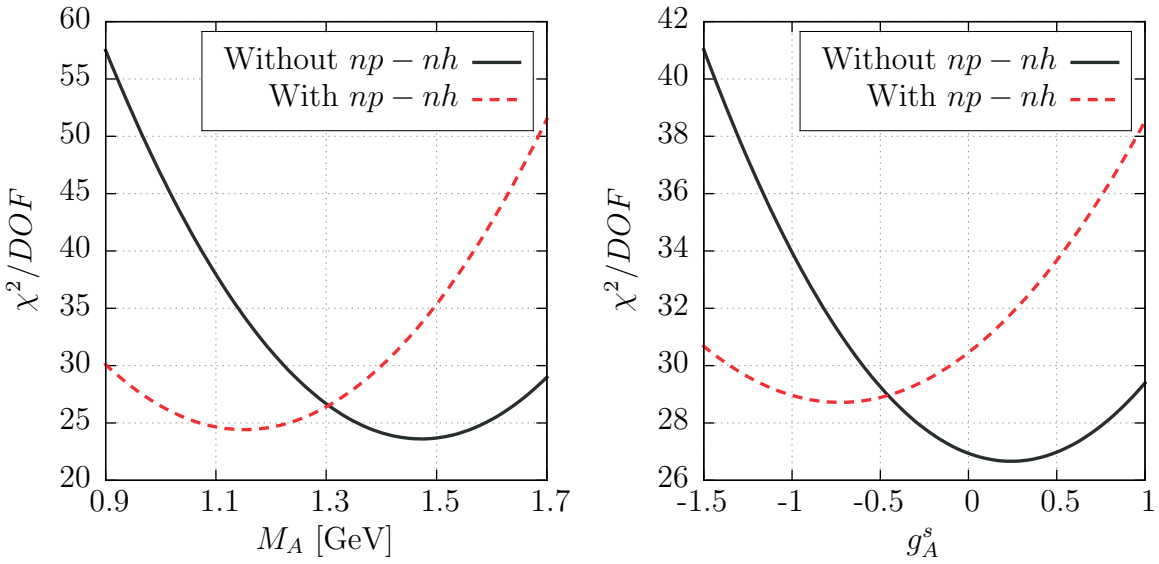

(a) χ^2 for NCEL sample.

(b) χ^2 for NCEL high energy sample.

Figure 4.2: The χ^2 distributions for NCEL and NCEL high energy samples.

4.3 The analysis with the two-body current contribution

Following the same steps the analysis was repeated including the $np-nh$ contribution. Transverse Enhancement model was used[3], as in MCs this is the only available model for NC $np-nh$ processes up to date. Assuming $g_A^s = 0$ the minimum of the χ^2 for the distribution of the total reconstructed energy of the final state nucleons was found for the axial mass value $M_A = 1.15 \pm 0.11$ GeV with $\chi^2_{min}/DOF = 24.4/50$ (CL = 99.9%). The extraction of the strangeness from the ratio η, assuming $M_A = 1.15$, leads to the value $g_A^s = -0.72 \pm 0.55$ with the $\chi^2_{min}/DOF = 28.7/29$ (CL = 48.1%), which is inconsistent with zero (as assumed in the first fit). As it was discussed, the two-body current events contribute mostly to the denominator of the ratio η making its value smaller. Also, a lower M_A makes the ratio η smaller. To compensate for both effects a lower value of g_A^s can be expected.

The inconsistency described above was motivating to make a simultaneous fit of both theoretical model parameters (see Subsec. 4.3.1). For various reasons described in details in Subsec. 4.3.2, the ratio η was no longer taken into considerations.

[3]The possible impact of the other model choice is discussed in Subsec. 4.3.2.

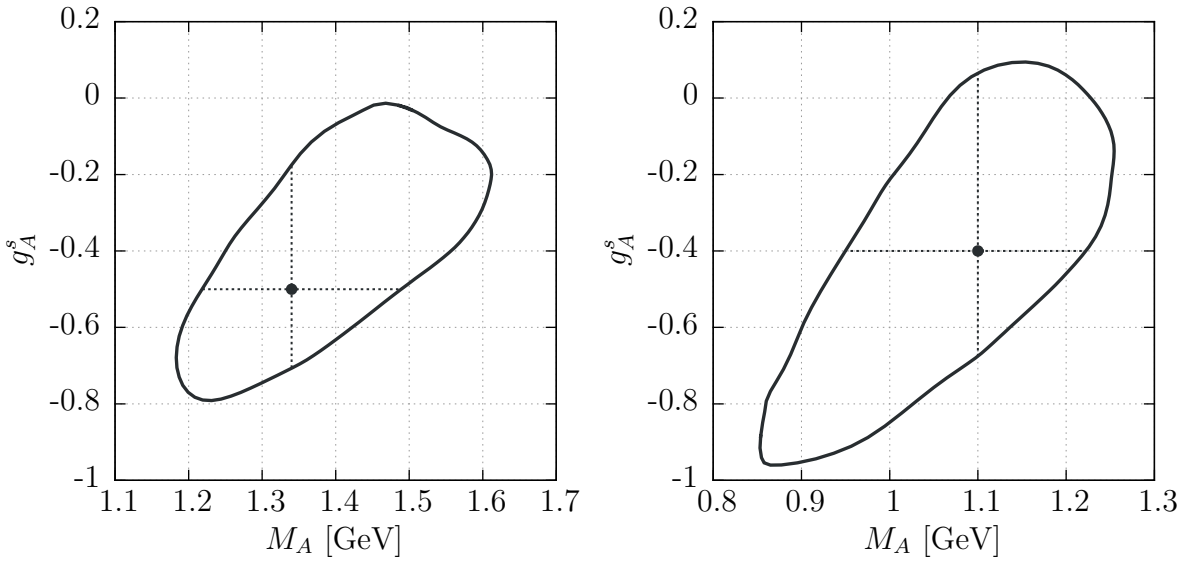

(a) Without $np-nh$ (b) With $np-nh$

Figure 4.3: 1σ error contour for (M_A, g_A^s) parameters obtained from χ^2 (Eq. 4.4) for the NCEL sample. Dots are located at χ^2 minima.

4.3.1 Simultaneous extraction of M_A and g_A^s

The procedure for simultaneous extraction of M_A and g_A^s is the same as before. Again, the fixed value of the axial mass ($M_A = 1.03$ GeV) was assumed for hydrogen. The χ^2 surface in M_A and g_A^s variables was calculated for the NCEL sample. The minimum of the χ^2 function was found for the following values:

- without $np-nh$ events:

$$M_A = 1.34^{+0.15}_{-0.12} \quad \text{and} \quad g_A^s = -0.5^{+0.3}_{-0.2}$$

  with $\chi^2_{min}/DOF = 22.0/50$;

- with $np-nh$ events:

$$M_A = 1.10^{+0.12}_{-0.15} \quad \text{and} \quad g_A^s = -0.4^{+0.5}_{-0.3}$$

  with $\chi^2_{min}/DOF = 22.7/50$.

Fig. 4.3 shows the results for the simultaneous two-dimensional fits without and with the $np-nh$ contribution included in the NuWro simulations, together with 68% confidence regions. The inclusion of the two-body current events makes the best fit

result for M_A consistent with the world average. It confirms that the difference between recent and older axial mass measurements can be explained by taking into account the $np-nh$ contribution. The value of the strange quark contribution is found to be consistent with zero.

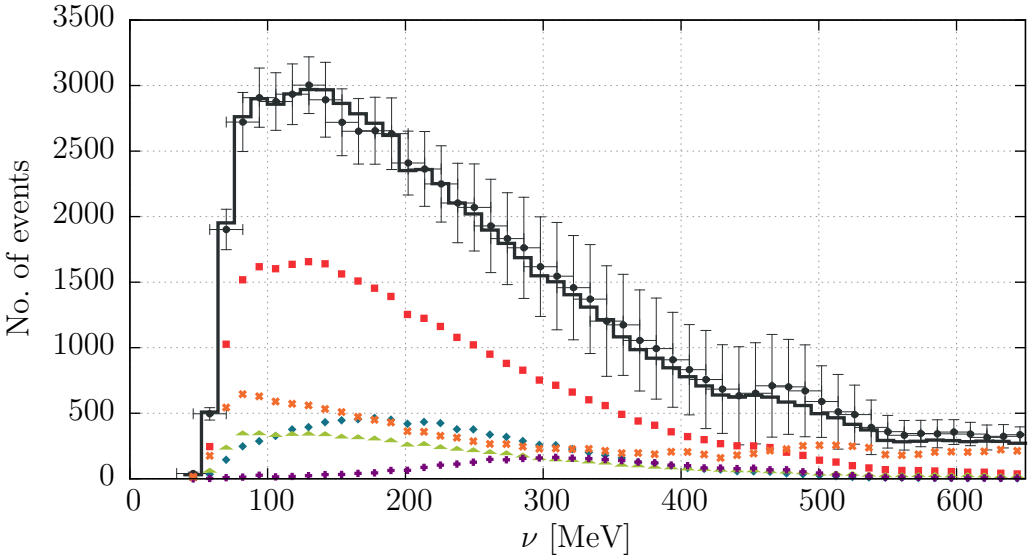

(a) NCEL sample

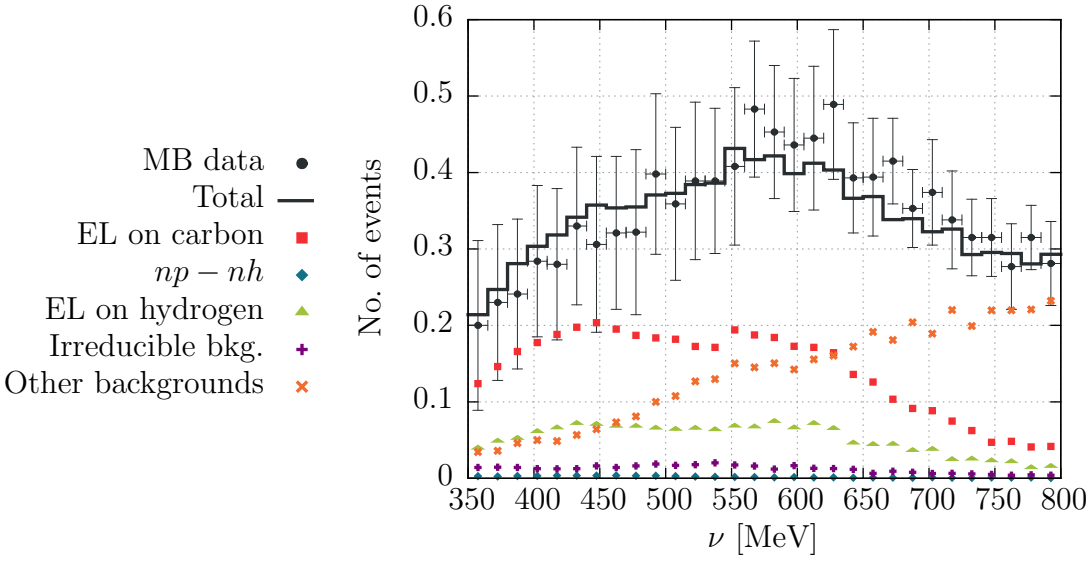

(b) NCEL high energy sample

Figure 4.4: NCEL and NCEL high energy sample distributions, broken down to individual contributions. The NuWro result is obtained with the $M_A = 1.10$ GeV and $g_A^s = -0.4$ values.

The simultaneous extraction of the M_A and g_A^s parameters was discussed in Ref. [149]. The χ^2 surface was calculated for the values of M_A and g_A^s from the region 1.0 GeV to 1.5 GeV and -0.5 to 0.5, respectively. The minimum of χ^2 was found for $M_A = 1.23$ GeV and $g_A^s = -0.5$. However, the author argued that due to a normalization variation g_A^s gets too far from $g_A^s = 0$ value. The further study for restricted value of $g_A^s = -0.2 \pm 0.1$ (suggested by the BNL E734 experiment Ref. [157]) lead him to the conclusion, that there is a little dependence on g_A^s in NCEL sample.

The NuWro prediction (broken down to individual contributions from elastic scattering on carbon and hydrogen, two-body current contribution, irreducible background and other backgrounds) for the best fit values of the M_A and g_A^s parameters is compared to the MB data in Fig. 4.4a. The contribution coming from the $np-nh$ events amounts to approximately 15% of the overall distribution affecting both its shape and the normalization. As the sum of the kinetic energies of all nucleons in the final state is investigated, the results is not very sensitive on the assumptions made on the $np-nh$ kinematics in 2.2.5.1.

The prediction for the ratio η obtained with the same M_A and g_A^s values together with the contributions to the numerator coming from various signal events is presented in Fig. 4.4b. The value of χ^2 obtained with $M_A = 1.10$ and $g_A^s = -0.4$ for the ratio is equal $\chi^2/DOF = 30.2/29$. It means that the reported values are consistent also with the proton enriched sample observable.

As mentioned in 2.4.4.2.1 the formation zone for the $np-nh$ events is assumed to be zero. In order to estimate how important the FZ effect can be for this analysis, the computations were repeated assuming the formation length for $np-nh$ events to be 1 fm. It turns out that this assumption does not affect the final results in a statistically relevant way.

The impact of the uncertainty of the value of p_{CC} parameter (see 2.2.5.2) was also investigated. The default value $p_{CC} = 0.6$ was replaced by $p_{CC} = 0.8$ and the computations were repeated. No significant influence on the final results was found.

4.3.2 The ratio η issue

The investigation of the NCEL high energy sample lead to the conclusion that the ratio η is very sensitive to many details of the theoretical model. From Fig. 4.4b it is clearly seen that η depends strongly on other backgrounds. Above 350 MeV of the kinetic energy a significant contribution comes from irreducible background, known with a precision not better than 20-30%. The choice of the $np-nh$ model strongly affects the final nucleons kinematics (see Fig. 2.7). One can expect that it also affects the number

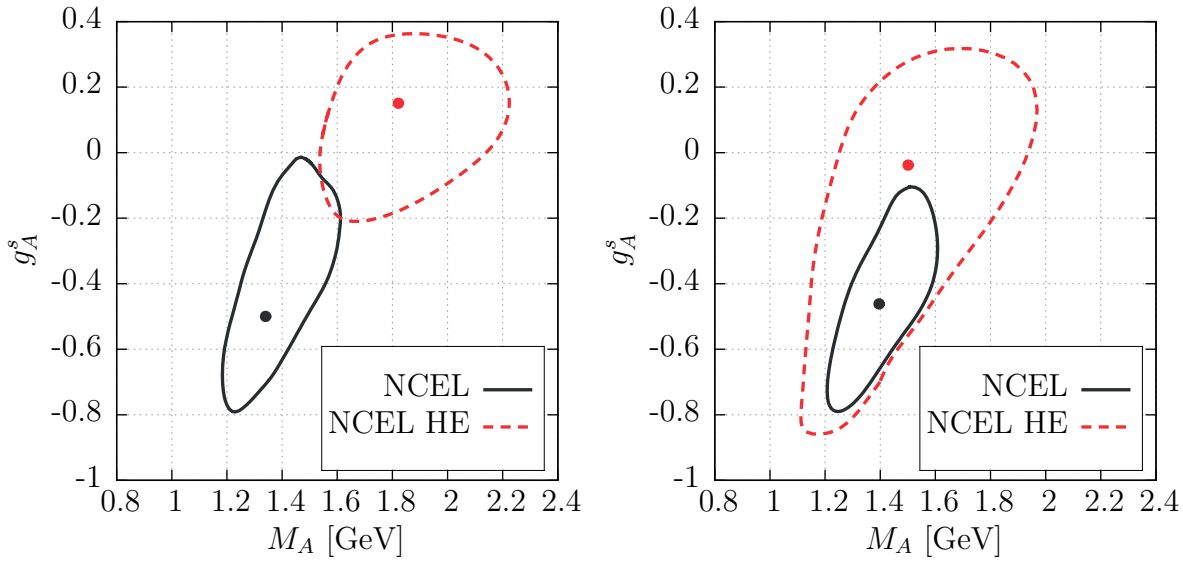

(a) With NuWro prediction for irreducible background

(b) With NUANCE prediction for irreducible background

Figure 4.5: 1σ error contour for the (M_A, g_A^s) parameters obtained from χ^2 (Eq. 4.4) for the NCEL and NCEL high energy samples without the $np-nh$ contribution. Dots are located at χ^2 minima.

of protons above the Cherenkov threshold and the predictions for the ratio η.

4.3.2.1 The ratio η and irreducible background

As it was discussed in Sec. 4.2, the prediction for irreducible background depends on including or not the π-less Δ decays. To check how it affects the results, the simultaneous extraction of the M_A and g_A^s parameters to both MB observables was done for two cases (without the $np-nh$ contribution):

1. the NuWro predictions for all five signals (see Subsec. 4.1.1) were used to calculate χ^2;
2. the NuWro predictions for first four signals and the NUANCE one for irreducible background were used to calculate χ^2.

The results are presented in Fig. 4.5[4]. When π-less Δ decays are not applied (Fig. 4.5a), two observables are barely consistent within 1σ error. In the other case (Fig. 4.5b), the predictions for NCEL and NCEL high energy samples are consistent.

[4]Please note, that due to the need for high computing power to calculate χ^2 surface the results suffers on statistical fluctuations. The plots are smoothed using Bezier curves.

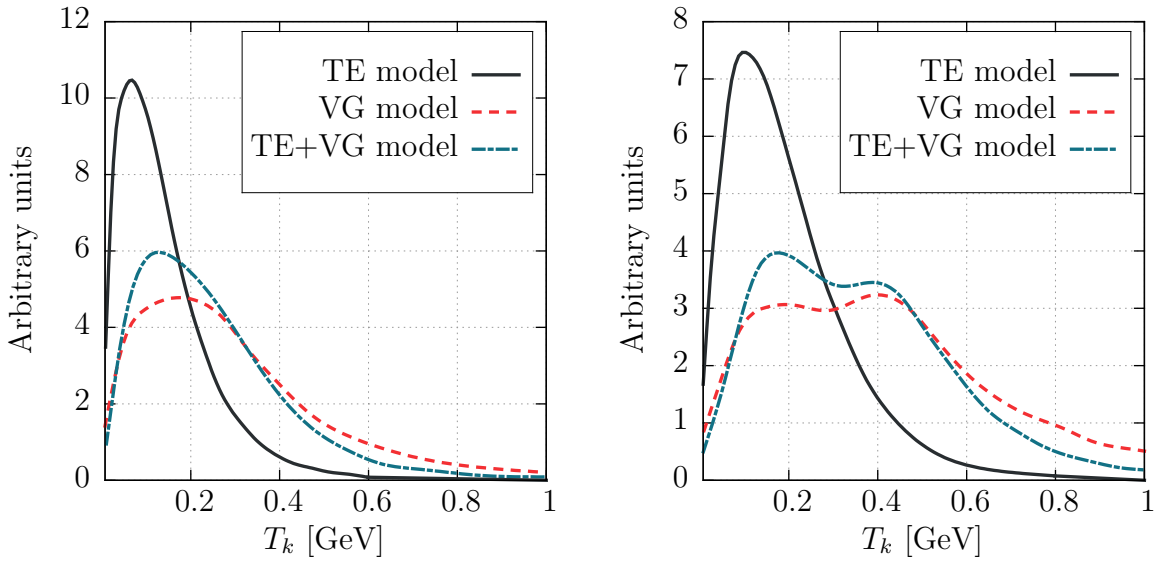

(a) The kinetic energy of the most energetic nucleon in the final state.

(b) The total kinetic energy of all nucleons in the final state.

Figure 4.6: The comparison of the nucleon kinematics in TE, Nieves and TE+Nieves models (for CC scattering off carbon with MB flux).

It is worth noting, that the ratio η strongly depends on the prediction for irreducible background, which does not happen in the case of NCEL sample.

4.3.2.2 The ratio η and the $np-nh$ model

As it was mentioned, the only available model for neutral current $np-nh$ events in NuWro is Transverse Enhancement model. The total cross section, introduced by the modification of the vector magnetic form factors, is in a good agreement with microscopic calculations. However, the QEL-based kinematics does not properly describe the energy transfer distribution (see Fig. 2.6), which affects final nucleon momenta.

To estimate the impact of using the phenomenological TE model instead of one of the theoretical calculations, the TE+Nieves toy model is introduced. The cross section and the lepton scattering angle are obtained from the TE differential cross section (Fig. 2.6d, but based on the established angle the lepton kinetic energy is obtained from the Nieves kinematics distribution (Fig. 2.6a) using MC methods (for NC processes lepton mass is set to zero).

In Fig. 4.6 there is the comparison of the nucleon kinematics in TE, Nieves and TE+Nieves models. The MB flux was used in the simulations and carbon was set as a target. The kinetic energy of the most energetic nucleon is shown in Fig. 4.6a and

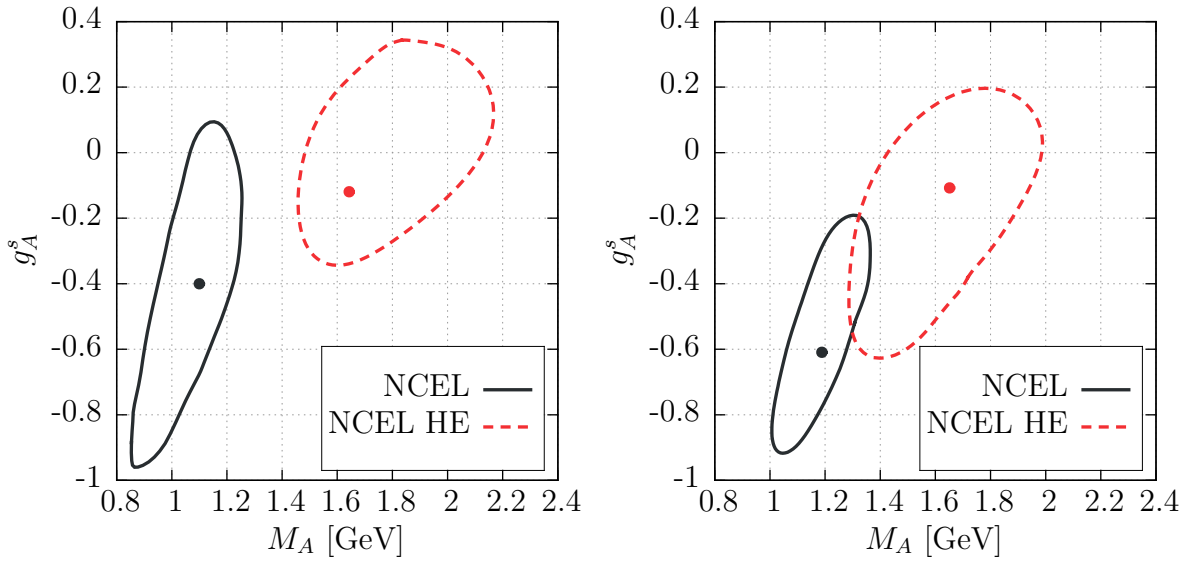

(a) TE model

(b) TE+Nieves model

Figure 4.7: 1σ error contour for the (M_A, g_A^s) parameters obtained from χ^2 (Eq. 4.4) for the NCEL and NCEL high energy samples with the $np-nh$ contribution. Dots are located at χ^2 minima.

the sum of kinetic energies of all nucleons in the final state is presented in Fig. 4.6b. The TE+Nieves "toy model" reconstructs the nucleon kinematics from original Nieves model quite well.

The extraction of the M_A and g_A^s parameters for both MB observables was done using pure TE and TE+Nieves models. The results are presented in Fig. 4.7. The analysis with pure TE model leads to the conclusion that NCEL and NCEL high energy samples are inconsistent within 1σ error. However, when TE+Nieves model is applied, the observables comply.

As one could expect, the ratio η is much more sensitive on the choice of the $np-nh$ model than NCEL sample. Further studies on the NC two-body contribution in the context of the MB data for high energy sample can discriminate between the models.

Summary

NuWro neutrino event generator was presented in the thesis. The primary neutrino interactions for charged and neutral currents were described:

- (quasi-)elastic scattering within the Llewellyn-Smith formalism;
- pion production through $\Delta(1232)$ resonance excitation within the Adler-Rarita-Schwinger formalism, together with non-resonant background;
- deep inelastic scattering within the quark-parton model;
- coherent pion production within the Rein-Sehgal model;
- two-body current contribution within Nieves, Martini, MEChM and Transverse Enhancement models.

Few approaches for the description of nuclei, including Fermi gas and spectral function, were presented. The results obtained using each of them were compared within several observables.

The final state interactions model was discussed in more detailed way. The propagation of nucleon and pion through nuclear matter was described within Metropolis and Oset models. The high-energy extensions for these models were proposed.

The formation time was introduced and most common parametrizations of this effect were presented. The impact of the formation time on the results was investigated.

NuWro predictions were compared to various experimental data and the results of other Monte Carlo generators.

Finally, the complete analysis of MiniBooNE data for neutrino-CH_2 neutral current elastic scattering were performed. It was the first analysis of this data made with the inclusion of the two-body current contribution.

Appendix A

Params.txt

NuWro uses by default the *params.txt* file located in "nuwro" directory. If the file does not exist, the one from "nuwro/data" folder is loaded. If both files are missing or some of the parameters are not set in the file, default values are used. In the table below one can find a detailed description of all parameters.

Parameter name	**Possible arguments**	**Default value**	**Description**
General settings			
number_of_events	any positive integer number	100 000	The number of equally weighted events to be saved in the output ROOT file *(eventsout.root)*.
number_of_test_events	any positive integer number	1 000 000	The number of events used to calculate cross sections (not saved by default).
user_events	0, 1	0	Used to turn on the fitting procedure: 0 - Run NuWro; 1 - Fit axial mass to MiniBooNE data for CCQE.

user_params *(use with user_events 1)*	x y z	-	Parameters for the axial mass extraction procedure: x - the minimum axial mass value; y - the maximum axial mass value; z - the axial mass step.
random_seed	any positive integer number	0	Controls the random seed persistence: 0 - use time(NULL) as a seed for the random number generator; 1 - read state from "random_seed" file or use seed=time(NULL), if the file was not found; n - use x as the seed for the random number generator.
mixed_order	0, 1	1	If 1, events are saved to the output file in random order.

save_test_events	0 - 2	0	Turn on to use test events in the analysis: 0 - test events are not saved; 1 - test events are finalized and stored in *weight.eventsout.root* file, the average weight is equal to the total cross section; 2 - test events of non-zero weights are finalized and stored in *weight.eventsout.root* file, the weights are respectively scaled, so the average weight is equal to the total cross section.
Beam specification			
beam_direction	$x\ y\ x$	0 0 1	The direction of the neutrino momentum in xyz coordinates.
beam_particle *(use with beam_type 0)*	$\pm$ 12, $\pm$ 14, $\pm$ 16	14	PDG number of the incident neutrino.

beam_type	0 - 4	0	Types of beams: 0 - a single neutrino flavor beam; 1 - a mixed flavor beam; 2 - a beam loaded from a ROOT file; 3 - a beam loaded from the histogram *(histout.txt)*; 4 - create *histout.txt* file based on a ROOT file *(than use beam_type 3 to run NuWro)*.
beam_energy *(use with beam_type 0)*	(1) E (2) E_{min} E_{max} (3) E_{min} E_{max} a_0 ... a_n	1000	The energy profile: (1) set a mono energetic beam; (2) set an uniform beam with energy range from E_{min} to E_{max}; (3) set a beam with energy range from E_{min} to E_{max}, $a_i / \sum_j^n a_j$ gives a probability the energy will be drawn from $(i*\varepsilon,\ (i+1)*\varepsilon)$ interval, where $\varepsilon = (E_{max} - E_{min})/n$.

beam_content *(use with beam_type 1)*	n x% + beam_energy	*empty*	The mixed beam definition: beam_content = BC_1 beam_content += BC_2 ... BC_i = n_i x_i% BE_i, n_i is a PDG number of the incident neutrino, x_i is a percent of this kind of neutrino in the beam, BE_i is the definition of the energy range (like in beam_energy).
beam_folder *(with beam_type 2,4)*	*path*	../flux	The path to the directory with ROOT files.
beam_file_first *(with beam_type 2,4)*	any positive integer number	1	The number of the first file in the folder to be read.
beam_file_limit *(with beam_type 2,4)*	any positive integer number	0	The number of files to be loaded (0 - read files to the last one in the directory).
beam_offset	x y z	0 0 0	The offset of the position of the interaction in xyz coordinates.

beam_placement *(in cascade mode only)*	0 - 2	0	The starting position of the particle: 0 - the propagation starts at the center of the nucleus; 1 - the propagation starts at a random place inside the nucleus; 2 - the propagation starts just under the surface of the nucleus.
One can also use predefined beam specifications instead of the above parameters. The list of beams can be found in "nuwro/data/beam" directory. To use one of those beams, one must use the following line: @beam/*beamfile.txt* where *beamfile.txt* is the name of the file from "nuwro/data/beam" directory.			
Target specification			
target_type	0, 1, 2	0	Types of targets: 0 - a single nucleus; 1 - a target composed from some nuclei; 2 - a detector geometry loaded from a ROOT file.
nucleus_p *(use with target_type 0)*	any positive integer number	6	A number of protons in the target nucleus.
nucleus_n *(use with target_type 0)*	any positive integer number	6	A number of neutrons in the target nucleus.
nucleus_E_b *(use with target_type 0)*	any positive number	34	The binding potential (sum of binding and Fermi energies).

nucleus_kf *(use with target_type 0)*	any positive number	220	The Fermi momentum.
nucleus_target	0 - 5	2	Nucleus models used in a primary interaction: 0 - free nucleon; 1 - Fermi gas; 2 - local Fermi gas; 3 - Bodek-Ritchie model; 4 - spectral function; 5 - deuterium.
nucleus_model	0, 1	1	Nucleus density profiles for FSI: 0 - constant density; 1 - realistic density profile.
target_content *(use with target_type 1)*	*a b c*x *d e f*	-	The composed target definition: target_content = TC_1 target_content += TC_2 ... $TC_i = a_i\ b_i\ c_i$x $d_i\ e_i\ f_i$, a_i is the number of protons, b_i is the number of neutrons, c_i is the number of i-th kind of nucleus in the target, d_i (optional) is the binding energy, e_i (optional) is the Fermi momentum, f_i (optional) is the nucleus model (like in nucleus_target).

geo_file *(use with target_type 2)*	*filename*	see description	The path to the file with the detector geometry (default *target/ND280_v9r7p5.root*).
geo_name *(use with target_type 2)*	*geometry name*	see description	The name of the geometry in the file (default *ND280Geometry_v9r7p5*).
geo_o *(use with target_type 2)*	*x y z*	0 0 0	The coordinates of the center of the box.
geo_d *(use with target_type 2)*	*x y z*	see description	The half dimension of the box (default 2000 5000 5000).
geo_volume *(use with target_type 2)*	*master volume name*	-	The name of the *master volume* in the detector file.
One can also use predefined target specifications instead of the above parameters. The list of targets can be found in "nuwro/data/target" directory. To use one of those beams, one must use the following line: @target/*targetfile.txt* where *targetfile.txt* is the name of the file from "nuwro/data/target" directory.			
Interaction settings			
dyn_qel_cc	0, 1	1	Turn on/off charge current quasi-elastic process.
dyn_qel_nc	0, 1	1	Turn on/off neutral current elastic process.
dyn_res_cc	0, 1	1	Turn on/off charge current resonance pion production..
dyn_res_nc	0, 1	1	Turn on/off neutral current resonance pion production.
dyn_dis_cc	0, 1	1	Turn on/off charge current deep inelastic scattering.

dyn_dis_nc	0, 1	1	Turn on/off neutral current deep inelastic scattering.
dyn_coh_cc	0, 1	1	Turn on/off charge current coherent pion production.
dyn_coh_nc	0, 1	1	Turn on/off neutral current coherent pion production.
dyn_mec_cc	0, 1	1	Turn on/off charge current meson exchange current process.
dyn_mec_nc	0, 1	1	Turn on/off neutral current meson exchange current process.
Quasi-elastic			
qel_vector_ff_set	1 - 6	2	Electromagnetic form factors parametrization: 1 - dipole form; 2 - BBBA05 (Ref. [138]); 3 - BBA03 (Ref. [158]); 4 - JLab (Ref. [159]); 5 - NN10 with two photon exchange effect (Ref. [155]).

qel_axial_ff_set	1 - 4	1	Axial form factors parametrization: 1 - dipole form; 2 - 2-fold parabolic modification; 3 - 3-fold parabolic modification; 4 - 4-fold parabolic modification.
qel_strange	0, 1	0	Turn on/off the strange quark contribution to the NC axial form factors.
qel_strangeEM	0, 1	0	Turn on/off the strange quark contribution to the NC vector form factors.
delta_s	any number	-0.15	g_A^s (see Subsec. 2.2.2).
qel_cc_axial_mass	any positive number	1200	The axial mass value for charge current form factors.
qel_nc_axial_mass	any positive number	1350	The axial mass value for neutral current form factors.
qel_s_axial_mass	any positive number	1200	The axial mass value used in the dipole strange form factor.

qel_rpa	0 - 3	0	RPA settings: 0 - do not use RPA; 1 - use RPA without effective mass of nucleon; 2 - use effective mass of nucleon without RPA (test only); 3 - use RPA with effective mass of nucleon (test only).
flux_correction	0, 1	1	Turn on/off flux correction.
sf_method	0 - 3	0	Spectral function settings (for CCQE): 0 - do not use spectral function; 1 - use grid spectral function (for ^{12}C, ^{16}O, ^{40}Ar, ^{40}Ca, ^{56}Fe); 2 - use factorized spectral function (for ^{16}O, ^{40}Ar, ^{40}Ca).
cc_smoothing	0, 1	1	If 1, the impossible quasi-elastic reaction (like CC ν scattering off proton) are skipped.

Pion production			
delta_FF_set	1 - 7	1	Δ production form factors: 1 - dipole form; 2 - Paschos and Lalakulich, 2.12 $M_A = 1.05 GeV$ BNL fit (Ref. [160]); 3 - Paschos and Lalakulich, 2.12 $M_A = 0.84 GeV$ ANL fit (Ref. [160]); 4 - Paschos and Lalakulich, page 4, bottom right (Ref. [160]); 5 - Paschos and Lalakulich, page 5, top left (Ref. [160]); 6 - Eq. 13 from Ref. [161]; 7 - based on chiral quark model from Ref. [162].
pion_axial_mass *(for delta_FF_set 1)*	any positive number	0.94	The axial mass value used in dipole parametrization of the resonance pion production form factor.
pion_C5A *(for delta_FF_set 1)*	any positive number	1.19	The C_A^5 value used in dipole parametrization of the resonance pion production form factor.
spp_precision	any positive number	500	Controls the precision in RES-DIS boundary region. Should not be changed.

red_dis_cut	any positive number	1600	Boundary of RES-DIS transition. Should not be changed.
coh_mass_correction	0, 1	1	Turn on/off Rein Sehgal correction to charge current coherent pion production.
coh_new	0, 1	1	Change between old (0) and improved (1) implementation of coherent pion production.
Two-body current			
mec_kind	1 - 4	1	Two-body current models: 1 - Transverse Enhancement model (Ref. [60]); 2 - based on Marteau model (Ref. [65]); 3 - Nieves et al. model (Ref. [63]); 4 - Martini et al. model (Ref. [65, 66]).
mec_ratio_pp	any positive number from [0,1]	0.6	The fraction of mixed initial nucleon pairs for charge current interaction. For neutral current the fraction is calculated as 1/(2*mec_ratio_pp + 1).
Final state interactions settings			
kaskada_on	0, 1	1	Turn on (1) / off (0) final state interactions.

kaskada_w	any positive number	7	The value of the effective potential subtracted from the nucleons energy leaving the nucleus.
kaskada_redo	0, 1	0	If on, given output file (*eventsout.root* by default) is loaded, the primary vertex is copied and only final state interactions are simulated. New output file with *".fsi.root"* suffix is created.
kaskada_writeall	0, 1	0	If on, all particles created during final state interactions are saved in *all* vector.
step	any positive number	0.2	Length of max step in the cascade in fm.
xsec	0, 1	1	Cross section models for pion-nucleon interactions: 0 - based on Ref. [97]; 1 - based on Ref. [101].
pauli_blocking	0, 1	1	Turn on/off Pauli blocking.
formation_length *(with formation_zone 7)*	any positive number	1	Formation length in fm.
tau	any positive number	8	The parameter control the formation length for *ranft* and *rl* models.
first_step	0, 1	0	If off, the formation zone is applied only for the particles created during final state interactions.

formation_zone	(0) nofz (1) skat8 (2) cosyn (3) cohl (4) ranft (5) rl (6) delta (7) const (8) fz (9) trans	fz	Formation zone models: (0) formation zone is off; (1) SKAT parametrization (Ref. [126]); (2) parametrization based on Color Transparency measurements (Ref. [163]); (3) coherence length (Ref. [164]); (4) parametrization based on hadron-hadron and hadron-nucleus collision (Ref. [165]); (5) as (4) but with fixed transverse momentum equal zero. (6) for resonance pion production. Based on Δ lifetime (Ref. [2]); (7) constant value; (8) default model: (3) for quasi-elastic scattering, (6) for resonance pion production, (4) for deep inelastic scattering and (0) for meson exchange current. (9) only for nuclear transparency analysis.

Appendix B

Response matrices

The graphical representation of response matrices used in MiniBooNE unfolding procedure (described in Sec. 4.1) is presented for each sample of data.

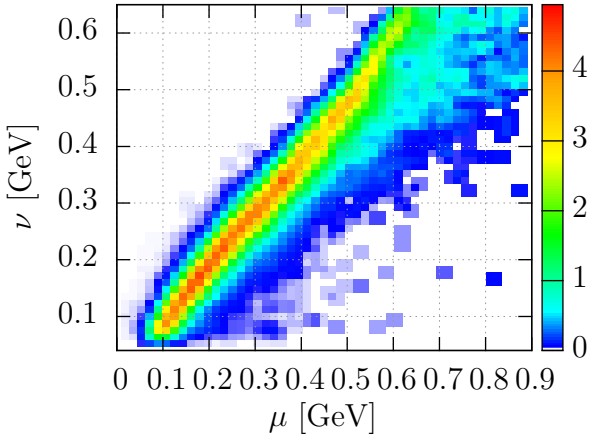

(a) NCEL scattering on hydrogen.

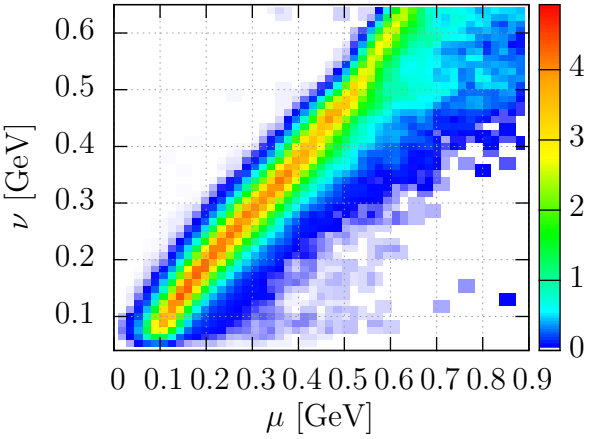

(b) NCEL scattering on a proton from carbon unaffected by FSI.

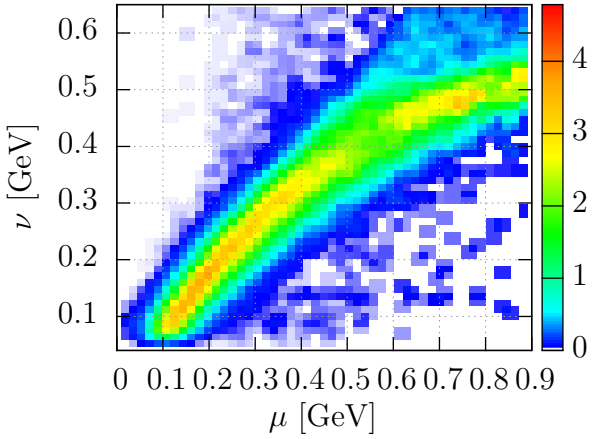

(c) NCEL scattering on a proton from carbon affected by FSI.

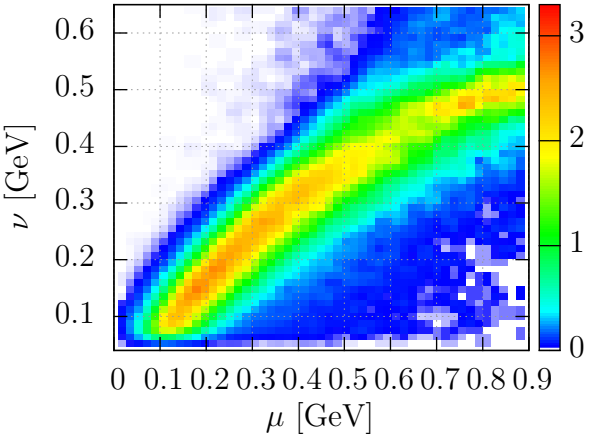

(d) NCEL scattering on a neutron from carbon.

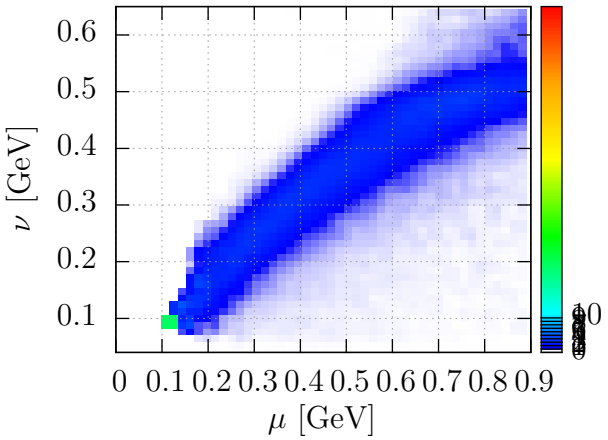

(e) Irreducible background.

Figure B.1: Response matrices for the NCEL sample.

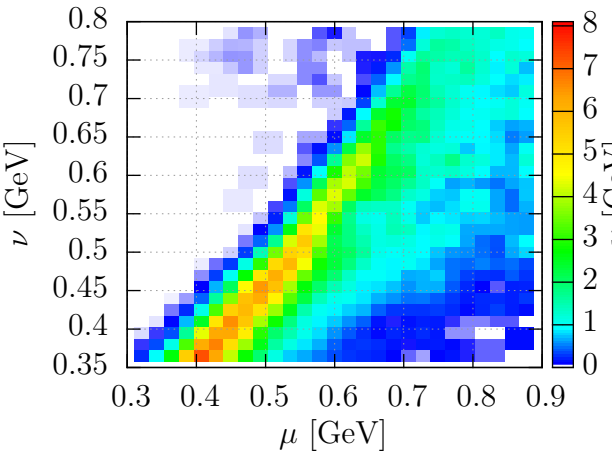

(a) NCEL scattering on hydrogen.

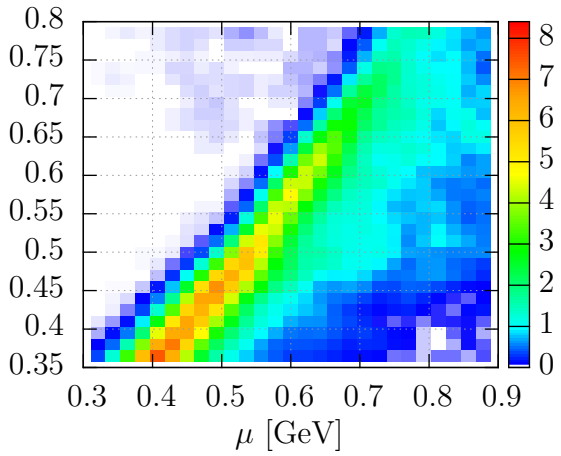

(b) NCEL scattering on a proton from carbon unaffected by FSI.

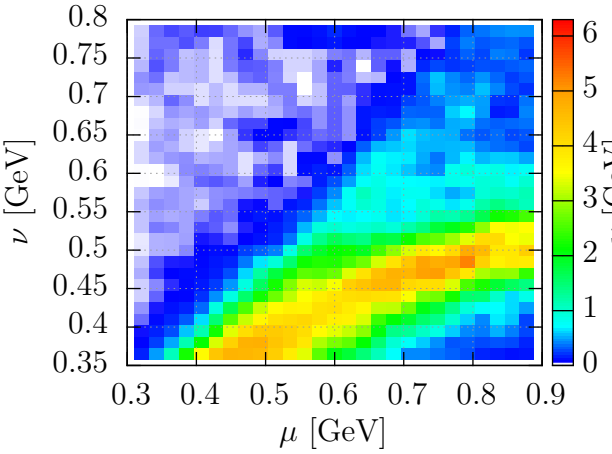

(c) NCEL scattering on a proton from carbon affected by FSI.

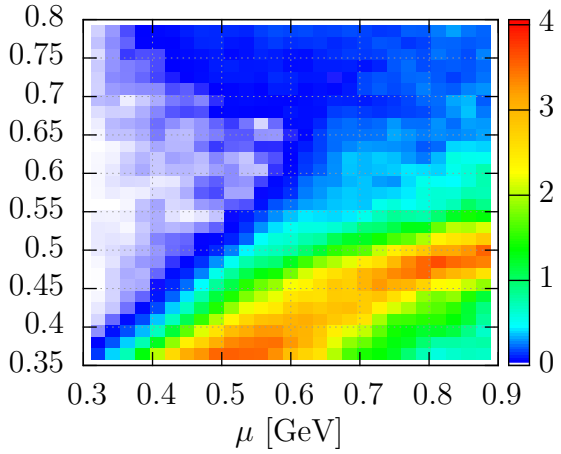

(d) NCEL scattering on a neutron from carbon.

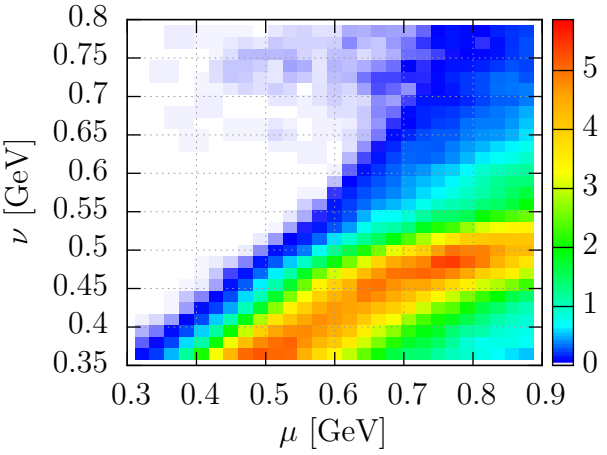

(e) Irreducible background.

Figure B.2: Response matrices for the NCEL high energy sample.

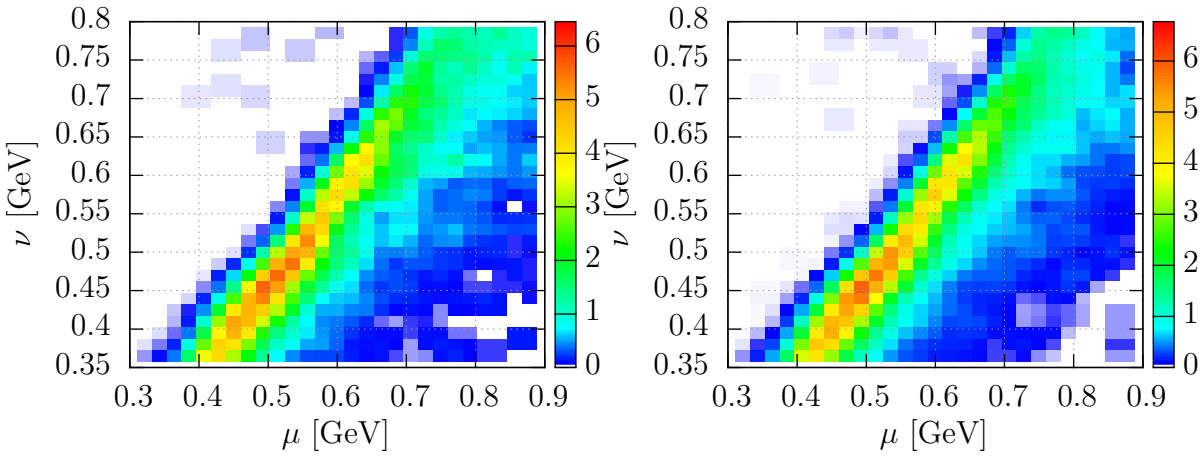

(a) NCEL scattering on hydrogen.

(b) NCEL scattering on a proton from carbon unaffected by FSI.

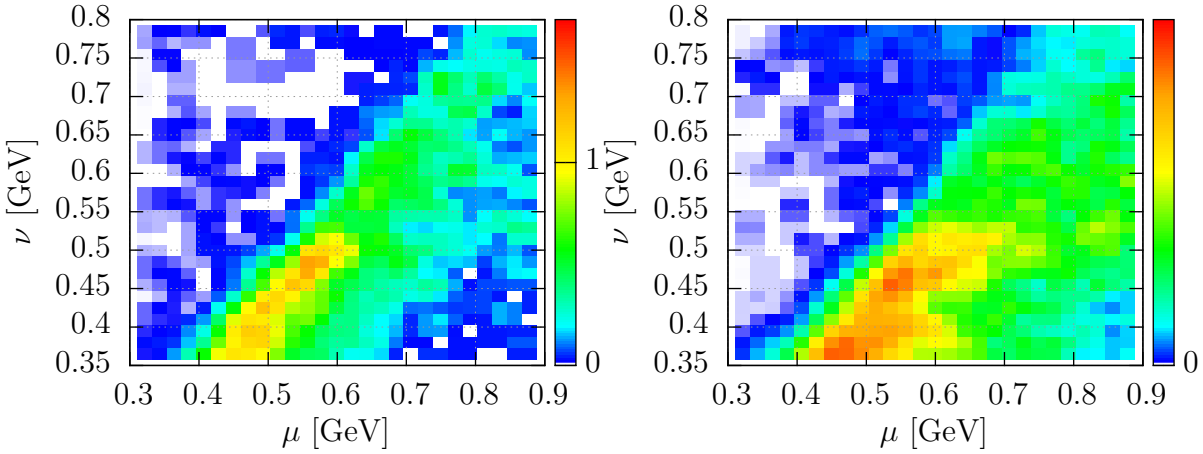

(c) NCEL scattering on a proton from carbon affected by FSI.

(d) NCEL scattering on a neutron from carbon.

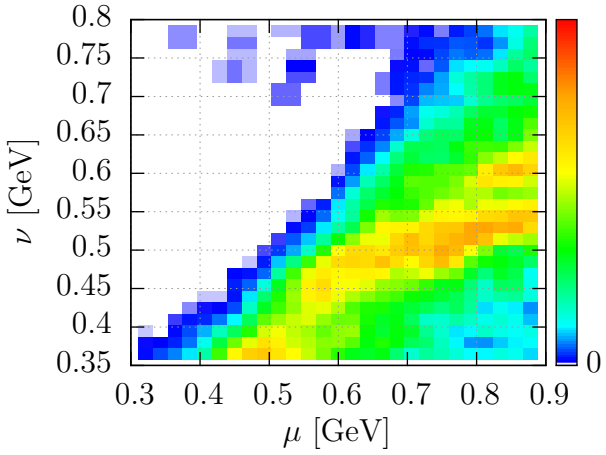

(e) Irreducible background.

Figure B.3: Response matrices for the NCEL proton enriched sample.

References

[1] Tomasz Golan et al. "Extraction of Axial Mass and Strangeness Values from the MiniBooNE Neutral Current Elastic Cross Section Measurement". Phys.Rev. C88 (2013), p. 024612.

[2] Tomasz Golan, Cezary Juszczak, and Jan T. Sobczyk. "Final State Interactions Effects in Neutrino-Nucleus Interactions". Phys.Rev. C86 (2012), p. 015505.

[3] Tomasz Golan. "A comparison of Monte Carlo generators" . arXiv: 1402.1608 [hep-ph] (2014).

[4] T. Golan, J.T. Sobczyk, and J. Zmuda. "NuWro: the Wroclaw Monte Carlo Generator of Neutrino Interactions". Nucl.Phys.Proc.Suppl. 229-232 (2012), p. 499.

[5] Tomasz Golan, Cezary Juszczak, and Jan T. Sobczyk. "Final state interactions model in NuWro Monte Carlo event generator". AIP Conf.Proc. 1405 (2011), pp. 219–222.

[6] M. Ziembicki et al. "The SMRD subdetector at the T2K near detector station". Acta Phys.Polon. B41 (2010), pp. 1579–1584.

[7] Maddalena Antonello et al. "Study of Pion Production in nu(mu) CC Interactions on O-16 Using Different MC Generators". Acta Phys.Polon. B40 (2009), pp. 2519–2535.

[8] K. Abe et al. "Measurement of the intrinsic electron neutrino component in the T2K neutrino beam with the ND280 detector" . arXiv: 1403.2552 [hep-ex] (2014).

[9] K. Abe et al. "Measurement of the neutrino-oxygen neutral-current interaction cross section by observing nuclear de-excitation γ-rays" . arXiv: 1403.3140 [hep-ex] (2014).

[10] K. Abe et al. "Recent Results from the T2K Experiment". Nucl.Phys.Proc.Suppl. 246-247 (2014), pp. 23–28.

[11] K. Abe et al. "Precise Measurement of the Neutrino Mixing Parameter theta23 from Muon Neutrino Disappearance in an Off-axis Beam" . arXiv: 1403.1532 [hep-ex] (2014).

[12] K. Abe et al. "Observation of Electron Neutrino Appearance in a Muon Neutrino Beam" . arXiv: 1311.4750 [hep-ex] (2013).

[13] K. Abe et al. "Measurement of Neutrino Oscillation Parameters from Muon Neutrino Disappearance with an Off-axis Beam". Phys.Rev.Lett. 111 (2013), p. 211803.

[14] K. Abe et al. "Evidence of Electron Neutrino Appearance in a Muon Neutrino Beam". Phys.Rev. D88 (2013), p. 032002.

[15] K. Abe et al. "Measurement of the Inclusive NuMu Charged Current Cross Section on Carbon in the Near Detector of the T2K Experiment". Phys.Rev. D87 (2013), p. 092003.

[16] K. Abe et al. "The T2K Neutrino Flux Prediction". Phys.Rev. D87 (2013), p. 012001.

[17] K. Abe et al. "First Muon-Neutrino Disappearance Study with an Off-Axis Beam". Phys.Rev. D85 (2012), p. 031103.

[18] K. Abe et al. "Measurements of the T2K neutrino beam properties using the INGRID on-axis near detector". Nucl.Instrum.Meth. A694 (2012), pp. 211–223.

[19] K. Abe et al. "Indication of Electron Neutrino Appearance from an Accelerator-produced Off-axis Muon Neutrino Beam". Phys.Rev.Lett. 107 (2011), p. 041801.

[20] K. Abe et al. "The T2K Experiment". Nucl.Instrum.Meth. A659 (2011), pp. 106–135.

[21] C. Rubbia et al. "Underground operation of the ICARUS T600 LAr-TPC: first results". JINST. 6 (2011), P07011.

[22] *NuWro web page*. URL: `http://borg.ift.uni.wroc.pl/nuwro/`.

[23] Yoshinari Hayato. "A neutrino interaction simulation program library NEUT". Acta Phys.Polon. B40 (2009), pp. 2477–2489.

[24] C. Andreopoulos et al. "The GENIE Neutrino Monte Carlo Generator". Nucl.Instrum.Meth. A614 (2010), pp. 87–104.

[25] D. Casper. "The Nuance neutrino physics simulation, and the future". Nucl.Phys.Proc.Suppl. 112 (2002), pp. 161–170.

[26] CERN. *ROOT library*. URL: http://root.cern.ch.

[27] H. De Vries, C.W. De Jager, and C. De Vries. "Nuclear charge and magnetization density distribution parameters from elastic electron scattering". Atom.Data Nucl.Data Tabl. 36 (1987), pp. 495–536.

[28] *T2K collaboration*. URL: http://t2k-experiment.org/.

[29] L. Fields et al. "Measurement of Muon Antineutrino Quasi-Elastic Scattering on a Hydrocarbon Target at $E_\nu \sim 3.5$ GeV". Phys.Rev.Lett. 111 (2013), p. 022501.

[30] G.A. Fiorentini et al. "Measurement of Muon Neutrino Quasi-Elastic Scattering on a Hydrocarbon Target at $E_\nu \sim 3.5$ GeV". Phys.Rev.Lett. 111 (2013), p. 022502.

[31] *NuWro repository*. URL: http://borg.ift.uni.wroc.pl/gitweb/?p=nuwro.

[32] Cezary Juszczak. "Running NuWro". Acta Phys.Polon. B40 (2009), pp. 2507–2512.

[33] *Tomasz Golan web page*. URL: http://www.ift.uni.wroc.pl/~tgolan/.

[34] S.J. Barish et al. "Study of Neutrino Interactions in Hydrogen and Deuterium: Inelastic Charged Current Reactions". Phys.Rev. D19 (1979), p. 2521.

[35] N. J. Baker et al. "Total cross sections for neutrino-nucleon charged-current interactions in the 7-foot bubble chamber". Phys. Rev. D. 25 (3 1982), pp. 617–623.

[36] Q. Wu et al. "A Precise measurement of the muon neutrino-nucleon inclusive charged current cross-section off an isoscalar target in the energy range 2.5 ¡ E(nu) ¡ 40-GeV by NOMAD". Phys.Lett. B660 (2008), pp. 19–25.

[37] Y. Nakajima et al. "Measurement of inclusive charged current interactions on carbon in a few-GeV neutrino beam". Phys.Rev. D83 (2011), p. 012005.

[38] P. Adamson et al. "Neutrino and Antineutrino Inclusive Charged-current Cross Section Measurements with the MINOS Near Detector". Phys.Rev. D81 (2010), p. 072002.

[39] Artur M. Ankowski and Jan T. Sobczyk. "Construction of spectral functions for medium-mass nuclei". Phys.Rev. C77 (2008), p. 044311.

[40] S.J. Barish et al. "Study of Neutrino Interactions in Hydrogen and Deuterium. 1. Description of the Experiment and Study of the Reaction Neutrino d -¿ mu- p p(s)". Phys.Rev. D16 (1977), p. 3103.

[41] A.A. Aguilar-Arevalo et al. "First Measurement of the Muon Neutrino Charged Current Quasielastic Double Differential Cross Section". Phys.Rev. D81 (2010), p. 092005.

[42] C.H. Llewellyn Smith. "Neutrino Reactions at Accelerator Energies". Phys.Rept. 3 (1972), pp. 261–379.

[43] C.F. Perdrisat, V. Punjabi, and M. Vanderhaeghen. "Nucleon Electromagnetic Form Factors". Prog.Part.Nucl.Phys. 59 (2007), pp. 694–764.

[44] Kaoru Hagiwara et al. "Review of particle physics. Particle Data Group". Phys.Rev. D66 (2002), p. 010001.

[45] G.T. Garvey, W.C. Louis, and D.H. White. "Determination of proton strange form-factors from neutrino p elastic scattering". Phys.Rev. C48 (1993), pp. 761–765.

[46] W. M. Alberico, S. M. Bilenky, and C. Maieron. "Strangeness in the nucleon: neutrino-nucleon and polarized electron-nucleon scattering". Phys. Rep. 358 (2002), pp. 227–308.

[47] Gian Luigi Fogli and G. Nardulli. "A New Approach to the Charged Current Induced Weak One Pion Production". Nucl.Phys. B160 (1979), p. 116.

[48] Stephen L. Adler. "Photoproduction, electroproduction and weak single pion production in the (3,3) resonance region". Annals Phys. 50 (1968), pp. 189–311.

[49] Stephen L. Adler. "Application of Current Algebra Techniques to Soft Pion Production by the Weak Neutral Current: V,a Case". Phys.Rev. D12 (1975), p. 2644.

[50] K.M. Graczyk et al. "C(5)A axial form factor from bubble chamber experiments". Phys.Rev. D80 (2009), p. 093001.

[51] Dieter Rein and Lalit M. Sehgal. "Neutrino Excitation of Baryon Resonances and Single Pion Production". Annals Phys. 133 (1981), pp. 79–153.

[52] Richard P. Feynman. "Very high-energy collisions of hadrons". Phys.Rev.Lett. 23 (1969), pp. 1415–1417.

[53] Elliott D. Bloom and Frederick J. Gilman. "Scaling, Duality, and the Behavior of Resonances in Inelastic electron-Proton Scattering". Phys.Rev.Lett. 25 (1970), p. 1140.

[54] E. Predazzi E. Leader. *An Introduction to Gauge Theories and Modern Particle Physics*. Cambrige University Press.

[55] M. Gluck, E. Reya, and A. Vogt. "Dynamical parton distributions of the proton and small x physics". Z.Phys. C67 (1995), pp. 433–448.

[56] A. Bodek and U.K. Yang. "Modeling deep inelastic cross-sections in the few GeV region". Nucl.Phys.Proc.Suppl. 112 (2002), pp. 70–76.

[57] Torbjorn Sjostrand et al. "High-energy physics event generation with PYTHIA 6.1". Comput.Phys.Commun. 135 (2001), pp. 238–259.

[58] S. Galster et al. "Coincidence experiment on inelastic electron-proton scattering in the region of the delta(1236) at q-squared=-0.35 and 1.0 (gev/c)squared". Phys.Rev. D5 (1972), pp. 519–527.

[59] J. Nieves, I. Ruiz Simo, and M.J. Vicente Vacas. "Inclusive Charged–Current Neutrino–Nucleus Reactions". Phys.Rev. C83 (2011), p. 045501.

[60] A. Bodek, H.S. Budd, and M.E. Christy. "Neutrino Quasielastic Scattering on Nuclear Targets: Parametrizing Transverse Enhancement (Meson Exchange Currents)". Eur.Phys.J. C71 (2011), p. 1726.

[61] M. Martini, M. Ericson, and G. Chanfray. "Neutrino quasielastic interaction and nuclear dynamics". Phys.Rev. C84 (2011), p. 055502.

[62] Jose Enrique Amaro et al. "Gauge and Lorentz invariant one pion exchange currents in electron scattering from a relativistic Fermi gas". Phys.Rept. 368 (2002), pp. 317–407.

[63] J. Nieves, I. Ruiz Simo, and M. J. Vicente Vacas. "Inclusive charged-current neutrino-nucleus reactions". Phys. Rev. C. 83 (4 2011), p. 045501.

[64] R. Gran et al. "Neutrino-nucleus quasi-elastic and 2p2h interactions up to 10 GeV" . arXiv: 1307.8105 [hep-ph] (2013).

[65] Jan T. Sobczyk. "Modeling nuclear effects in neutrino interactions in 1-GeV region" . arXiv: nucl-th/0307047 [nucl-th] (2003).

[66] M. Martini et al. "Unified approach for nucleon knock-out and coherent and incoherent pion production in neutrino interactions with nuclei". Phys. Rev. C. 80 (6 2009), p. 065501.

[67] E. Oset and L.L. Salcedo. "Delta self-energy in nuclear matter". Nucl.Phys. A468 (1987), pp. 631–652.

[68] Teppei Katori. "Meson Exchange Current (MEC) Models in Neutrino Interaction Generators" . arXiv: 1304.6014 [nucl-th] (2013).

[69] Jan T. Sobczyk. "Multinucleon ejection model for Meson Exchange Current neutrino interactions". Phys.Rev. C86 (2012), p. 015504.

[70] D. W. Higinbotham. *Using the (e,e'X) reaction to understand nucleons inside the nucleus*. talk given at INT Workshop 13-54W, Neutrino-Nucleus Interactions for Current and Next Generation Neutrino Oscillation Experiments. 2013.

[71] Dieter Rein and Lalit M. Sehgal. "Coherent pi0 Production in Neutrino Reactions". Nucl.Phys. B223 (1983), p. 29.

[72] Stephen L. Adler. "Tests of the Conserved Vector Current and Partially Conserved Axial-Vector Current Hypotheses in High-Energy Neutrino Reactions". Phys.Rev. 135 (1964), B963–B966.

[73] V. Flaminio et al. "COMPILATION OF CROSS-SECTIONS. 1. PI+ AND PI- INDUCED REACTIONS" (1983).

[74] D. Rein and L.M. Sehgal. "PCAC and the Deficit of Forward Muons in pi+ Production by Neutrinos". Phys.Lett. B657 (2007), pp. 207–209.

[75] J.E. Amaro et al. "Neutrino induced weak pion production off the nucleon and coherent pion production in nuclei at low energies". AIP Conf.Proc. 1189 (2009), pp. 224–229.

[76] S. Willocq et al. "Coherent production of single pions and rho mesons in charged current interactions of neutrinos and anti-neutrinos on neon nuclei at the Fermilab tevatron". Phys.Rev. D47 (1993), pp. 2661–2674.

[77] M. Aderholz et al. "Coherent production of pi+ and pi- mesons by charged-current interactions of neutrinos and antineutrinos on neon nuclei at the Fermilab Tevatron". Phys. Rev. Lett. 63 (21 1989), pp. 2349–2352.

[78] H. Faissner et al. "Observation of Neutrino and Anti-neutrino Induced Coherent Neutral Pion Production Off ^{27}Al". Phys.Lett. B125 (1983), p. 230.

[79] E. Isiksal, D. Rein, and J.G. Morfin. "EVIDENCE FOR NEUTRINO AND ANTI-NEUTRINOS INDUCED COHERENT PI0 PRODUCTION". Phys.Rev.Lett. 52 (1984), pp. 1096–1099.

[80] H.J. Grabosch et al. "COHERENT PION PRODUCTION IN NEUTRINO AND ANTI-NEUTRINO INTERACTIONS ON NUCLEI OF HEAVY FREON MOLECULES". Z.Phys. C31 (1986), p. 203.

[81] P.P. Allport et al. "Coherent Production of π^+ Mesons in Neutrino - Neon Interactions". Z.Phys. C43 (1989), pp. 523–526.

[82] F. Bergsma et al. "Measurement of the Cross-section of Coherent π^0 Production by Muon Neutrino and Anti-neutrino Neutral Current Interactions on Nuclei". Phys.Lett. B157 (1985), p. 469.

[83] P. Vilain et al. "Coherent single charged pion production by neutrinos". Phys.Lett. B313 (1993), pp. 267–275.

[84] E.J. Moniz et al. "Nuclear Fermi momenta from quasielastic electron scattering". Phys.Rev.Lett. 26 (1971), pp. 445–448.

[85] S.K. Singh and E. Oset. "Inclusive quasielastic neutrino reactions in C-12 and O-16 at intermediate-energies". Phys.Rev. C48 (1993), pp. 1246–1258.

[86] T.S. Kosmas and E. Oset. "Charged current neutrino nucleus reaction cross-sections at intermediate-energies". Phys.Rev. C53 (1996), pp. 1409–1415.

[87] C. Juszczak, J.A. Nowak, and J.T. Sobczyk. "Spectrum of recoil nucleons in quasi-elastic neutrino nucleus interactions". Eur.Phys.J. C39 (2005), pp. 195–200.

[88] P.K.A. de Witt Huberts. "Proton spectral functions and momentum distributions in nuclei from high resolution (e, e-prime p) experiments". J.Phys. G16 (1990), pp. 507–544.

[89] D. Rohe et al. "Correlated strength in nuclear spectral function". Phys.Rev.Lett. 93 (2004), p. 182501.

[90] Omar Benhar et al. "Electron- and neutrino-nucleus scattering in the impulse approximation regime". Phys.Rev. D72 (2005), p. 053005.

[91] R. Shneor et al. "Investigation of proton-proton short-range correlations via the C-12(e, e-prime pp) reaction". Phys.Rev.Lett. 99 (2007), p. 072501.

[92] A. Tang et al. "n-p short range correlations from (p,2p + n) measurements". Phys.Rev.Lett. 90 (2003), p. 042301.

[93] R. Subedi et al. "Probing Cold Dense Nuclear Matter". Science. 320 (2008), pp. 1476–1478.

[94] O. Benhar et al. "Spectral function of finite nuclei and scattering of GeV electrons". Nucl.Phys. A579 (1994), pp. 493–517.

[95] Omar Benhar, Alessandro Lovato, and Noemi Rocco. "Two particle-two hole final states in quasi elastic neutrino-nucleus interactions" . arXiv: 1312.1210 [nucl-th] (2013).

[96] A. Lovato et al. “Neutral weak current two-body contributions in inclusive scattering from ^{12}C” . arXiv: 1401.2605 [nucl-th] (2014).

[97] N. Metropolis et al. “Monte Carlo Calculations on Intranuclear Cascades. I. Low-Energy Studies”. Phys.Rev. 110 (1958), pp. 185–203.

[98] N. Metropolis et al. “Monte Carlo Calculations on Intranuclear Cascades. 2. High-Energy Studies and Pion Processes”. Phys.Rev. 110 (1958), pp. 204–219.

[99] O. Buss et al. “Transport-theoretical Description of Nuclear Reactions”. Phys.Rept. 512 (2012), pp. 1–124.

[100] V.R. Pandharipande and Steven C. Pieper. “Nuclear transparency to intermediate-energy nucleons from (e, e’p) reactions”. Phys.Rev. C45 (1992), pp. 791–798.

[101] L.L. Salcedo et al. “Computer simulation of inclusive pion nuclear reactions”. Nucl.Phys. A484 (1988), p. 557.

[102] E. Oset, L.L. Salcedo, and D. Strottman. “A Theoretical Approach to Pion Nuclear Reactions in the Resonance Region”. Phys.Lett. B165 (1985), pp. 13–18.

[103] Patrick de Perio. “NEUT pion FSI”. AIP Conf.Proc. 1405 (2011), pp. 223–228.

[104] *SAID*. URL: `http://gwdac.phys.gwu.edu/`.

[105] I. Navon et al. “True Absorption and Scattering of 50-MeV Pions”. Phys.Rev. C28 (1983), p. 2548.

[106] D. Ashery et al. “True Absorption and Scattering of Pions on Nuclei”. Phys.Rev. C23 (1981), pp. 2173–2185.

[107] M.K. Jones et al. “Pion absorption above the Delta (1232) resonance”. Phys.Rev. C48 (1993), pp. 2800–2817.

[108] R.A. Giannelli et al. “Multiproton final states in positive pion absorption below the Delta (1232) resonance”. Phys.Rev. C61 (2000), p. 054615.

[109] S.M. Levenson et al. “INCLUSIVE PION SCATTERING IN THE DELTA (1232) REGION”. Phys.Rev. C28 (1983), pp. 326–332.

[110] B.G. Ritchie. “Parametrization of total and differential cross-sections for pi d; p p below 1-GeV”. Phys.Rev. C44 (1991), pp. 533–536.

[111] S. Mukhopadhyay et al. “Pion absorption by He3 at the Delta resonance energy”. Phys.Rev. C43 (1991), pp. 957–972.

[112] T. Alteholz et al. "A Large solid angle study of pion absorption on He3". Phys.Rev.Lett. 73 (1994), pp. 1336–1339.

[113] B. Kotlinski et al. "Pion absorption reactions on N, Ar and Xe". Eur.Phys.J. A9 (2000), pp. 537–552.

[114] Kinga Partyka. "Exclusive 1mu+np topologies in ArgoNeuT". NuInt12. 2012.

[115] Ornella Palamara. "QE or not QE, that is the question". INT workshop, Seattle. 2013.

[116] L.D. Landau and I. Pomeranchuk. "Limits of applicability of the theory of bremsstrahlung electrons and pair production at high-energies". Dokl.Akad.Nauk Ser.Fiz. 92 (1953), pp. 535, 735.

[117] Leo Stodolsky. "Formation Zone Description in Multiproduction" (1975).

[118] S. J. Brodsky. *in Proceedings of the Thirteenth International Symposium on Multiparticle Dynamics, Volen- dam, The Netherlands, 1982, edited by W. Kittel et al. (World Scientific, Singapore, 1983).*

[119] A.H. Mueller. *in Proceedings of the Seventeenth Recontre de Moriond Conference on Elementary Particle Physics, Les Arcs, France, 1982 edited by J. Tran Thanh Van (Editions Fronriers, Gif-sur-Yvette, France, 1982).*

[120] X. Qian et al. "Experimental tudy of the A(e,e'π^+) Reaction on ^{1}H, ^{2}H, ^{12}C, ^{27}Al, ^{63}Cu and ^{197}Au". Phys.Rev. C81 (2010), p. 055209.

[121] J. Ranft. "Hadron Production in Hadron - Nucleus and Nucleus-nucleus Collisions in a Dual Parton Model Modified by a Formation Zone Intranuclear Cascade". Z.Phys. C43 (1989), p. 439.

[122] A. Fasso et al. "The Physics models of FLUKA: Status and recent developments". eConf. C0303241 (2003), MOMT005.

[123] P. Astier et al. "A Study of backward going p and pi in neutrino(muon) CC interactions with the NOMAD detector". Nucl.Phys. B609 (2001), pp. 255–279.

[124] A. Bialas. "Length of the Formation Zone From Inclusive Hadron - Nucleus Collisions". Z.Phys. C26 (1984), p. 301.

[125] G. Battistoni, P.R. Sala, and A. Ferrari. "The treatment of nuclear effects for neutrino interactions in the FLUKA code". Acta Phys.Polon. B37 (2006), pp. 2361–2369.

[126] D.S. Baranov et al. "An estimate for the formation length of hadrons in neutrino interactions" (1984).

[127] D. Abbott et al. "Quasifree (e, e-prime p) reactions and proton propagation in nuclei". Phys.Rev.Lett. 80 (1998), pp. 5072–5076.

[128] T.G. O'Neill et al. "A-dependence of nuclear transparency in quasielastic A (e, e-prime p) at high Q**2". Phys.Lett. B351 (1995), pp. 87–92.

[129] B. Clasie et al. "Measurement of nuclear transparency for the A(e, e-prime' pi+) reaction". Phys.Rev.Lett. 99 (2007), p. 242502.

[130] S. Nakayama et al. "Measurement of single pi0 production in neutral current neutrino interactions with water by a 1.3-GeV wide band muon neutrino beam". Phys.Lett. B619 (2005), pp. 255–262.

[131] Alexis A. Aguilar-Arevalo et al. "Measurement of nu(mu) and anti-nu(mu) induced neutral current single pi0 production cross sections on mineral oil at E(nu) O(1- GeV)". Phys.Rev. D81 (2010), p. 013005.

[132] Y. Kurimoto et al. "Measurement of Inclusive Neutral Current Neutral π^0 Production on Carbon in a Few-GeV Neutrino Beam". Phys.Rev. D81 (2010), p. 033004.

[133] Giuseppe Battistoni et al. "The FLUKA code: Description and benchmarking". AIP Conf.Proc. 896 (2007), pp. 31–49.

[134] G. Battistoni et al. "Neutrino interactions with FLUKA". Acta Phys.Polon. B40 (2009), pp. 2491–2505.

[135] G. Battistoni et al. "Generator of neutrino-nucleon interactions for the FLUKA based simulation code". AIP Conf.Proc. 1189 (2009), pp. 343–346.

[136] H. Gallagher. "The NEUGEN neutrino event generator". Nucl.Phys.Proc.Suppl. 112 (2002), pp. 188–194.

[137] A. Bodek and J.L. Ritchie. "Further Studies of Fermi Motion Effects in Lepton Scattering from Nuclear Targets". Phys.Rev. D24 (1981), p. 1400.

[138] R. Bradford et al. "A New parameterization of the nucleon elastic form-factors". Nucl.Phys.Proc.Suppl. 159 (2006), pp. 127–132.

[139] A. Bodek and U.K. Yang. "Modeling neutrino and electron scattering inelastic cross- sections in the few GeV region with effective LO PDFs TV Leading Order". Nucl.Phys.Proc.Suppl. (2003).

[140] T. Yang et al. "A hadronization model for the MINOS experiment". AIP Conf.Proc. 967 (2007), pp. 269–275.

[141] Steven Dytman. "Neutrino event generators". AIP Conf.Proc. 896 (2007), pp. 178–184.

[142] Krzysztof M. Graczyk and Jan T. Sobczyk. "Lepton mass effects in weak charged current single pion production". Phys.Rev. D77 (2008), p. 053003.

[143] A.A. Aguilar-Arevalo et al. "Measurement of muon neutrino quasi-elastic scattering on carbon". Phys.Rev.Lett. 100 (2008), p. 032301.

[144] *45th Karpacz Winter School in Theoretical Physics. Neutrino interactions: from theory to Monte Carlo simulations.*

[145] A.A. Aguilar-Arevalo et al. "Measurement of ν_μ-induced charged-current neutral pion production cross sections on mineral oil at $E_\nu \in 0.5 - 2.0$ GeV". Phys.Rev. D83 (2011), p. 052009.

[146] A.A. Aguilar-Arevalo et al. "Measurement of Neutrino-Induced Charged-Current Charged Pion Production Cross Sections on Mineral Oil at $E_\nu \sim 1$ GeV". Phys.Rev. D83 (2011), p. 052007.

[147] Philip Rodrigues. "Comparing pion production models and MiniBooNE data". NuInt12. 2012.

[148] Nathan Mayer Steve Dytman Tomasz Golan. "The comparison of MC generators". NuInt12. 2012.

[149] Denis Perevalov. "Neutrino-nucleus neutral current elastic interactions measurement in MiniBooNE". PhD thesis. FERMILAB, 2009. URL: `http://www-boone.fnal.gov/publications/Papers/denis_thesis.pdf`.

[150] A.V. Butkevich and D. Perevalov. "Neutrino neutral-current elastic scattering on 12C". Phys.Rev. C84 (2011), p. 015501.

[151] Artur M. Ankowski. "Consistent analysis of neutral- and charged-current neutrino scattering off carbon". Phys.Rev. C86 (2012), p. 024616.

[152] Andrea Meucci, Carlotta Giusti, and Franco Davide Pacati. "Relativistic descriptions of final-state interactions in neutral-current neutrino-nucleus scattering at MiniBooNE kinematics". Phys.Rev. D84 (2011), p. 113003.

[153] *MiniBooNE Neutral Current Elastic Data Release*. URL: `http://www-boone.fnal.gov/for_physicists/data_release/ncel/`.

[154] Denis Perevalov. *private communication.*

[155] Krzysztof M. Graczyk, Piotr Plonski, and Robert Sulej. "Neural Network Parameterizations of Electromagnetic Nucleon Form Factors". JHEP. 1009 (2010), p. 053.

[156] Krzysztof M. Graczyk. "Two-Photon Exchange Effect Studied with Neural Networks". Phys.Rev. C84 (2011), p. 034314.

[157] L.A. Ahrens et al. "Measurement of Neutrino - Proton and anti-neutrino - Proton Elastic Scattering". Phys.Rev. D35 (1987), p. 785.

[158] Howard Scott Budd, A. Bodek, and J. Arrington. "Modeling quasielastic form-factors for electron and neutrino scattering" . arXiv: hep-ex/0308005 [hep-ex] (2003).

[159] E.J. Brash et al. "New empirical fits to the proton electromagnetic form-factors". Phys.Rev. C65 (2002), p. 051001.

[160] Olga Lalakulich and Emmanuel A. Paschos. "Resonance production by neutrinos. I. J = 3/2 resonances". Phys.Rev. D71 (2005), p. 074003.

[161] L. Alvarez-Ruso, S. K. Singh, and M. J. Vicente Vacas. "Charged current weak electroproduction of the Δ resonance". Phys. Rev. C. 57 (5 1998), pp. 2693–2699.

[162] D. Barquilla-Cano, A.J. Buchmann, and E. Hernandez. "Axial N-¿Delta(1232) and N-¿N*(1440) transition form factors". Phys.Rev. C75 (2007), p. 065203.

[163] Wim Cosyn. "Exploring the limits of a hadronic picture of nuclei through pion and nucleon removal reactions". PhD thesis. Ghent University, 2009. URL: `http://lib.ugent.be/fulltxt/RUG01/001/350/817/RUG01-001350817\_2010\_0001\_AC.pdf`.

[164] A. Rubbia G. Battistoni A. Ferrari and P.R. Sala. *The FLUKA nuclear cascade model applied to neutrino interactions.* talk given at NuInt02. 2002.

[165] J. Ranft. "Hadron production in hadron-nucleus and nucleus-nucleus collisions in a dual parton model modified by a formation zone intranuclear cascade". Zeitschrift für Physik C Particles and Fields. 43.3 (1989), pp. 439–446.